Università degli Studi di Palermo

AREA RICERCA E TRASFERIMENTO TECNOLOGICO
SETTORE DOTTORATI E CONTRATTI PER LA RICERCA
U. O. DOTTORATI DI RICERCA

Dottorato in Scienze Molecolari e Biomolecolari
Dipartimento di Scienze e Tecnologie Biologiche, Chimiche e Farmaceutiche
SSD BIOS-03/A BIOS-04/A

BIOLOGICAL CHARACTERIZATION OF THE EFFECTS INDUCED BY AQUEOUS EXTRACTS FROM LEAVES AND RHIZOMES OF *P. OCEANICA* (L.) DELILE,1813 AND COELOMIC FLUID OF *H. TUBULOSA* (GMELIN,1790) ON HEPG2 HEPATOCARCINOMA CELLS AND AN *IN VITRO* MODEL OF HUMAN BLOOD-BRAIN BARRIER

IL DOTTORE
DOTT.SSA GIULIA ABRUSCATO

IL COORDINATORE
PROF.SSA GIOVANNA PITARRESI

IL TUTOR
PROF. VINCENZO ARIZZA

CO TUTOR
PROF. CLAUDIO LUPARELLO

CICLO XXXVII
ANNO CONSEGUIMENTO TITOLO 2024

TABLE OF CONTENTS

2.2 STATISTICS

2.3 RESULTS

2.3.1 Effects of *P. oceanica's* extracts on short-term viability and long term proliferative potential of HepG2 cells

2.3.2 Effects of *P. oceanica's* extracts on cell-cycle status and apoptosis induction in HepG2 cells

2.3.3 Effects of *P. oceanica's* extracts on mitochondrial membrane polarization and redox status in HepG2 cells

2.3.4 Effects of *P. oceanica's* extracts on HepG2 cells' autophagic activity

2.3.5 Inhibition of the locomotory ability of HepG2 Cells exposed to *P.oceanica's* extracts

2.3.6 Contribution of 14 of the 100 proteins found on the biological activity obtained

2.3.7 Quali-quantitative determination of the phenolic components of GLE, BLE and RE.

3. ANTIDIABETIC EFFECT: EFFECT OF EXTRACTS FROM *P. OCEANICA* (GLE AND RE) AND THE COELOMIC FLUID OF *H. TUBULOSA* (CFE)

3.1 MATERIALS AND METHODS

3.1.1 Cell culture and treatment

3.1.2 Pas Staining

3.1.3 Extracellular glucose determination

3.1.4 Flow cytometric assays

3.1.4.1 Flow cytometric assays for glucose uptake determination

3.1.4.2 Flow cytometric assays for Glut-2 and Glut-4 exposure on the plasma membrane

3.1.5 Conventional and qRT-PCR

3.1.6 Western Blotting.

3.2 STATISTICS

3.3 RESULTS

3.3.1 GLE and CFE stimulate glycogen accumulation in HepG2 cells

LIST OF ABBREVIATIONS

µg	Microgram
µL	Microliter
AJ	Adherent Junction
AVOs	Acidic Vesicular Organelles
BBB	Blood Brain Barrier
BLE	Beached leaves extract
BLECs	Brain Like Endothelial cells
BSA	Bovine Serum Albumin
CFE	Coelomatic Fluid extract
CNS	Central nervous system
DAPK	Death associated protein kinase
DRE	Dynamic range enhancement
ESI	Electrospray ionization
FACS	Fluorescence activated cell sorter
FBS	Fetal Bovine Serum
GLE	Green leaves extract
HCC	Hepatocellular Carcinoma
HPLC	High performance liquid chromatography
IC_{50}	Half maximal inhibitory concentration
MCP	Microchannel plate
MFI	Mean Fluorescence Intensity
MMP	Mitochondrial Transmembrane Potential
MMPs	Matrix metalloproteases
MS	Mass spectometry
mTOR	Mammalian target of rapamycin
NaFlu	Sodium Fluoresceine
P62/SQSTSM1	p62 sequestosome 1
PBS-CMF	PBS Calcium-Magnesium Free
Pe	Endothelial Permeability Coefficient
PE	Plating Efficiency
PI	Propidium Iodide

pNA	p-nitroanilide
qRT-PCR	Quantitative Real Time PCR
RE	Rhizomes extract
RH	Ringer Hepes
ROS	Reactive Oxygen Species
SF	Surviving Fraction
TJ	Tight Junction
TNFα	Tumor Necrosis Factor Alpha
λ	Wavelenght.

1. INTRODUCTION

1.1 AQUATIC SPECIES AND THEIR BENEFICIAL EFFECTS: *POSIDONIA OCEANICA* AND *HOLOTHURIA TUBULOSA*

Seas and oceans, which cover three-quarters of the Earth's surface, host an enormous variety of organisms and represent a richest source of marine natural bioactives yet to be exploited. Among the marine phanerogams, *Posidonia oceanica* (L.) (Delile, 1813; Liliopsida, Najadales: Posidoniacee) is the most widely distributed and abundant endemic member in the Mediterranean Sea. This slow-growing plant consists of buried roots and modified stems (called rhizomes, which give rise to groups of long strap-like green leaves), and forms dense and extensive underwater meadows, thus colonizing vast areas that account for about 1.5% of the surface of the Mediterranean Sea.

Figure 1. Underwater meadows of *P.oceanica* (ResearchGate, photo of Dimitris Poursanidis).

It is listed as a protected species by several international conventions and plays a central ecological role as an indicator of the overall environmental quality of the coastal areas, including the Sicilian coast, where it covers 76,000 hectares (Bellissimo et al., 2020). On the other hand, dealing with biomedical applications, it is known that, similarly to many other aquatic species, *P. oceanica* is a rich reservoir of numerous primary and secondary metabolites; therefore, extracts from this species have been the subject of preclinical investigations aimed at designing new preventive and/or treatment agents effective against various diseases. Early reports assessed the antimicrobial activity of rhizome and grass extracts (Bernard & Pesando, 1989; Berfad, 2014) and also demonstrated the dose-dependent glucose lowering and vasoprotective effects of *P. oceanica*'s preparations in a diabetic rat

model (Gokce & Haznedaroglu, 2008). In addition, the antioxidant, antiaging, antiinflammatory and antiglycation activities of the leaf extracts have been recently recognized (Cornara et al., 2018; Messina et al., 2021; Vasarri et al., 2020, 2021). A limited number of papers have also examined the antitumoral potential of *P. oceanica*'s extracts. Specifically, Barletta et al. (2015); Leri et al. (2018); Vasarri et al. (2021) described the capacity of hydrophilic preparations to inhibit matrix metalloproteases (MMPs) gene and protein expressions in human fibrosarcoma and neuroblastoma cells modulating the cells' autophagic flux and also blocking the enzymatic activity of secreted MMPs, thereby impairing the locomotory and invasive attitudes of the cells. Furthermore, as shown by (Farid, 2018), different extracts of *P. oceanica* exhibited varying antiproliferative activity against human breast, colon, liver, and larynx cancer cells, thus prompting further investigation into the anticancer potential of the preparations. Among marine invertebrates, edible sea cucumbers belonging to the class Holothuroidea of the phylum Echinodermata have been shown to exert numerous beneficial effects on human health due to the wide range of bioactive molecules present in their different body parts which are endowed with diversified properties (e.g., antioxidant, neuroprotective, and antitumoral) (Hossain et al., 2022; Shou et al., 2023).

Figure 2. A *Holothuria tubulosa* sea cucumber specimen (Luparello et al., 2022).

Holothuria tubulosa is an edible Mediterranean species, extensively distributed, that lives on muddy rocks or sandy bottoms within meadows of *P. oceanica.* It has a light brown or reddish surface covered with numerous long, dark conical papillae and three lines of mobile tubular legs along the ventral face (Bay-Nouailhat A., 2006). Some reports in the literature have been focused on the nutritional and pharmacological values of the extracts and isolated compounds obtained from this sea cucumber. A study carried out on experimentally

edematous mice assessed the anti-inflammatory role of a methanolic extract from *H. tubulosa* through the partial inhibition of cyclooxygenase-2 activity (Zhu et al., 2020).The low M.W. fucoidan isolated from the body wall of *H. tubulosa* has been shown to attenuate the inflammatory reaction related to metabolic disease both *in vitro* and *in vivo*. The significant fatty acid content of *H. tubulosa*'s tegument, in addition to being endowed with an important nutritional quality, has been shown to exert antioxidant and free radical-scavenging effects *in vitro* (Zmemlia et al., 2020) . In addition, the total body extracts of this sea cucumber promoted apoptosis-based cytotoxicity against cancer cells, and the enzymatic hydrolysates of the body wall proved to be a source of angiotensin-converting enzyme (ACE) inhibitory peptides (Alper & Güneş, 2020;Mecheta et al., 2020).Moreover, its coelomocytes, mediating cells of the immune system, have been shown to be the source of the antimicrobial peptides holothuroidin-1 and -2 (Schillaci et al., 2013). In echinoderms, the coelomic fluid represents a significant part of their body mass. It provides a pseudo-vascular system designed for transport and immune response and hosts a complex mixture of soluble molecules, mostly proteins, constitutively secreted by different parts of the invertebrate's body. The use of the cell-free water extract from the coelomic fluid (CFE) of *H. tubulosa* has previously demonstrated its *in vitro* anti-breast and liver cancer effects (Luparello et al., 2022; 2019). In fact, if supplied to cancer cell cultures, the preparation inhibited cell viability and proliferation by impairing cell cycle progress, locomotion, mitochondrial activity, reactive oxygen species (ROS) production, and autophagic flux, in some cases stimulating apoptotic death. A comprehensive proteomic analysis of the CFE identified a subgroup of proteins potentially responsible for its anti-liver cancer activity.

1.2 HEPATOCELLULAR CARCINOMA

Hepatocellular carcinoma (HCC) is an aggressive cancer histotype that accounts for more than 90% of primary liver cancers and is rated as the fifth most common cancer type worldwide and the second main cause of cancer death in men (Asafo-Agyei, 2023). The prognosis of HCC, which often gives rise to extensive metastasis and shows a high recurrence rate after resection or ablation, is generally unfavorable. As reported by Philips et al. (2021), in 2018, the estimated global incidence rate of liver cancer per 100,000 person-years was 9.3, while the corresponding mortality rate was 8.5. In general, all cirrhosis-inducing conditions can increase the risk of HCC. Oxidative stress, inflammation, and continuous cycles of necrosis and regeneration are fundamental mechanisms in the development of the neoplasia and, within this altered microenvironment, the damaged

hepatocytes accumulate genetic alterations and undergo progressive de-differentiation, leading to oncogenic transformation (Brar et al., 2018). Advances in the knowledge of the dysregulation of various signaling pathways responsible for uncontrolled cell propagation, metastasis, and recurrence of HCC cells have led to the identification of compounds that could inhibit the specific targets of signal transduction by acting on cell cycle, cell migratory behavior, apoptosis and autophagy that if altered or lost represent a key mechanism in neoplastic spread and treatment resistance (Farzaneh et al., 2021). Many of these beneficial compounds are being investigated as potential additives for functional foods or food-packaging so that their regular intake might contribute to the maintenance of the health in the organs of the digestive apparatus. However, the development of targeted therapies requires biological characterization of the molecular mechanism of action of the agents under investigation.

1.3 DIABETES MELLITUS

Diabetes mellitus is a metabolic disorder characterized by chronic hyperglycemia due to the incapacity to produce sufficient insulin (type 1) or to use it efficiently (type 2). More in detail the former, also called insulin-dependent or juvenile, is characterized by deficiency of insulin secretion due to autoimmune destruction of pancreatic β cells. Genetic tests or serologic tests for autoantibodies, e.g., autoantibodies to cell islets and to insulin are commonly used for the diagnosis of this type of diabetes. The second form, defined non-insulin dependent or adult-onset, is characterized by insuline resistance and the following insuline deficiency is not of autoimmune derivation. Unlike for type 1, affected individuals do not require insulin for survival (A.D.A, 2013). At the cellular level, normally, hepatocytes internalize glucose through the membrane glucose transporters GLUT-2 and -4. Specifically, GLUT-2 regulates glucose levels in an insulin-independent manner and mediates transport in both directions by exploiting concentration gradients and thus enhancing glucose uptake by cells (Mueckler & Thorens, 2013; Fu et al., 2023). Therefore modulation of GLUT expression by the transcription factor hepatocyte nuclear factor HNF-1α is a crucial event in the regulation of glucose metabolism. GLUT-4, on the other hand, is a transporter whose presence in the membrane is insulin-dependent through the activation of the pathway IRS-1/PI3K/Akt (Furtado et al., 2002). Briefly insulin binds to its receptor, resulting in the activation of the intrinsic tyrosine kinase, which causes in turn the phosphorylation in Tyr of the IRS-1 protein. These preliminary events determine the binding and activation of phosphatidylinositol 3-phosphate, which will activate protein kinase Akt-2 responsible for

the phosphorylation of many substrates, including proteins that stimulate the membrane translocation of GLUT-4 (Saltiel & Kahn, 2001; Taniguchi et al., 2006). Alterations in the expression levels of genes involved in these pathways may be responsible for the onset of diabetes, described above, that is a serious threat to human health considering that, worldwide, more than a half billion people are living with diabetes, 96% of the mellitus type, and that this number is expected to more than double in the next 30 years (Ong et al., 2023). Many pharmacological resources are available to help the control of blood glucose levels, but many side effects are associated with the use of these drugs. On the other hand, as reported in Zhang et al., (2019) and Abdel Raoof et al. (2018) the development of naturally derived anti-diabetic compounds has attracted much attention as a safe, effective, available, and low-cost alternative, that holds promise for its potential beneficial effects, while keeping in mind that rigorous scientific validation is essential for their medical use.

1.4 THE BLOOD-BRAIN BARRIER AND NEUROINFLAMMATORY DISEASES

The BBB is a selective barrier that regulates the passage of substances between the bloodstream and the CNS, protecting it from potential neurotoxic agents.This barrier is localized in endothelial cells that line the blood vessels contributing to the maintenance of homeostasis. Unlike peripheral endothelial cells, brain endothelial cells exhibit a low rate of transcytosis and a limited paracellular permeability guaranteed by multiprotein junctional complexes, such as of tight junctions (TJs) and adherent junctions (AJs) (Versele et al., 2022), whose more used protein markers are Claudin-5 and VE-Cadherin, respectively. Claudin-5 is a key tight junction protein that prevents the passage of potentially harmful substances from the blood to the brain. On the other hand, VE-cadherin is an adherens junction-specific protein that mediates adhesion between endothelial cells, which is critical for the maintenance of cell cohesion and structural architecture of the BBB. Alterations at VE-Cadherin levels, in response to various physiological and pathological stimuli, may indicate vascular instability and increased permeability. After damage to the BBB an increase in VE-Cadherin expression may be helpful in restoring barrier integrity since it tends to strengthen the adherens junctions between endothelial cells, limiting the leakage of fluid and inflammatory cells from blood to brain tissue, thus protecting the latter from further damage.The causes of damage to the BBB and responsable for the development of neuroinflammatory diseases can be various, such as brain injury, autoimmune diseases, infections, and stress. In fact, these latter induce the immune system to release inflammatory cytokines whose prolonged release can cause chronic neuroinflammation. The major

neuroinflammatory disorders include multiple sclerosis, Alzheimer and Parkinson's diseases.

1.5 AIM OF THE RESEARCH

In the present study, preparations obtained from marine species were used to test their beneficial effects on cell cultures *in vitro*; in particular, aqueous extracts prepared from *P. oceanica*'s rhizomes (RE) and leaves, both fresh (green; GLE) and beached (brown; BLE) and the aqueous extract of the coelomic fluid from *Holothuria tubulosa* (CFE), used for previous investigations. The HepG2 liver cell line, derived from a 15-year-old Caucasian male affected by differentiated hepatocellular carcinoma (Donato et al., 2015), was chosen as the *in vitro* model system for a tumor of the digestive apparatus, being one of the most used in drug toxicity studies. Dealing with the novel potential anticancer preparations from *P.oceanica*'s extracts, in a first set of assays we examined whether and to what extent RE, GLE and BLE could exert cytotoxic effects against HepG2 cells in culture. In particular, the viability and locomotory behavior, cell cycle distribution, apoptosis and autophagy modulation, mitochondrial membrane polarization, and cell redox state were selected as biological endpoints. Next, since the liver is the main organ in which glucose metabolism and storage take place and the main target for the molecular alterations of glucose uptake and utilization, and since HepG2 cells express many differentiated hepatic functions, including glycogen storage and insulin signalization (Donato et al., 2015), these cells were also chosen to test the glucose-lowering and potential antidiabetic activity of GLE, RE and CFE. In particular, using a combination of cytochemical, flow cytometric, PCR, and protein blot techniques, we examined the role of GLE, RE and CFE in glucose consumption, internalization, and accumulation and in the upregulation and surface translocation of the two glucose transporters GLUT-2 and -4 (Karim, 2012). We also studied the changes in expression, synthesis, and/or activation of the GLUT2-related transcription factor hepatocyte nuclear factor-1α (HNF1α) (Kim et al., 2017) and the GLUT4-translocation regulatory factors insulin receptor substrate-1 (IRS-1) and AKT/pAKT (Ramachandran & Saravanan, 2015). Finally, given the high presence of phenolic compounds in GLE and RE which have been shown to possess anti-oxidant, antiinflammatory and neuroprotective properties *in vitro* our aim was also to evaluate their potential anti-inflammatory effect, in the context of CNS inflammatory diseases, by analyzing the effects induced on a TNF-α inflamed human blood-brain barrier (BBB) model. Before proceeding with these latter studies, however, we selected the concentrations to be used performing MTT assays and

Griess reactions on LPS-treated RAW 264.7 cell cultures, commonly used as an *in vitro* model for the study of inflammation. Specifically, the effects of GLE and RE on BBB permeability, nitric oxide production and release, integrity of junctional complexes (both adherens and tight) and on the expression of ICAM-1 and VCAM-1 markers of inflammation after TNFα exposure were analyzed by qRT-PCR, Western blot and immunofluorescence.

2. CYTOTOXIC ACTIVITY EXERTED BY GLE AND RE : FOCUS ON AUTOPHAGY AND APOPTOSIS

2.1 MATERIALS AND METHODS

2.1.1 *Preparation of green leaves extract (GLE), Brown Leaves extract (BLE) and Rhizomes extract (RE) of P.oceanica*

Fresh samples of *P. oceanica* characterized by green leaves and rhizomes were collected by scuba diving off the coast of the Gulf of Palermo (Sicily, Italy), while stranded brown leaves were collected on the coastal beach at the same location.The plant material was extensively washed under fresh water to remove sandy debris and manually cleaned to remove epiphytes. For the extraction, 5 g of rhizomes, green and brown leaves were individually pulverized in a mortar in the presence of liquid nitrogen. The aqueous extracts obtained by individual resuspension of the powders in 2 M acetic acid (1:3 g/mL) plus a 1:200 antiprotease cocktail (P8340, Sigma, St. Louis, MO, USA) were homogenized with an Ultra-Turrax T-25 digital instrument (IKA, Staufen, D), sonicated with an ultrasonic processor (Sonics & Materials Inc., Danbury, CT, USA), and centrifuged at 15,500 rpm for 20 min at 4 ◦C. The supernatants were sterilized with filter (pore size = 0.22 μm),lyophilized with an Alpha 2-4 LD plus instrument (Martin Christ, Osterode am Harz,D), resuspended in a minimum volume of sterile distilled water and stored at -20°C until use.

2.1.1.1 Chromatographic Analysis

Aliquots of 10 mg of each sample were dissolved/diluted in 1.0 mL methanol in an autosampler vial and sonicated for 5 min. The analysis was performed with an Alliance 2695 (Waters), a high-performance liquid chromatography (HPLC) system equipped with an autosampler, degasser and column heater, coupled with a quadrupole time-of-flight mass spectrum (Waters Q-TOF Premier). The compounds were separated with a Thermo Hypersil Gold column, 5 cm, 2.1 mm, 1.9 μm particle size, at a temperature of 30°C and with an injected volume of 5 μL. Triplicate injections of all samples were carried out with a thermostatic autosampler maintained at 15°C. For HPLC analysis, solvent A (water, with 0.1 v/v% formic acid) was mixed with solvent B (methanol, with 0.1 v/v% formic acid) with the following gradient schedule:from 0 to 1 min, 95% A (flow rate0.25 mL/min);from 1 to 15 min, 100% B; from 15 to 20 min, the same percentage of solvent B; from 20 to 21 min, 100% B; from 21 to 26 min, 95% A for column rebalancing. The mass spectrometry (MS) experiments were carried out by the dynamic range enhancement (DRE) acquisition mode

to avoid microchannel plate (MCP) saturation and maintain good sensitivity, thereby ensuring a proper quantification of the compounds present in both high concentration and trace levels. Electrospray ionization (ESI) was used in a negative ion mode under the following conditions : capillary voltage, 2.0 KV; desolvation temperature, 300 °C; sampling cone,0.0 V; extraction cone, 2.0 V; ion guide, 2 V; source temperature, 80 °C; cone gas N2, flow 35.0 L/h; desolvation gas N2, flow 300.0 L/h; scan time, 1 s; delay between scans, 0.1 s. The acquisition mass interval was 100-1000 m/z; for data collection with an accurate mass selection, an appropriate block mass was selected.

2.1.1.2 *Proteomic Analysis*

GLE and RE were centrifuged and the supernatants were placed on 10-kDa membrane filters for subsequent solvent exchange. Protein concentrations were identified with a NanoDrop 3300 (Thermo Fisher, Waltham, MA, USA), then enzymatic digestion was performed as previously reported (Luparello et al., 2022a; 2022b).Shortly, the proteins present in the sample were reduced with RapiGest and dithiothreitol (Thermo Fisher), then alkylated with iodoacetamide (Thermo Fisher) and finally digested with LysC-Trypsin and Trypsin (Mass Spec grade, Promega, Madison, WI, USA) in two steps. Proteolysis was stopped by the addition of formic acid (Thermo Fisher). Then, the samples were dried and desalted using C18 spin columns (Thermo Fisher) and stored at -20 ◦C until analysis. Aliquots of each sample (total nominal amount = 3 μg protein) were then processed with an Ultimate 3000 (Dionex, Sunnyvale, CA, USA) coupled to a Bruker Maxis II ETD mass spectrometer (Bruker Daltonics GmbH, Bremen, D) via a CaptiveSpray nanobooster ion source. Peptides were separated with an ACQUITY UPLC M-Class Peptide BEH C18 column (Waters, Milford, MA, USA). Proteins were identified by searching in the FASTA Uniprot Alismatales database (accessed Feb. 20, 2023), using the Byonic program (version 4.5.2., Protein Metrics Inc.). Based on the results, a protein database was developed and Scaffold was used for protein quantification, using a 95% threshold for peptides ,1% false protein discovery rate, and a minimum of 2 peptides per protein (version 4.11, Proteome Software). Quantitative proteomic information was provided by Quantitative Scaffold Analysis.

2.1.2 *Cell culture and viability assay*

HepG2 cells were cultured at 37°C and 5% CO_2 in a humidified atmosphere using DMEM (Sigma), supplemented with 10% Fetal Bovine Serum (Sigma) and antibiotics (100 U/mL penicillin and 100 µg/mL streptomycin; Sigma). Cell viability tests were performed by exclusion test with trypan blue (Strober, 2015). Cells were seeded at a density of 5500 cells/well in 96-well plates and, after overnight adhesion, incubated for 24 h either with DMEM alone for control conditions, or with GLE, RE or BLE at different concentrations in a range between 10 and 100 µg dry extract/mL. In each experimental condition a cell viability ratio was calculated as the ratio between treated cells and controls; the IC_{50} (half maximal inhibitory concentration) for GLE and RE was evaluated using the CompuSyn software (Chou et al., 2004). In parallel, HepG2 cells were co-exposed to 1nM rapamycin (macrolide antibiotic that actives autophagy (Librizzi et al., 2012) and IC_{50} of GLE or RE and subjected to trypan blue exclusion tests.

2.1.3 *Clonogenic assay*

The clonogenic assay was performed according to Ramos et al. (2005). HepG2 cells were seeded and treated for 24 h with either extract at their IC_{50}. At the end of the treatment, the cells were trypsinizated and seeded in 6-wells plates at a density of 200 cells/well with fresh medium. After an incubation of 10 days at 37°C and 5%CO_2 the colonies were stained with crystal violet and counted. The obtained data were used to determine the plating efficiencies (PE) and surviving fraction (SF), as follows :

$$PE = \text{number of colonies counted/number of cells plated}$$

$$SF = PE \text{ of exposed cells/PE of control} \times 100$$

2.1.4 *Wound-healing assay*

The wound healing assay was performed as described in Luparello et al. (2022a, b). HepG2 cells were seeded in 6-well plates (88.000 cells/well) and after the confluence was reached the monolayer wasscraped with a 200 µL pipette tip. Culture media were replaced with DMEM alone (control) or with medium containing GLE or RE at their IC_{50}. Selected wound sites were photographed with a phase-contrast microscope at different time points within 24

hours from the start of the experiment. Finally, wound areas were quantified by ImageJ/Fiji and reported as mean area %+/- s.e.m.

2.1.5 *Flow Cytometry Assays*

For these assays, cells were seeded in 6-well plates at a density of 88.000 cells/well, incubated for 24 h to allow for adhesion and for further 24 h with GLE or RE at their IC_{50} or in control conditions. Experiments were performed in triplicate (Luparello et al., 2019a; 2019 b; Luparello et al., 2022a; 2022b;), using a FACSCanto flow cytometer (BD Biosciences, Franklin Lakes, NJ, USA) and taking into account 10,000 events for the evaluation. Results were analyzed with Floreada, an online tool available at https://floreada.io/. Cell debris, which had low FSC values, were excluded from the analysis by gating in the FSC *vs.* SSC plot ; additionally duplicates and cell multiplets were excluded from any cell cycle analysis by gating in the FSC-H *vs*. FSC-A plot.

2.1.5.1 *Cell-cycle Analysis*

For the analysis of the distribution of cells in the different phases of the cell cycle treated and control cells were fixed with cold 70% ethanol, incubated with 40 µg /mL RNase A and stained with 20 µg/mL propidium iodide.

2.1.5.2 *Apoptosis Assay*

Phosphatidylserine externalization, representative of apoptosis induction, was assessed in control and treated cells with the Annexin V-FITC kit (Canvax Biotech, Cordoba, Spain) using recombinant annexin-V conjugated to the green fluorescent FITC dye in conjunction with propidium iodide (PI) to discriminate viable, early-apoptotic, late-apoptotic, or necrotic cells.

2.1.5.3 *Analysis of Mitochondrial Transmembrane Potential (MMP)*

The MMP was analyzed with the JC-10 Mitochondrial Membrane Potential Assay kit (Abcam, Cambridge, UK) using the cationic lipophilic JC-10 dye, a ratiometric fluorescent indicator sensitive to modifications of MMP. In intact cells, JC-10 aggregates in the

mitochondrial matrix and its fluorescence emission shifts from green (520 nm) to red (570 nm). Conversely, in the case of MMP dissipation, it remains monomeric in the cytosol emitting green fluorescence. A positive control, obtained by incubating the cells with 1 µM valinomycin, a K+ ionophore that dissipates MMP, was assayed in parallel.

2.1.5.4 *Reactive Oxygen Species (ROS) Detection*

The intracellular level of ROS in control and treated cells was analyzed with the ROS Detection Assay kit (Canvax Biotech), monitoring the extent of deacetylation and oxidation of the probe 2,7 dichlorodihydrofluorescein diacetate in the fluorescent 2,7 dichlorodihydrofluorescein species, following the manufacturer's instructions.

2.1.5.5 *Acidic Vesicular Organelles (AVO)' Accumulation Analysis*

AVO's accumulation was assessed by fixing treated and control cells with cold 70% ethanol and staining with 100 µg acridine orange/mL (Sigma) for 20 min in the dark.

2.1.6 *Caspase Activity Assay*

Caspase activity was assessed using the Caspase Family Colorimetric Substrate kit II Plus (Abcam) in cells seeded in 6-well plates at a concentration of 88,000 cells/plate and incubated for 24 h in control conditions or exposed to GLE or RE at their IC_{50}.

2.1.7 *Cell Lysates and Western Blot*

Total protein samples were obtained from treated and control HepG2 cells by incubation in a lysis buffer (7 M Urea, 2% CHAPS, and 10 mM DTT) containing a protease inhibitor cocktail (Sigma) (Chiarelli et al., 2021). Separation of protein samples (25 µg) was carried out by 13% SDS-polyacrylamide gel electrophoresis and after the transfer on nitrocellulose membranes they were incubated with the primary antibodies overnight at 4°C. The antibodies used were rabbit anti-p62/SQSTM1 (P0068, Sigma; working dilution 1:500), rabbit anti-Beclin-1 (SC-11427, Santa Cruz Biotechnology, Delaware, CA, USA; working dilution 1:500), rabbit anti-LC3 (L8918, Sigma; working dilution 1:1000), mouse anti-HSP60 (H3524, Sigma; working dilution 1:500), and rabbit anti-actin (Ab8227, Abcam;

working dilution 1:1000). After membrane washing the membranes were incubated with peroxidase-conjugated anti-mouse or anti-rabbit secondary antibodies (W4021 and W4011, Promega Corporation, Madison, WI, USA) at room temperature for 1 h. The Molecular imager Versadoc MP imaging System (Bio-Rad, Hercules, CA, USA) was used to visualize the protein bands after staining with the Immun StarTM WesternCTM chemiluminescent kit (Bio-Rad). Finally, the bands' quantitative analysis was performed using Quantity One v.4.6.6 software (Bio-Rad), referring to actin band intensity as the loading control.

2.1.8 *RNA extraction, Reverse Transcription and qRT-PCR*

Total RNA samples were extracted from cells cultured and grown in 25 cm^2 flasks and then incubated for 24 h in control conditions or exposed to either GLE or RE at their IC_{50}, using the PureLink RNA Mini kit (ThermoFisher, Waltham, MA, USA) with on-column DNase treatment (PureLink DNase set, ThermoFisher). Bleach gel electrophoresis (Aranda et al., 2012) was used to evaluate the quality and the integrity of the RNAs which were quantitated spectrophotometrically. The cDNAs were synthesized from 250 ng of total RNA using 10 U of Transcriptor reverse transcriptase (Roche, Manheim, Germany) and random hexamer primers; their quality was checked through PCR amplification in the presence of 1 U/µL of Taq DNA polymerase (TAQ-RO, Roche) and the forward and reverse primers for β-actin. Gene expression levels of *BAD, BAX*, *BCL2*, *JUN* and *FOS* were investigated through qRT-PCR using the SYBR-Green method, the specific sets of primers listed in Table 1, and an Applied Biosystems 7500 Real-Time PCR system. The 25 µL PCR mixtures were prepared with 2 µL of cDNA, 300 nM primers (forward and reverse) and 12.5 µL of Power SYBR-Green PCR MasterMix (Applied Biosystems, Waltham, MA, USA). The sample quantification was obtained using the $2^{-\Delta\Delta Ct}$ method; the normalization was performed to β-actin and the relative expression levels were evaluated calculating the ratio between the normalized value of the target gene in each treated experimental conditions and that in control condition.

Gene (Primer)	Sequence (5′→3′)	Reference
BAD (Forward)	GTTCCAGATCCCAGAGTTTGAGC	(Luparello et al., 2008)
BAD (Reverse)	TTAAAGGAGTCCACAAACTCGTCACT	
BAX (Forward)	ATGGACGGTCCGGGGAGCAGC	(Luparello et al., 2008)
BAX (Reverse)	CCCCAGTTGAAGTTGCCGTCAG	

BCL2 (Forward)	GCCTTTGTGGAACTGTACGGC	(Luparello et al., 2008)
BCL2 (Reverse)	GGCAGTAAATAGCTGATTCGACGTT	
DAPK (Forward)	GATGGCAACATGCCTATCGTG	(Luparello et al., 2008)
DAPK (Reverse)	GATGAAGAGTCCTCGGTGCGTAT	
JUN (Forward)	CCCCAAGATCCTGAAACAGA	(Luparello et al., 2012)
JUN (Reverse)	CCGTTGCTGGACTGGATTAT	
FOS (Forward)	CCAACTTTATCCCCACGGTGAC	(Ronchetti et al., 2013)
FOS (Reverse)	TGGCAATCTCGGTCTGCAAC	
ACTB (Forward)	GGAAGGTGGACAGCGAGGCC	(Li et al., 2014)
ACTB (Reverse)	GTGACGTGGACATCCGCAAAG	

Table 1. Primers used for PCR amplification.

2.2 STATISTICS

The normality tests were performed by SigmaPlot 11.0 software (SYSTAT, San Jose, CA, USA). For Western blot experiments, data were analyzed by unpaired two-tailed Student's t-test with GraphPad Prism 9 software (GraphPad, San Diego, CA, USA).

2.3 RESULTS

2.3.1 *Effects of P.oceanica's extracts on short-term viability and long-term proliferative potential of HepG2 cells*

The cytotoxic effects of GLE, BLE and RE were evaluated through the trypan blue exclusion assay and, in case of dose-dependent viability inhibition, the IC_{50} was determined. Cell exposure for 24 h to GLE and RE exerted a concentration-dependent decrease in cell viability, whereas treatment with BLE at all concentrations was ineffective at modifying cell viability. For this reason the latter preparation was excluded from the subsequent analyses. On the basis of the results obtained in the dose-response assays, 83 and 11.5 µg of dry extract /mL were the estimated IC_{50} for GLE and RE, respectively, and they were used in all the following experiments.

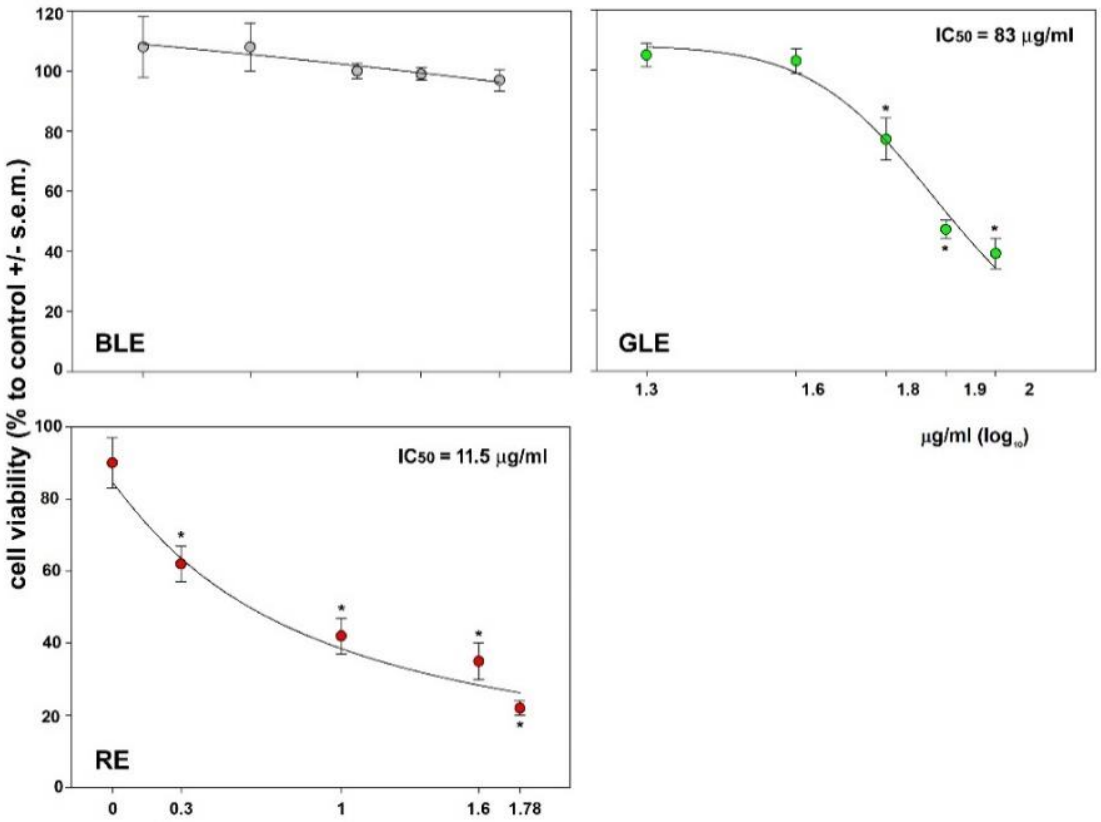

Figure 3. Representative graphs of cell viability rates following exposure of HepG2 cells to different concentrations of GLE, BLE and RE (mean ± s.e.m of three independent experiments).

In a second set of assays, the clonogenic assay (also known as colony formation assay) was performed to investigate the ability of the cells to continue proliferating or, conversely, to undergo to reproductive death after treatments with GLE or RE. To this purpose, we evaluated the long-term ability of individual cells to give rise to colonies of at least 50 individuals after 24 hours of exposure to the IC_{50} of the extracts (Franken et al., 2006). Representative micrographs of the stained colonies and the PE and SF values under both experimental conditions, obtained from colony counting in triplicate experiments, are shown in Figure 4.

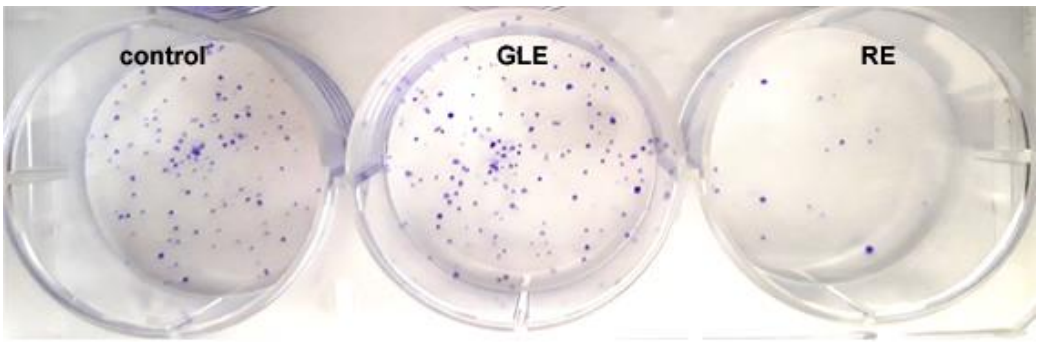

	control	GLE	RE
PE	0.46 +/- 0.08	0.47 +/- 0.03	0.08 +/- 0.01
SF		1.03 +/- 0.07	0.17 +/- 0.03

Figure 4. Representative images of clonogenic assays of HepG2 cells under control conditions or exposed to the IC_{50} of GLE or RE for 10 days. The corresponding plating efficiencies (PE) and surviving fractions (SF) are shown in the attached table (mean ± s.e.m. of three independent experiments).

The obtained results indicate that, unlike to the exposure of cells to GLE which was ineffective in modifying cell behavior, the exposure to RE resulted in a significant reduction of cells' replicating capacity, down to about 16% of that of the untreated control, thus suggesting the occurrence of phenotypic effects that could be distributed over time and develop after a certain number of cell divisions.

2.3.2 *Effects of P.oceanica's extracts on cell-cycle status and apoptosis induction in HepG2 cells*

In the light of the observed reduction in cell viability following short-term treatment with the extracts, we evaluated the distribution of HepG2 cells along cell cycle phases under control conditions and after 2 and 24 hours of exposure to GLE or RE. As shown in Figure 5, the treatment of cells for 2 hours produced no significant change in the percentage of the cell populations in the cycle phases. In contrast, after 24 h of exposure we detected a shared accumulation of cells in the sub-G_0/G_1 phase (more pronounced in the case of GLE exposure) and a decrease in the percentage of cells in the other stages, with the exception of RE-treated cells at the G_2/M stage, whose amount remained significant and comparable to that of controls. This suggests that, unlike the generalized cell damage induced by RE that extends to the entire cycle, treatment with GLE could result in a sustained impairment of the DNA checkpoint in G_2, with a consequent arrest of cycle progress at G_2/M, an event that commonly precedes HepG2 cells' apoptosis (Chao et al., 2014; Li et al., 2019). We next

examined whether the observed alteration of the cell cycle and the increase in the proportion of sub-G_0/G_1 hypodiploid cells could be, at least in part, attributed to an apoptosis-promoting effect of the extracts on HepG2 cells. Cultures grown under control conditions or exposed to GLE or RE for 14 or 24 h were analyzed for phosphatidylserine externalization in combination with PI staining; the data obtained are shown in Figure 6 and indicate that, at an early stage of exposure (14 h), the percentage of the viable annexin-V-/PI cells was reduced from about 89% of controls to about 72% after both treatments. On the other hand, the percentage of early apoptotic cells (annexin-V+/PI-) increased from about 9% of the controls to about 25%. As expected, after 24 hours of exposure the number of viable cells was drastically reduced by about 6 (for GLE) and 8% (for RE), while the percentage of late apoptotic cells (annexin-V+/PI+) increased to about 92% (for GLE) and 89% (for RE) of the population. This result is consistent with flow cytometry data on the observed accumulation of cells in the sub-G_0/G_1 fraction after 24 h of exposure to the extracts. No significant difference was found for the necrotic cell populations, i.e., annexin-V-/PI+, under the investigated experimental conditions.

Real-time PCR analyses were performed to detect the changes in *BCL-2*, *BAX*, *BAD*, *FOS,* and *JUN* mRNA trascription at 4 and 14 hours of exposure to GLE and RE (Figure 7). As suggested by Golestani Eimani et al. (2014), since the balance between anti-apoptotic members (Bcl-2) and pro-apoptotic members (Bax and Bad) of the Bcl-2 family (Kale et al., 2018) is a better indicator of apoptosis sensitivity, we focused on Bcl-2/Bax and Bcl-2/Bad expression ratios instead of individual expression patterns. Under the experimental conditions used, the >1 ratios found with both extracts after 4 h of treatment decreased after 14 h of culture, more drastically in the presence of GLE. In particular, the Bcl-2/Bax ratio decreased from 1.71 to 0.44 with GLE and from 2.04 to 1.19 with RE, while the Bcl-2/Bad ratio decreased from 2.49 to 0.35 with GLE and from 3.52 to 1.19 with RE. It is generally recognized that the products of the immediate early genes *FOS* and *JUN*, which are involved in the formation of the transcription factor AP-1, control various cellular functions, including apoptosis (Singh & Czaja, 2007). In particular, the decreased level of *FOS* expression was found to be associated with cell death induced by suppression of the expression of Cyclin D1 and G_0/G_1 arrest in colorectal cancer cells and also with c-Jun/ATF2-mediated neuronal apoptosis, while the increase of *JUN* trancription level was responsible for caspase activation and apoptosis induction in myeloma cells (Podar et al., 2007; Yuan et al., 2009; Gao et al., 2020). Regarding HepG2 cells, it has been shown that overexpression of *JUN* down-regulates cyclin A2, thus leading to G_1 arrest (Yang et al., 2013). In liver tissue, the decline in the expression of *FOS* with sustained high levels of *JUN* expression is an hallmark of

irreversible damage and correlates with the onset of programmed hepatocellular death (Schlossberg et al., 1996). As displayed in the figure, and in line with the cited reports, the up-regulation of *JUN* and concomitant down-regulation of *FOS* were detected at the beginning and end of exposure to both extracts.

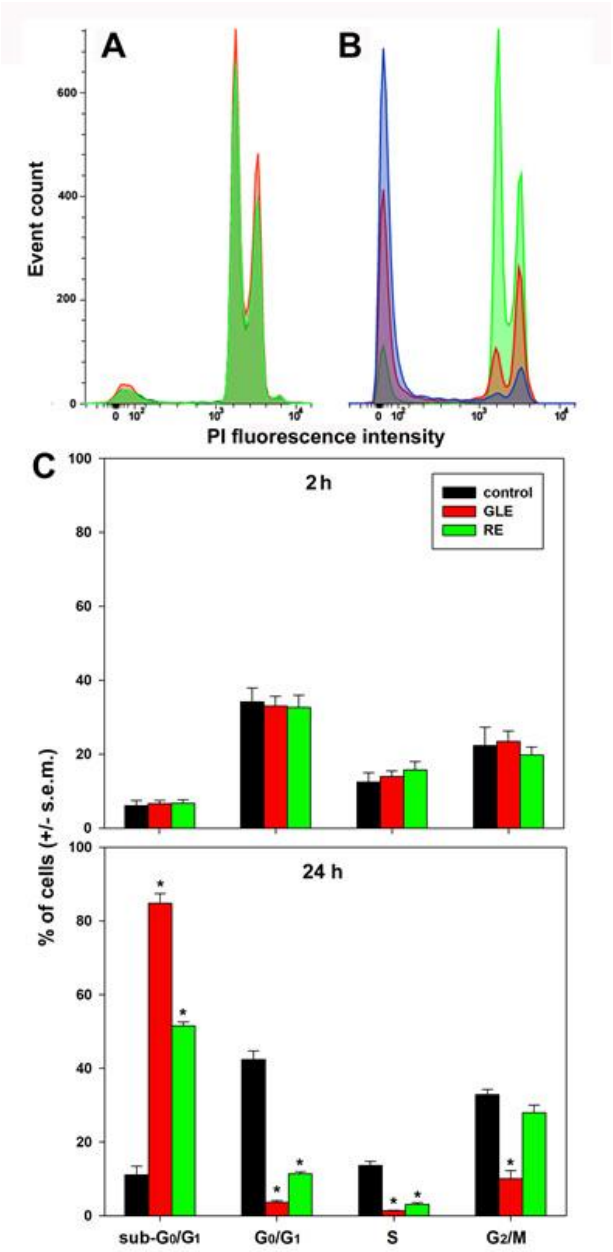

Figure 5. Representative DNA profiles of control (green), GLE (blue), and RE-treated (red) HepG2 cells after 2 (A) and 24 h (B) of exposure. (C) Bar graphs show the effect of GLE and RE on the cell-cycle distribution of HepG2 cells after 2 and 24 h of treatment compared with controls. The error bars indicate the standard error of the mean (s.e.m.) of three independent measurements. * normality test *vs*. control passed.

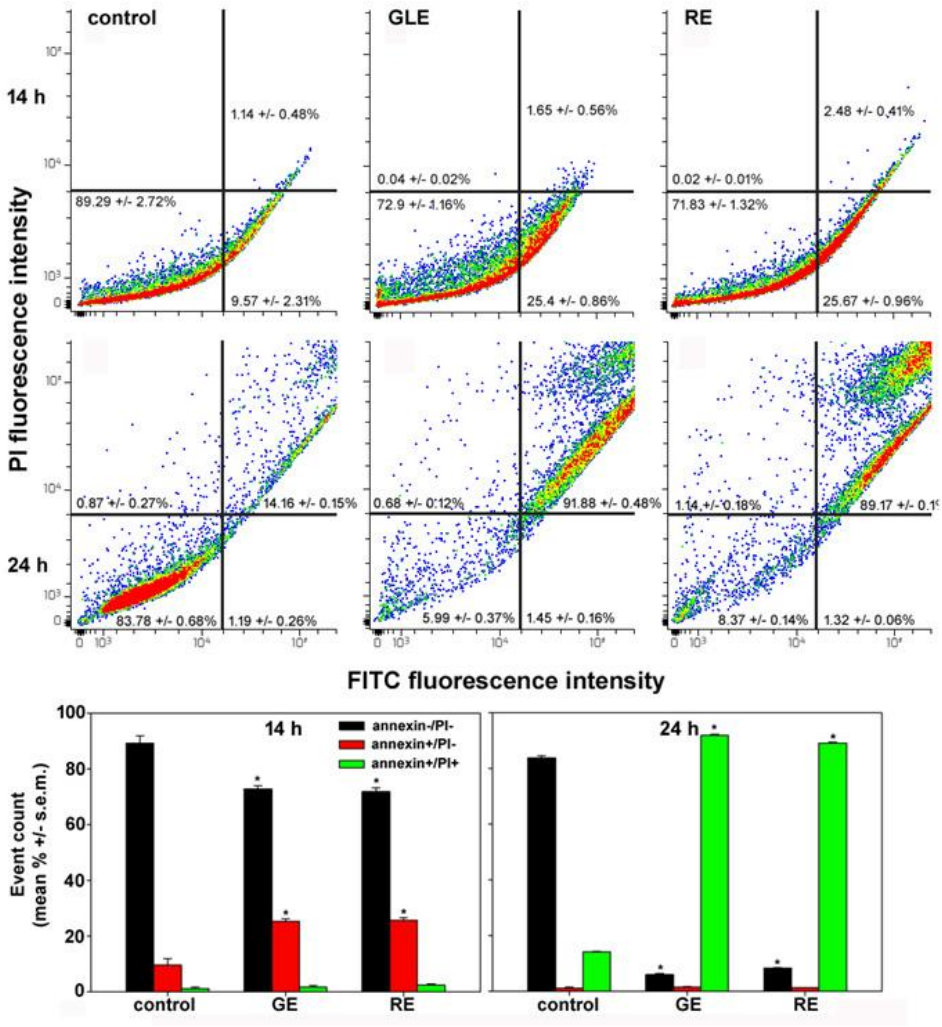

Figure 6. (A) Flow cytometry assays for apoptosis in HepG2 cells cultured under control conditions or exposed to IC_{50} of GLE or RE for 14 or 24 hours. The graphs show the results of representative experiments, and the percentages, shown as mean ± s.e.m. of three independent assays, refer to viable annexin-V-/PI- cells (lower left quadrant), early apoptotic annexin-V+/PI- cells (lower right quadrant), late apoptotic annexin-V+/PI+ cells (upper right quadrant) and necrotic annexin-V-/PI+ cells (upper left quadrant). (B) Bar graphs summarize the data for live, early apoptotic and late apoptotic control and treated cells from triplicate experiments. * normality test *vs*. control passed.

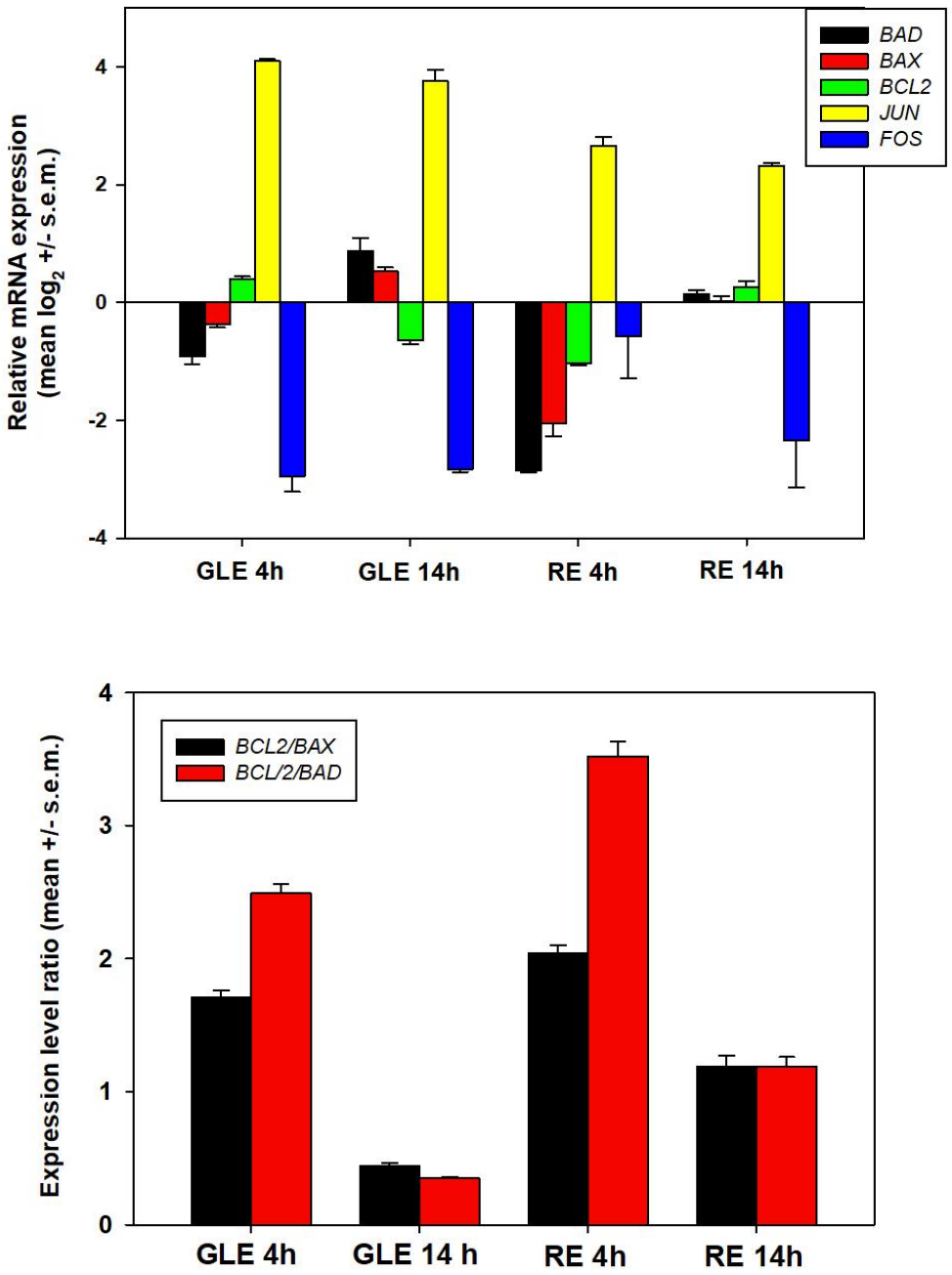

Figure 7. (Upper graph) Real-time PCR analysis of expression of *BAD*, *BAX*, *BCL2*, *JUN* and *FOS* in HepG2 cells cultured under control conditions or exposed to the IC_{50} of GLE or RE for 4 and 14 hours. Gene expression values are normalized to *ACTB*. (Lower graph) Expression ratios of *BCL2*/*BAX* and *BCL2*/*BAD* in HepG2 cells exposed to the IC_{50} of GLE or RE for 4 and 14 hours. Error bars indicate the standard error of the mean (s.e.m.) of three independent measurements. All data passed the normality test compared with the control.

In addition, to obtain more details about the activation of specific caspases following exposures, we submitted control and treated cell lysates to spectrophotometric

measurements in the presence of p-NA-conjugated substrates for caspases 1 to -6 and -8 to -9. Figure 8 shows that exposure to both extracts resulted in the activation of caspases-1, -2 and -6, whereas, in the presence of GLE alone, the additional and prominent activation of caspase-3 was observed. No statistically significant results were obtained for caspases 4, -5, -8 and -9.

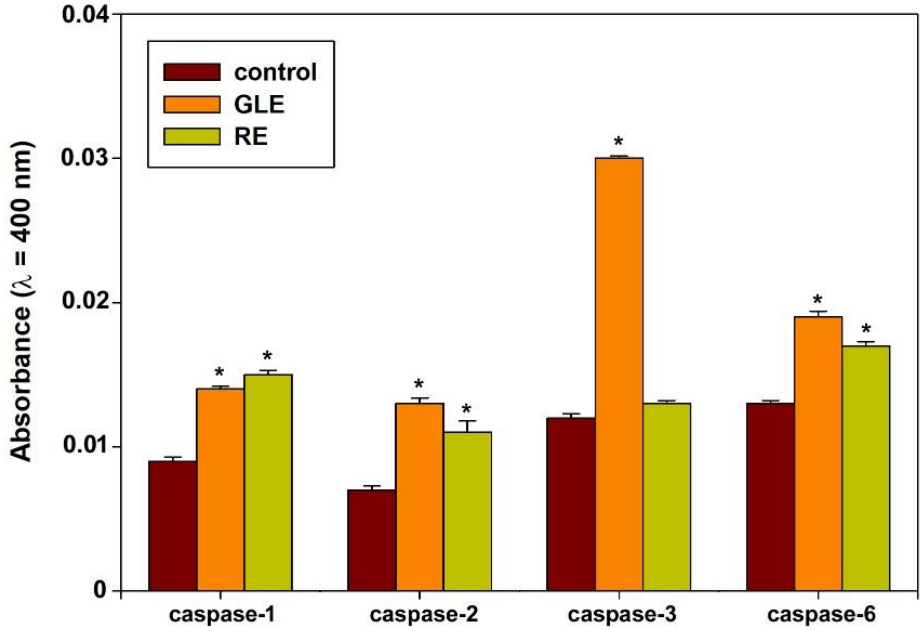

Figure 8. Determination of caspase activity in HepG2 cells cultured under control conditions or exposed to the IC_{50} of GLE or RE for 24 hours. The error bars indicate the standard error of the mean (s.e.m.) of three independent measurements. * normality test *vs*. Control passed.

2.3.3 *Effects of P.oceanica's extracts on mitochondrial membrane polarization and redox status in HepG2 cells*

We examined whether cell exposure to GLE or RE could affect mitochondrial function by examining the status of MMPs with the lipophilic cationic dye JC10. To this purpose, we assessed the percentage of cells with either intense red or bright green/dim red fluorescence (indicative of intact or collapsed MMPs, respectively) after 4, 14, and 24 hours. Figure 9 shows that, differently from GLE, treatment with RE resulted in the gradual increase of the cell population exhibiting mitochondrial depolarization. Specifically, in the three time intervals considered, the cells emitting dim red light increased from about 31, 31 and 28% of the controls to about 57, 61 and 78%, respectively. However, in no experimental condition,

the obtained values increased to the levels of the valinomycin-treated positive controls (98-99%), indicating the persistence of a subpopulation of HepG2 cells with intact mitochondrial functions. It is known that mitochondria are the main source of intracellular ROS, although these can also be produced by other intracellular components, such as endoplasmic reticulum-bound enzymes (Auten & Davis, 2009; Zaidieh et al., 2019). On the other hand, HepG2 cells represent a useful model for examining ROS production mainly from mitochondrial sources, since cytochrome P450 family 2 subfamily E member 1 (CYP2E1), an endoplasmic reticulum ROS-generating enzyme, is poorly expressed in the cell line (Jiang et al., 2015). The accumulation of different types of ROS (hydrogen peroxide, peroxynitrite, hydroxyl radicals, nitric oxide and peroxy radicals) after 4 and 24 hours of exposure to GLE or RE was examined by flow cytometry. As reported for other experimental models (Belyaeva et al., 2008; Kenny et al., 2019; Luparello et al., 2022a;2022b), under each condition studied, two distinct cell subpopulations endowed with low (ROS-) and high rates (ROS+) of ROS generation were detected. The mean fluorescence intensity (MFI) values of the events associated with ROS+ subpopulations, as well as the overall proportion of ROS+ cells within the entire populations, were calculated and reported in Figure 10. A reduction in ROS generation could be observed already after 4 h of incubation with both extracts, with an average decrease of 69% (for GLE) and 57% (for RE) in exposed cells compared with controls, respectively (mean MFI of control cells = 11,989, mean MFI of GLE-treated cells = 3831, mean MFI of RE-treated cells = 5184; $p < 0.05$). The reduction in the amount of ROS was reversed after 24 h of treatment with RE alone (mean MFI of control cells = 6710, mean MFI of treated cells = 6465; no statistical significance), while the level of ROS produced in HepG2 cells treated with GLE remained lower, although slightly (58%), than that of control cells (Mean MFI of control cells = 6710, mean MFI of treated cells = 2821; $p < 0.05$). In addition, the proportions of ROS+ subpopulations of treated cells were always lower than those of controls and decreased over the time interval studied, accounting for about 19% (at 4 h) and 2% (at 24 h) with GLE and about 47% (at 4 h) and 14% (at 24 h) with RE, as predicted by the progressive cell impairment and death.

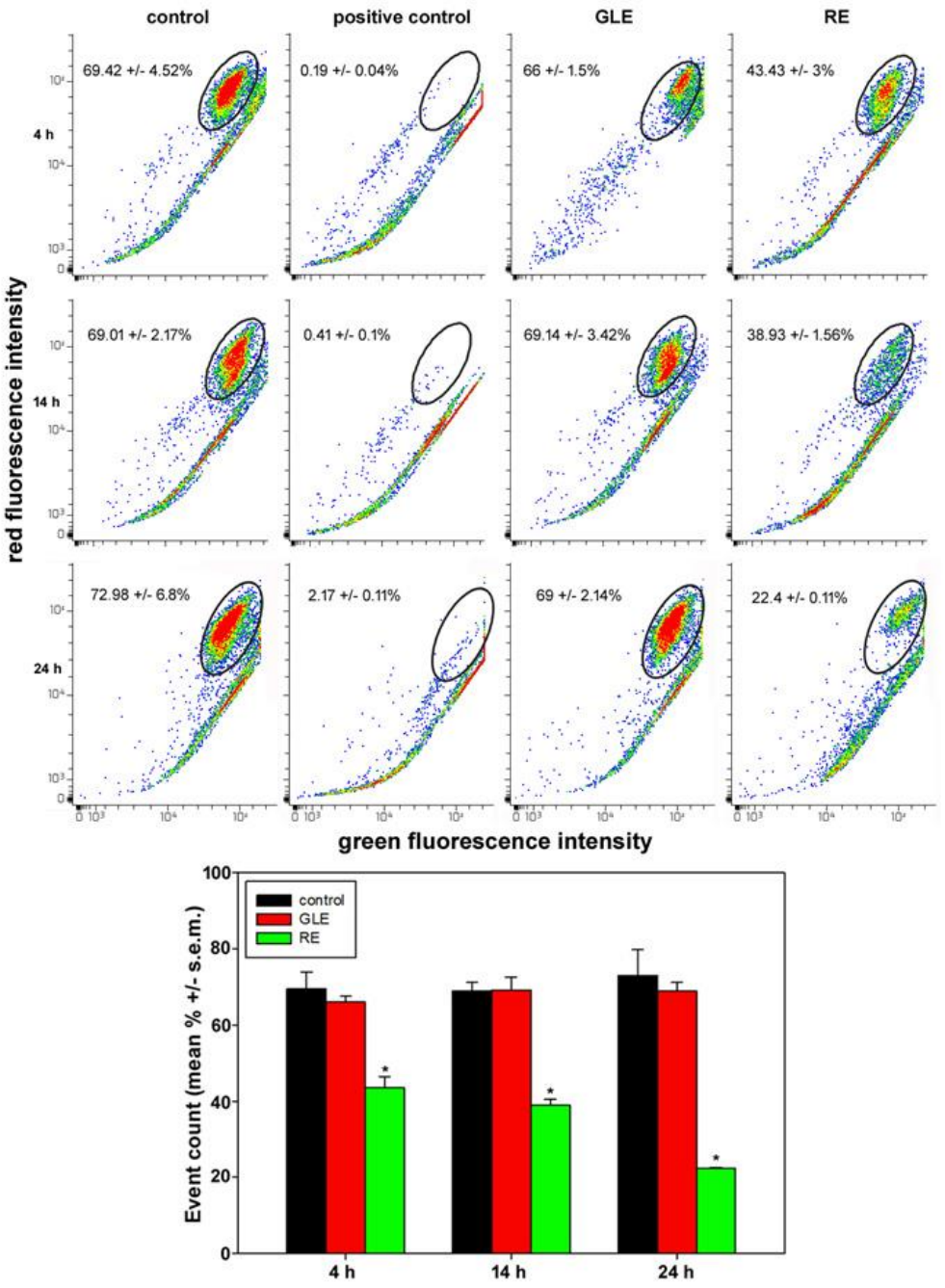

Figure 9. (Upper panel) flow cytometric assays for MMP in HepG2 cells cultured for 4, 14 and 24 under control conditions or exposed to 1 μM valinomycin (positive control) or the IC_{50} of GLE or RE. The graphs show the results of representative experiments, and the percentages in each box, shown as mean ± s.e.m. of three independent assays, refer to the intense red-emitting cells with intact MMP in the gated area. (Lower image) bar graph summarizing data for control and treated cells with intact MMP obtained from triplicate experiments. * normality test *vs*. control passed.

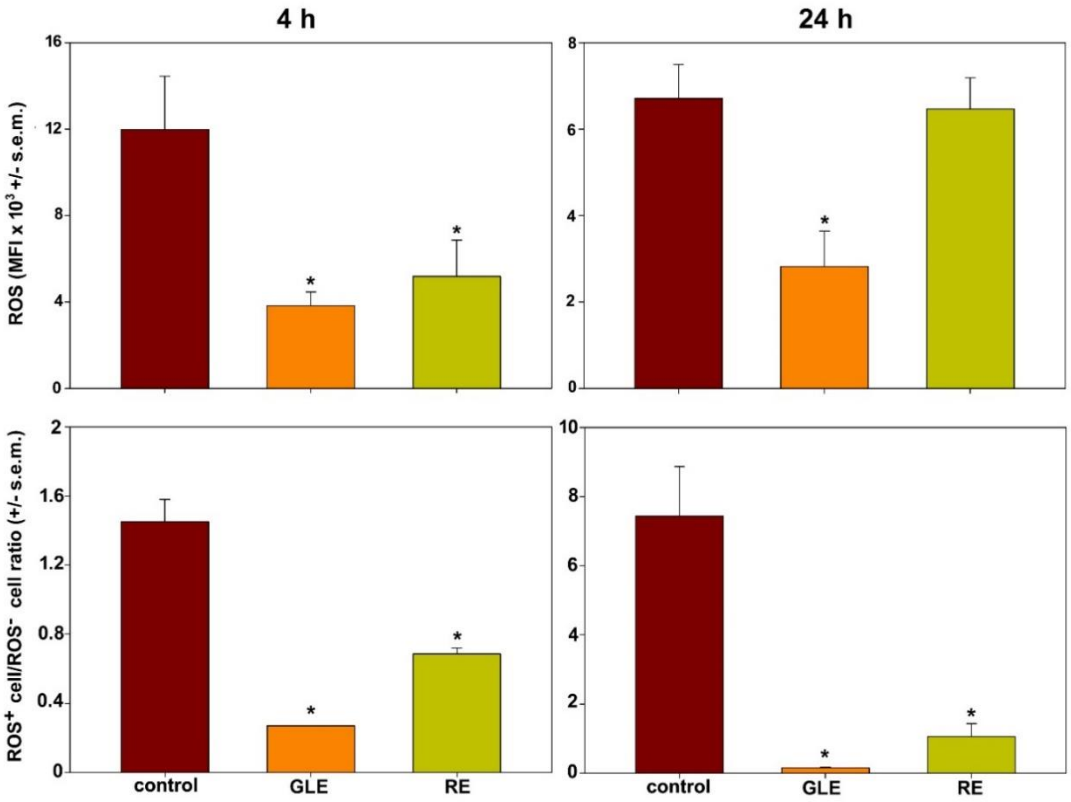

Figure 10. Histograms showing ROS-associated MFI in ROS+ subpopulations (upper graphs) and ROS+ cell/ROScell ratio (lower graphs) of HepG2 cells grown under control conditions or exposed to the IC_{50} of GLE or RE for 4 and 24 hours. The error bars indicate the standard error of the mean (s.e.m.) of three independent measurements. * normality test *vs*. control passed.

2.3.4 *Effects of P.oceanica's extracts on HepG2 cells' autophagic activity*

We then examined whether the extracts could affect the autophagic flux of HepG2 cells by analyzing in parallel the accumulation of AVO and the intracellular presence of LC3, Beclin-1, p62/SQSTM1 and hsp60 protein markers at early (4 h), intermediate (14 h) and late (24 h) stages of exposure. LC3 protein is recognized to be anchored in the membrane of the autophagosome after conversion of LC3-I (cytoplasmic form) to LC3-II (autophagosome membrane-associated form). Beclin-1 is known to regulate autophagy, being an essential effector that plays important roles in the crosstalk with the apoptosis pathway. The dissociation of Beclin-1 from Bcl-2 is essential for its autophagic activity. Unlike LC3, which is a marker of final autophagosome formation, Beclin-1 participates in the early stages of autophagy, promoting the nucleation of the autophagic vesicle and recruiting proteins from the cytosol. P62/SQSTM1 protein is commonly found in the inclusion bodies containing polyubiquinated protein and provides important protein information on proteins

destined for autophagic degradation. Finally, considering the involvement of polyubiquitinated proteins destined for autophagic degradation as indicated by the p62/SQSTM1 protein, we investigated the amount of hsp60, an indicator of cyto-protection, being a component of the machinery for proper protein folding. (Decuypere et al., 2012; Klionsky et al., 2021a; Pace et al., 2013). In addition, the expression levels of the *DAPK* gene were monitored at the early and at intermediate stages by qRT- PCR. In fact, it is well known that the expression of DAPK in various cell lines, also in HepG2 cells, leads to the increased formation, trafficking and fusion of autophagosomes and also to the increased levels of Beclin-1, thus being considered a potent and unique inducer of the autophagic process (Farag & Roh, 2019; P. Singh et al., 2016). As shown in Figure 11, two distinct cell subpopulations showing low AVO- and high rate (AVO+) of acridine orange fluorescence were highlighted in the plot analyses. It's recognized that HepG2 cells are endowed with a high basal level of autophagy (Luparello et al. 2022a; 2022b) and, as a result, the percentage of AVO+ cells was found to be about 90, 84 and 71% at 4, 14 and 24 h of culture in untreated cells. Following exposure to the IC_{50} of GLE or RE, two different results were obtained. In fact, in the first experimental condition, the percentage of AVO+ cells after 4 h decreased to about 48%, and the extension of the exposure time to 14 and 24 h did not cause a further reduction in AVO+ cells (about 47% after 14 h; about 44% after 24 h); in contrast, exposure to RE resulted in the almost complete disappearance of the fraction of AVO+ cells, whose amount decreased to about 68, 50 and 4% of the total population after 4, 14 and 24 hours of treatment. The Western Blot results on the expression levels of autophagy- and cytoprotection-related proteins are shown in Figure 12. We investigated the LC3-II/LC3-I ratio to monitor the level of autophagic flux during the relative exposure times. After 4 hours, an initial up-regulation of the ratio was observed after both exposures, with an approximately 1.8- and 2.2-fold increase for GLE- and RE-treated cells, respectively, compared with controls, followed by an approximately 0.1- and 0.2-fold decrease at 14 hours from the start of exposure. After 24 hours, a further slight decrease in the ratios was observed in both experimental conditions (GLE-treated cells = approximately 0.1-fold ; RE-treated cells = approximately 0.2-fold). Concerning Beclin-1, after 4 h of GLE treatment, its level was found to be about 0.8-fold lower than in the control ; in contrast, a comparable level of Beclin-1 was found in the presence of RE.

After 14 hours, however, Beclin-1 was down-regulated in both treated samples, although to different degrees and more pronouncedly in RE-treated cells (about 0.4-fold). The same trend was also observed after 24 hours in both experimental conditions. After 4 hours of treatment, the level of p62/SQSTM1 increased of about 0.3-fold in GLE-treated cells

compared with the untreated sample, while in the RE-treated cells it was comparable to that of the control. Similarly, after 14 hours, a time during which physiologically control cells express high levels of p62/SQSTM1, its levels increased for GLE-treated cells (about 0.4-fold) and reduced for RE-treated cells (about 0.5-fold) with respect to control cells. This treatment period coincided, however, with the highest levels of p62/SQSTM1 in the whole experiment. After 24 hours, low levels of p62/SQSTM1 were detected in the controls compared with treated samples, showing a larger increase in RE- cells (about 1.5-fold) than in GLE-treated cells (about 0.5-fold). In general, it is noteworthy that p62/SQSTM1 levels in RE-treated cells remained constantly low in the three times of exposure. Finally, concerning hsp60, its levels decreased after 4 hours of treatment compared with the control, more prominently in GLE-treated cells (about 0.4-fold). After 14 hours, the level of hsp60 was elevated by about 0.2-fold compared with control only in the presence of GLE, while it remained comparable to control for RE-treated cells. After 24 hours, the level of hsp60 was reduced by about 0.9-fold in both treated conditions.

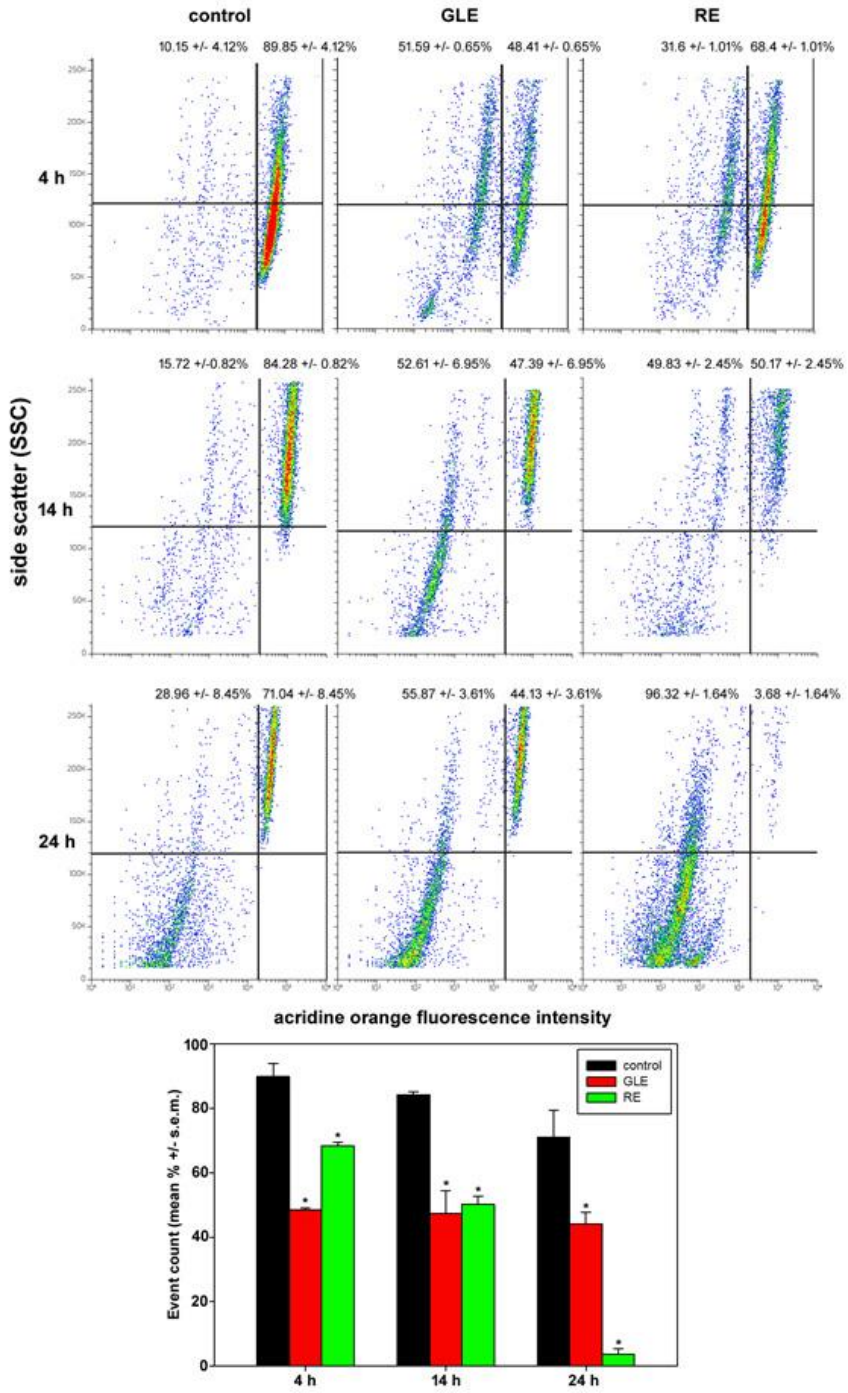

Figure 11. (Upper panel) flow cytometric assays for AVOs in HepG2 cells cultured under control conditions or exposed to the IC_{50} of GLE or RE for 4, 14 and 24 hours. The graphs show the results of representative experiments, and the percentages, shown as mean ± s.e.m. of three independent experiments, refer to AVO+ cells (right quadrants) and AVO- cells (left quadrants). (Lower image) bar graph summarizing the data for control and treated AVO+ cells obtained from triplicate experiments. * normality test *vs*. control passed.

As expected from the different extent of autophagy down-regulation indicated by flow cytometry and protein blot data, different patterns of *DAPK* expression were detected after

treatment with both preparations, confirming the previous results. In particular, an important decrease in its transcription rate was observed at 4 h of exposure in the presence of GLE and RE. Consistent with the gradual total disappearance of AVO+ cell population, the major down-regulation of *DAPK* remained stable within 14 h of RE treatment, while, consistent with the stabilization of AVO+ cells at values of about 50% of the total population, at 14 h of GLE exposure, the amount of DAPK mRNA returned to values slightly lower than those of control cells (Figure 13). Finally, the increased *C-JUN* transcription, which was reported in our experimental system, may be considered as a prelude to the inhibition of autophagy(Yogev et al., 2010). We next examined to what extent the inhibition of the autophagic process could be responsible for the observed cytotoxic effect after the exposure of HepG2 cells to GLE and RE. To this purpose, cells were co-incubated with the IC_{50} of GLE or RE and 1 nM of the autophagy stimulator rapamycin (sirolimus), which acts through inhibition of mTOR (mammalian target of rapamycin) serine/threonine kinase. As shown in Figure 14 the co-exposure was able to significantly reverse the decrease in cell number only in the presence of GLE ; in contrast, no significant effect was found after co-administration of RE and rapamycin, thus confirming the occurrence of more extensive and diffuse damage induced by exposure of HepG2 cells to this specific preparation.

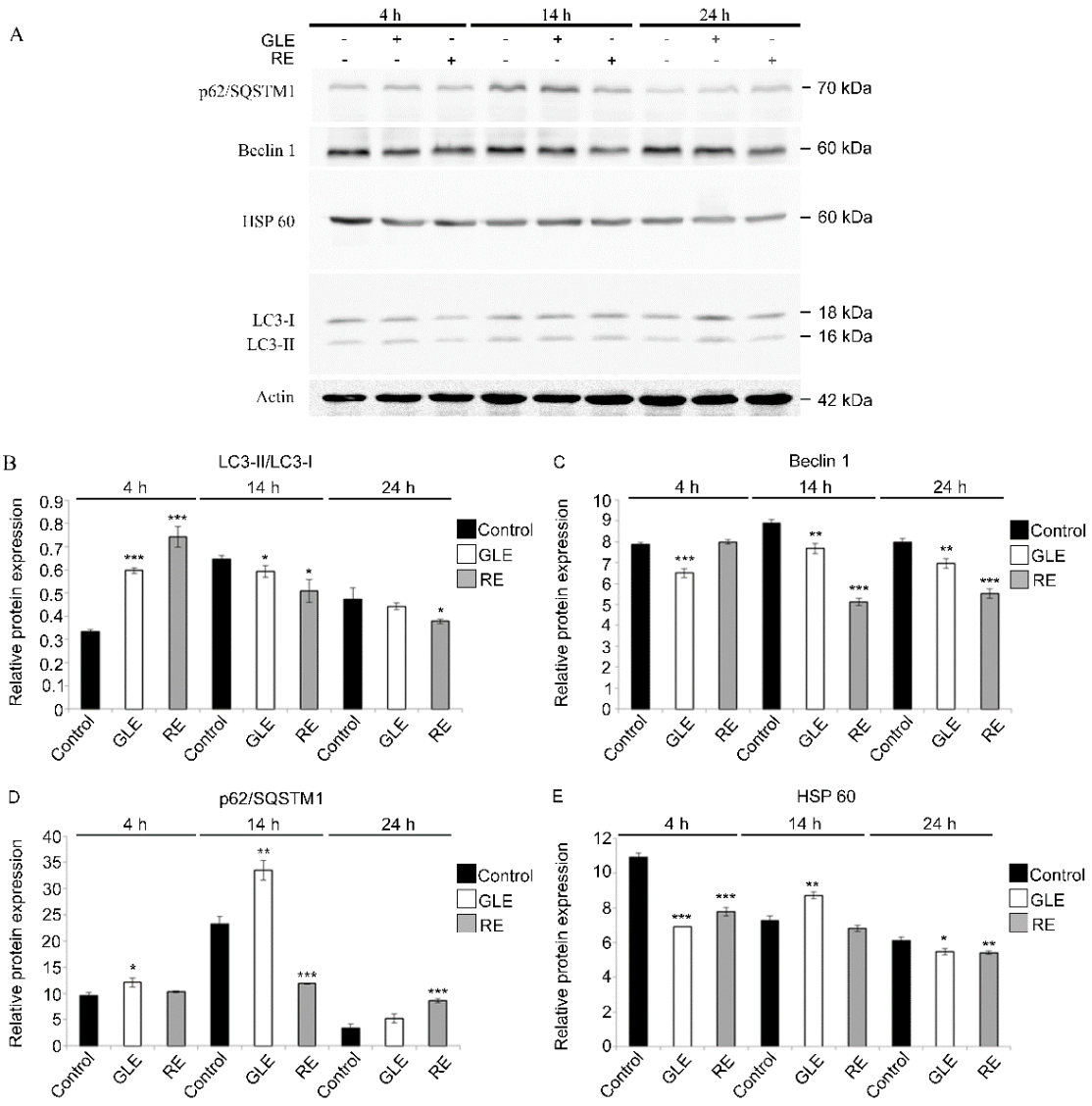

Figure 12. Immunoblotting and quantitative analysis. (A) Total lysates of control and GLE or RE-treated cells after 4 h, 14 h and 24 h exposure, immunoreacted with anti-p62/SQSTM1, - Beclin-1, -HSP 60, -LC3 and -actin antibodies. The histograms show the densitometric analysis of the bands obtained for (B) LC3-II/LC3-I ratio, (C) Beclin-1, (D) p62/SQSTM1, and (E) HSP 60. Actin was used as a loading control, and in C-E, relative protein expression, reported as arbitrary units, was calculated as the ratio of protein band density to actin band density. Experiments were performed in triplicate, and data are expressed as mean ± standard deviation (n = 3 ± SD). * $p \leq 0.05$; ** $p \leq 0.01$; *** $p \leq 0.005$ compared with control for each treatment time.

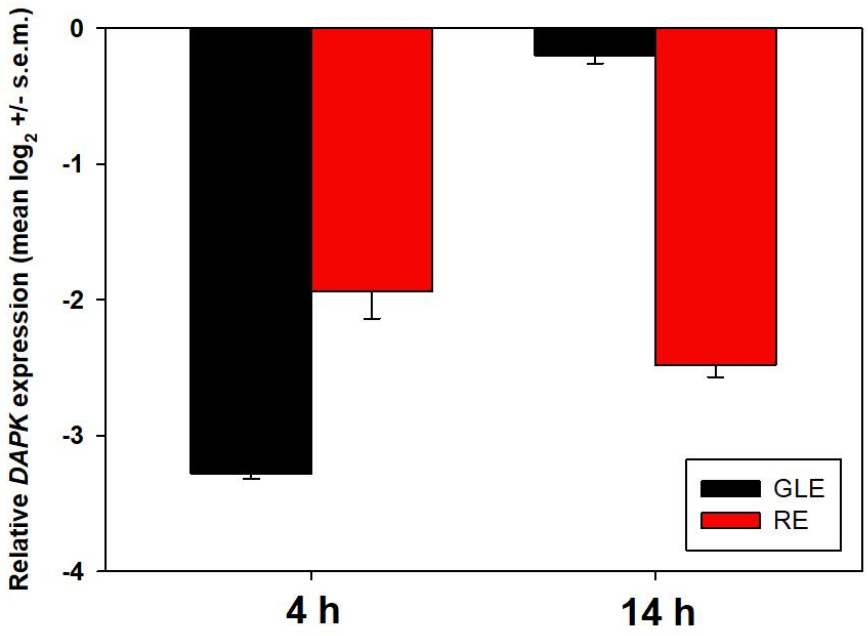

Figure 13. Real-time PCR analysis of *DAPK* expression in HepG2 cells cultured under control conditions or exposed to the IC_{50} of GLE or RE for 4 and 14 hours. Gene expression values are normalized to *ACTB*. The error bars indicate the standard error of the mean (s.e.m.) of three independent measurements. All data passed the normality test relative to the control.

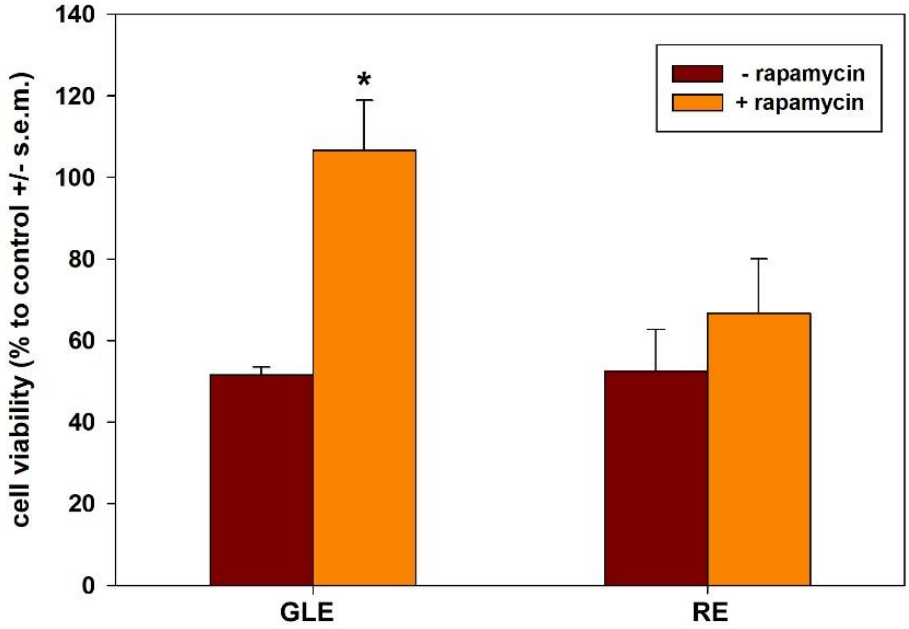

Figure 14. Histogram showing the effect exerted by co-treatment with 1 nM rapamycin on the decrease in HepG2 cell viability induced by GLE or RE after 24 hours of exposure. The error bars correspond to the standard error of the mean (s.e.m.) of three independent measurements. * normality test *vs*. control passed.

2.3.5 *Inhibition of the locomotory ability of HepG2 Cells exposed to P. oceanica's Extracts*

To examine the effect of incubation with the IC_{50} of GLE or RE on the locomotory ability of HepG2 cells, a wound healing assay was performed. It is known that, under control conditions, HepG2 cells show a motile attitude that allows them to drastically reduce the wounded area within 24 h. (Luparello et al., 2022 a; 2022b; Xie et al., 2017; Zheng et al., 2022). Consistent with these indications, the panel of micrographs in Figure 15 shows that untreated HepG2 cells were endowed with a locomotory ability, resulting in a progressive decrease in wounding (expressed as mean area % ± s.e.m): 37.5 ± 1.2 (0 h), 32.2 ± 0.1 (2 h), 27.4 ± 2.2 (4 h), 23.4 ± 1.1 (6 h) and 9.1 ± 1.7 (22 h) from the start of the experiment. Being not less than 24 h the doubling time of HepG2 cells (Desquiret et al., 2006; Furth et al., 1992), the effect observed at shorter times is not attributable to cell proliferation. On the other hand, the ability of HepG2 cells to migrate to the scratched area was inhibited by exposure to both extracts to different extents. Specifically, under both experimental conditions, the wound size was not changed within 6 h after scratching. The mean area % ± s.e.m. in the presence of GLE or RE was 37.8 ± 0.2 and 37.9 ± 0.9 (2 h), 37.5 ± 1.1 and 37.7 ± 1.2 (4 h), and 37.4 ± 1.2 and 37.7 ± 0.8 (6 h) from the start of the experiment, respectively. At 22 h after scratching, HepG2 cells cultured in the presence of GLE showed a moderate migratory attitude, resulting in the gap area reduction to 24 ± 0.6%, whereas, in the case of exposure to RE, the ability of cells to migrate into the denuded area appeared even lower and the wound size remained larger with an area of 31.8 ± 2.7%.

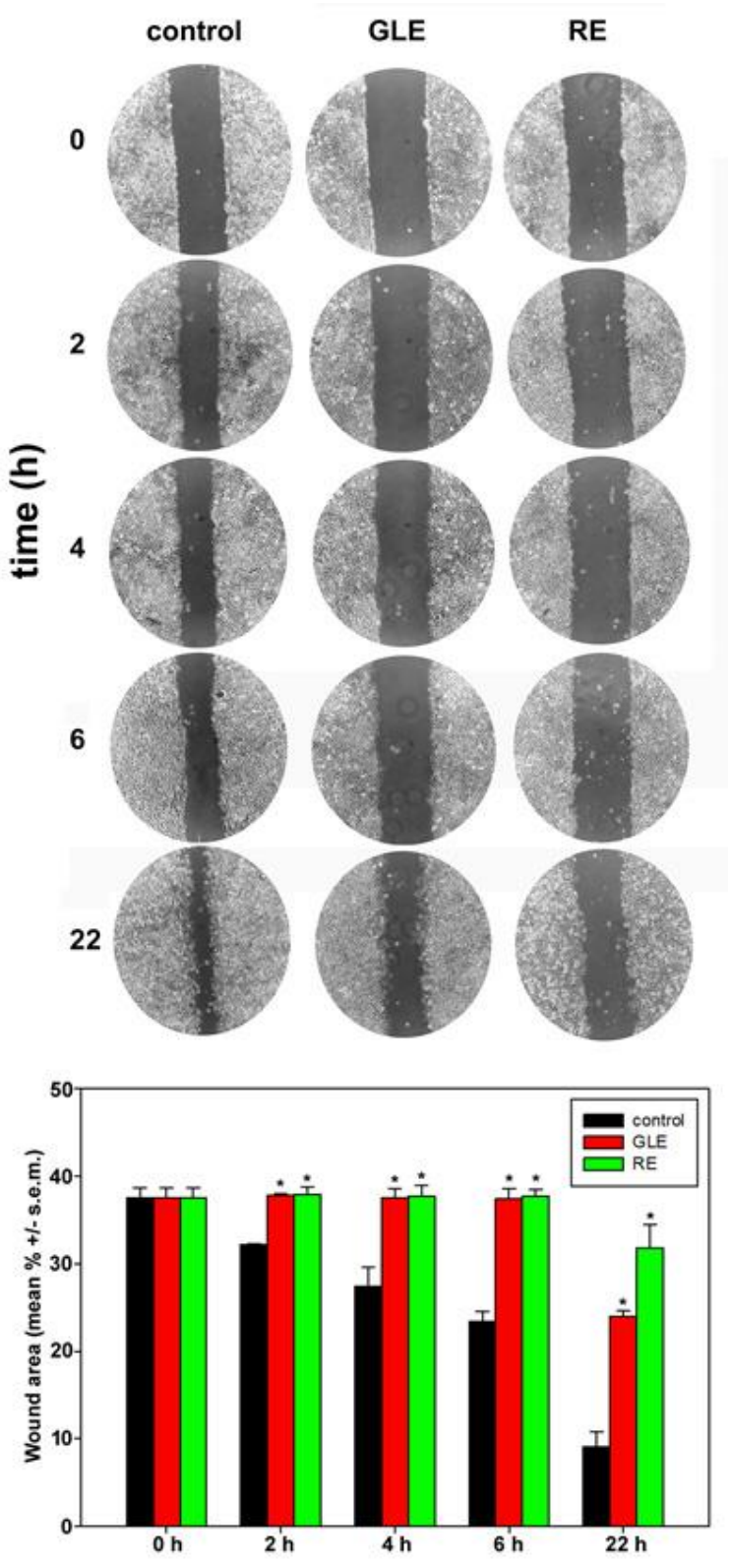

Figure 15. (Upper panel) Representative phase-contrast micrographs acquired during wound healing experiments at different time intervals under control conditions and in the presence of GLE or RE at their IC_{50}. The test was performed in triplicate. Microscopic magnification = 20×. (Lower image) bar graph summarizing data on wound closure by control and treated cells obtained from triplicate experiments. *Normality test *vs*. control passed.

2.3.6 *Contribution of 14 of the 100 proteins found on the biological activity obtained*

In light of the cytotoxic role played by GLE and RE on HepG2 cells and the sometimes-variable involvement of autophagy, apoptosis, redox state imbalance, and mitochondrial function derangement as revealed by the data previously shown, MS-based proteomic analyses were performed on the extracts after proteolysis of the samples as reported in 2.1.1.2. A total of 100 proteins were identified by searching the Alismatales database ; this was necessary, as protein sequence databases for *P. oceanica* are highly incomplete. This bioinformatic similarity search identified 14 proteins contained in the preparations that could be potentially associated with the various aspects related to the reported impairment of biological activities. The identity of the proteins and their relative semi-quantitative abundance in the GLE and/or RE samples are given in Table 2.

Accession number/ Protein description	**Organism**	**GLE amount**	**RE amount**
A0A843WDB0 ACB domain-containing protein	*Colocasia esculenta*	5.34E+04	3.72E+05
A0A1D1ZBB9 Adenosine kinase (Fragment)	*Anthurium amnicola*	4.68E+04	3.92E+04
A0A1D1YQU6 Adenosylhomocysteinase (Fragment)	*Anthurium amnicola*	1.06E+05	6.39E+05
A0A1D1YZX9 2-Cys peroxiredoxin BAS1-like, chloroplastic (Fragment)	*Anthurium amnicola*	5850	6.58E+04
A0A0K9PQ40 Ferredoxin-NADP reductase, chloroplastic	*Zostera marina*	1.37E+05	0
A0A1D1ZGY1 Glutathione reductase	*Anthurium amnicola*	0	1.31E+05
A0A0K9P699 Glutathione transferase	*Zostera marina*	0	2.01E+05
A0A0K9P881 Leucyl aminopeptidase	*Zostera marina*	9.56E+04	4.23E+04
A0A843XPL2 Mechanosensitive ion channel protein	*Colocasia esculenta*	7.32E+06	5.62E+06
A0A0K9Q3S1 Nucleoside-diphosphate kinase	*Zostera marina*	3.87E+04	2.31E+05
A0A0K9P7Q7			

Peptidyl-prolyl cis-trans isomerase	*Zostera marina*	0	1.96E+05
F8U875 Phosphoglucomutase (alpha-D-glucose-1,6-bisphosphate-dependent)	*Amorphophallus konjac*	0	1.22E+05
A0A0K9PHA0 Protein CutA 1, chloroplastic	*Zostera marina*	0	4.93E+05
A0A1D1XUN0 Superoxide dismutase	*Anthurium amnicola*	3.92E+05	1.95E+06

Table 2. Cytotoxic activity-associated proteins identified in GLE and RE.

2.3.7 Characterization of GLE, BLE and RE

Polyphenols were evaluated in GLE, BLE and RE; the results are shown in Table 3. Not all polyphenols identified were quantifiable, probably due to the extraction method used; these compounds were indicated as n.q. Interestingly, the three preparations showed a different polyphenol content. Higher polyphenols levels were observed in RE and, in particular, we observed a considerable amount of delphinidin-3 glucoside and quercetin-3-O-galactoside and a much lower, but still measurable, concentration of vanillic acid and procyanidins B2 and -3. In GLE and BLE, however, the most represented polyphenols are the caffeic acid methyl ester and p-hydroxybenzoic acid, respectively.

Polyphenol	**GLE (μg/g)**	**BLE (μg/g)**	**RE (μg/g)**
Delphinidin-3-glucoside	n.q	-	11.52
Quercetin 3-O-galactoside	n.q	-	10.81
Procyanidin dimer B type isomer 2	n.q	-	0.20
Procyanidin dimer B type isomer 3	n.q	n.q	0.30
Pro-Cyanidin-Dimer-B	n.q	n.q	-
Cyanidin 3-O-glucoside	-	n.q	-
Vanillic acid	-	-	0.6
Gallic acid	n.q	-	n.q.
Kaempferol 3-O-glucoside	-	-	n.q.
Kaempferol	n.q	-	-
Kaempferol 7-O-hexuronide	-	-	n.q.

Procyanidin trimer B type	-	-	n.q.
Gallic acid ethyl ester	-	-	n.q.
Catechin	n.q	n.q	n.q.
Epicatechin	-	-	n.q.
Myricetin	-	-	n.q.
Peonidin 3-O-hexoside isomer	-	-	n.q.
Malvidin 3-O-pentoside	-	-	n.q.
Quercetin 3-O-hexuronide	-	-	n.q.
Quercetin 3-O-(6″ -malonyl) hexoside	n.q	n.q	-
Resveratrol tetramer	-	-	n.q.
Caffeic acid methyl ester	0.37	-	-
Caffeic acid	n.q	n.q	-
p-Coumaric Acid	n.q.	-	-
Ellagic acid	n.q	-	-
p-Hydroxybenzoic acid	-	0.29	-
Ferulic acid	-	n.q	-
Myricetin	-	n.q	-
Myricetin 3-O-hexoside	-	n.q	-
Petunidin 3-O-(6″-acetyl) hexoside	-	n.q	-

Table 3. Quali-quantitative characterization of the phenolic components of GLE, BLE and RE. n.q. = not quantifiable.

3. ANTIDIABETIC EFFECT : EFFECT OF EXTRACTS FROM *P.OCEANICA* (GLE AND RE) AND THE COELOMIC FLUID OF *H.TUBULOSA* (CFE)

3.1 MATERIALS AND METHODS

3.1.1 Cell culture and treatment

HepG2 cells were cultured at the same condition than in paragraph 2.1.2. On the basis of the results from previous cell viability assays (Abruscato et al., 2023; Luparello et al., 2022), a concentration of 2 µg/ml for CFE and a concentration of 2,2 µg/ml and 60 µg/ml for GLE and RE respectively were selected as the maximum non-inhibitory concentrations on HepG2 cells and used for the following experiments

3.1.2 Pas Staining

HepG2 cells were seeded at a density of 88,000 cells/well in 6-well plates. Once subconfluent, cells were treated with either CFE, GLE or RE, with or without the supplement of 10^{-7} M insulin (Santa Cruz Biotechnology, Heidelberg, Germany), or only with insulin, for 24 h. Control untreated cells were assayed in parallel. The evaluation of glycogen accumulation was performed following the protocol reported by (Donato et al., 2015) Briefly, treated and untreated cells were fixed with 4% paraformaldehyde in PBS (Santa Cruz Biotechnology), covered with 0.5% periodic acid solution (Santa Cruz Biotechnology), and finally exposed to the Schiff's reagent (Santa Cruz Biotechnology). The preparations were observed under the microscope to assess the presence of glycogen granules.

3.1.3 Extracellular Glucose Determination

HepG2 cells were seeded at a density of 40,000 cells/well in 24-well plates. Once subconfluent, cells were treated with either CFE, GLE or RE, with or without the supplement of 10^{-7} M insulin (Santa Cruz Biotechnology, Heidelberg, Germany), or only with insulin, for 24 h. The amount of extracellular glucose was measured as previously described by (X. Zhang et al., 2019). Briefly, after 24 h of incubation in each experimental condition, cell culture media were collected and diluted 1 :1 with sterile distilled water. Subsequently, glucose levels were measured, in triplicate, using a blood glucose meter (Glucomen Areo 2k, Menarini Diagnostics, Firenze, Italy) and single-use test strips (Glucomen Areo Sensor, Menarini Diagnostics). The media from control untreated cells were assayed in parallel.

3.1.4 Flow cytometric assays

Flow cytometric analyses were carried out using the FACScanto instrument (BD Biosciences, Franklin Lakes, NJ, USA) with the evaluation of 10,000 single-cell events. The data obtained were analysed using the Floreada online tool available at the link https://floreada.io/. A gating in the FSC *vs.* SSC plot was performed to exclude cell debris with low FSC values from every analysis. For these assays, HepG2 cells were seeded at a density of 88,000 cells/well in 6-well plates and, once subconfluent, treated with the extracts and 10^{-7} M insulin for 24 h.

3.1.4.1 Flow cytometric assays for glucose uptake determination

The glucose uptake was determined as reported byCsepregi et al. (2018). Briefly, after 24h of incubation, cell culture media were discarded and replaced with Ca^{++}/Mg^{++}-containing PBS. Subsequently the cells were exposed to the fluorescent glucose analog 2-(N-(7-nitrobenz-2- oxa-1,3-diazol-4-yl) amino) -2-deoxyglucose (2-NBDG ; Peptide Institute, Osaka, Japan) for 1 h and trypsinized. The amount of 2-NBDG internalised by the cells was measured by flow cytometry in the FITC channel. Co-incubation with propidium iodide (PI) was performed to identify the fraction of dead cells. A preparation without the addition of 2-NBDG was assayed as a control.

3.1.4.2 Flow cytometric assays for GLUT-2 and -4 exposure on the plasma membrane

The exposure of GLUT-2 and -4 carriers on the plasma membrane has been quantitated by immunostaining as reported by Koshy et al. (2010) and Bruzzone et al. (2012). Briefly, after 24 h of treatment with the extracts, the cells were trypsinized, washed with ice-cold PBS and incubated with GLUT-2 or GLUT-4 polyclonal antibodies (bs-10379R-TR and bs-0384R-TR, Bioss, Boston, MA, USA ; working dilution 1 :100) dissolved in 3% BSA-containing PBS, for 20 minutes in the cold. Subsequently the preparation was incubated with the FITC-conjugated secondary antibody (AP132F, Sigma, working dilution 1 :80) for further 20 minutes. After an extensive washing, the cell preparations were analyzed by flow cytometry. An isotype control was included in the analysis.

3.*1.5 Conventional and qRT- PCR*

The analysis of gene expression was performed by conventional and qRT-PCR (Abruscato et al., 2023). Briefly the total RNAs from control and treated cells were extracted with the PureLink RNA Mini kit (ThermoFisher) using the in-column DNase treatment with the PureLink DNase set (ThermoFisher), as recommended by the manifacturer. Five hundreds ng of RNA for each sample were reverse transcribed using the RevertUP™ II Reverse transcriptase kit (Biotechrabbit, Berlin, Germany) and random hexamer primers. The conventional PCR analysis was performed using 2.5 µM of the appropriate forward and reverse primers (see Table 4), 1 U BIOTAQ^{TM} DNA polymerase (Meridian Bioscience, Cincinnati, OH/USA)/µL, 200 µM each of dNTPs, and 1 µL of the cDNA template, with following the thermal cycle : 1 denaturation step of 94°C for 2 min, 33 cycles of 94°C for 1 min, the appropriate annealing temperature for 1 min and 72°C for 1 min, and a final extension of the product for 5 min at 72°C .The amplified cDNAs were separated by 1% agarose gel electrophoresis and visualized by Gel Red staining (Biotium, Fremont, CA, USA) under the UV light. The quantitative analysis of the bands was performed with the ImageJ software and the normalization was carried out to *ACTB* band intensity, used as the internal control. The differential expression of *GLUT2*, *GLUT4*, and *HNF1A* genes was further investigated through the SYBR-Green-based qRT-PCR using the SYBR-Green qPCR MasterMix (MedChem Express, Monmouth Junction, NJ, USA) in an Applied Biosystems 7500 Real-Time PCR system, as previously reported by (Abruscato et al., 2023). The quantification was performed using the $2^{-\Delta\Delta Ct}$ method and the normalization was carried out between the expression levels of each target gene and that of *ACTB* as the internal control.

Gene (Primer)	Sequence (5′ → 3 ′)	Reference
GLUT2 (Forward)	GATGAACTGCCCACAATCTC	(Kang et al., 2014)
GLUT2 (Reverse)	CTGATGAAAAGTGCCAAGTG	
GLUT4 (Forward)	GTTAATCGGCATTCTGATCG	(Kang et al., 2014)
GLUT4 (Reverse)	GTGAAGACTGTGTTGACCAC	
AKT2 (Forward)	GCTAGGTGACAGCGTACCAC	(Mokashi et al., 2017)
AKT2 (Reverse)	GGCCTCTCGGTCTTCATCAG	
IRS1 (Forward)	TATCTGCATGGGTGGCAAGG	(Mokashi et al., 2017)

IRS1 (Reverse)	GGGTAGGCAGGCATCATCTC	
HNF1A (Forward)	GAATGCATCCAGAGAGGGGT	(Kang et al., 2014)
HNF1A (Reverse)	GTGGACCTTACTGGGGGAGA	
ACTB (Forward)	GGAAGGTGGACAGCGAGGCC	(Abruscato et al., 2023)
ACTB(Reverse)	GTGACGTGGACATCCGCAAAG	

Table 4. Primers used for PCR amplification.

3.1.6 Western Blotting

After 24 h of treatment with either extract, control and treated cells were trypsinized, collected and lysed in a buffer containing 7 M Urea, 2% CHAPS, 10 mM DTT and supplemented with a protease inhibitor cocktail (Sigma) (Abruscato et al., 2023). Equal amounts of protein lysates were separated by 13% SDS-PAGE and transferred to the nitrocellulose membrane. Subsequently the membranes were incubated with the following rabbit primary antibodies: anti-GLUT2 (bs-10379R-TR, Bioss, Boston, MA, USA; working dilution 1:500), anti-GLUT4 (bs-0384R-TR, Bioss; working dilution 1:500), anti-HNF1α (PAG775Hu01, Cloud-Clone Corp., Katy, TX, USA; working dilution 1:1000), anti-AKT (9272, Cell Signaling Technology, Danvers, MA, USA; working dilution 1:750), anti-pAKT (sc-7985-R, Santa Cruz Biotechnology, working dilution 1:500), and anti-actin (Ab8227, Abcam, Cambridge, UK; working dilution 1:1000) at 4°C overnight. After an extensive washing, the membranes were incubated with the peroxidase-conjugated anti-rabbit secondary antibody (Ab6721, Abcam; working dilution 1:3000) at room temperature for 1 h. The bands' visualization was performed using the molecular imager Versadoc MP imaging System (Bio-Rad, Hercules, CA, USA) and the Super Signal West Pico Plus substrate (ThermoFisher). The quantitative analysis of the bands was performed with the ImageJ software, with the normalization to the actin band intensity, used as internal control.

3.2 STATISTICS

The normality tests were performed with the SigmaPlot 11.0 software (SYSTAT, San Jose, CA, USA). For the Western blot experiments, the data were analyzed with the unpaired two-tailed Student's t-test using GraphPad Prism 9 software (GraphPad, San Diego, CA, USA).

3.3 RESULTS

3.3.1 *GLE and CFE stimulate glycogen accumulation in HepG2 cells*

In a first set of assays aimed to assess the effect of GLE, RE and CFE on glucose metabolism in HepG2 cells, PAS staining was performed to evaluate the intracellular accumulation of glycogen under the different culture conditions. As shown in the panel of representative micrographs in Figure 16, the PAS assay showed that, as expected, in the presence of insulin a marked reaction could be observed compared to the untreated control. Of note, exposure to GLE, RE and CFE gave contrasting results. In fact, differently from RE that showed no significant effect, the PAS staining in the presence of GLE and CFE was slightly more intense than that of cells treated with insulin, whereas the co-treatment with GLE and CFE plus insulin did not result in further substantial up-regulation of intracellular glycogen accumulation. The staining in the presence of co-treatment with RE and insulin was comparable to that of insulin alone.

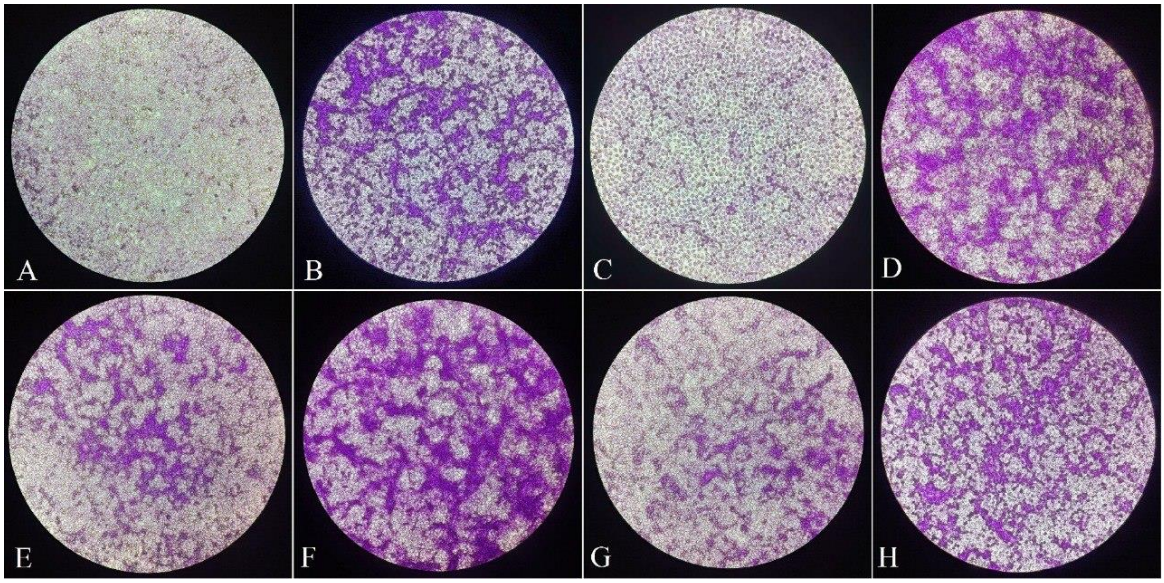

Figure 16. Representative micrographs of PAS-stained HepG2 cells cultured for 24 h in control condition (A) and in the presence of 2.2 µg/mL GLE (B), 60 µg/mL RE (C), 2 µg/mL CFE (D), 10^{-7} M insulin (E), 2.2 µg/mL GLE+ 10^{-7} M insulin (F), 60 µg/mL RE+ 10^{-7} M insulin (G) and 2 µg/mL CFE+ 10^{-7} M insulin (H). Microscopic magnification = 10X.

3.3.2 *Glucose consumption and glucose uptake by CFE-, RE- and GLE-treated HepG2 cells.*

The potential antidiabetic effect of GLE, RE and CFE in the presence or absence of insulin was further investigated through the glucose consumption and glucose uptake assays. To this purpose, glucose consumption was monitored by evaluating glucose content in the culture media of control and treated cells, whereas the 2-NBDG uptake assay was performed to determine the short-term glucose responsive action upon exposure to the extracts. As reported in Figure 17 the treatment with CFE and GLE for 24 h significantly decreased glucose concentration in the medium down to 82.1 +/- 3 % and 82.5 +/- 3.7 %, respectively *vs*. control, a value analogous to that obtained in the presence of insulin (81.1 +/- 3.2%). Conversely, no statistically significant difference was found after treatment with RE. No synergistic effect has been highlighted after co-exposure to CFE or GLE and insulin (84.1+/- 3.2 % and 84.8 +/- 3.9 % respectively). Also, co-incubation with RE and insulin resulted in a glucose consumption comparable to that of cells exposed to the sole insulin. Therefore, based on the irrelevance of glucose measurement and PAS assay results, co-incubation conditions were not included in the subsequent experiments. In support of the glucometric data, the obtained flow cytometric data (Figure 18) of the internalization of 2-NBDG showed that after 1 h of treatment only CFE and GLE induced a significant and immediate response leading to the stimulation of 2-NBDG internalization up to +4.8 +/- 0.03 fold and 2.6+/-0.03 fold respectively *vs.* Control. Conversely, no significant short-term uptake increase was found after exposure to RE (about +0.3 ± 0.3 folds) or the sole insulin (about +0.1 ± 0.2 folds).

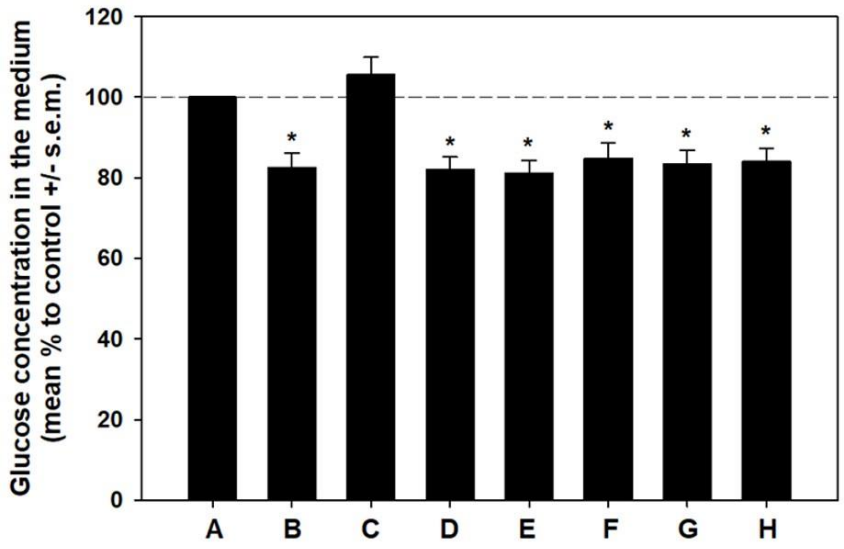

Figure 17. Bar graph showing the percentage of glucose concentration in the media of HepG2 cells cultured in the presence of 2.2 µg/mL GLE (B), 60 µg/mL RE (C), 2 µg/mL CFE(D), 10^{-7} M insulin (E), 2.2 µg/mL

GLE+ 10^{-7} M insulin (F), 60 µg/mL RE + 10^{-7} M insulin (G) or 2 µg/mL CFE+ 10^{-7} M insulin (H) *vs.* control (A). The error bars indicate the standard error of the mean (s.e.m.) of three independent measurements. *normality test *vs.* control passed.

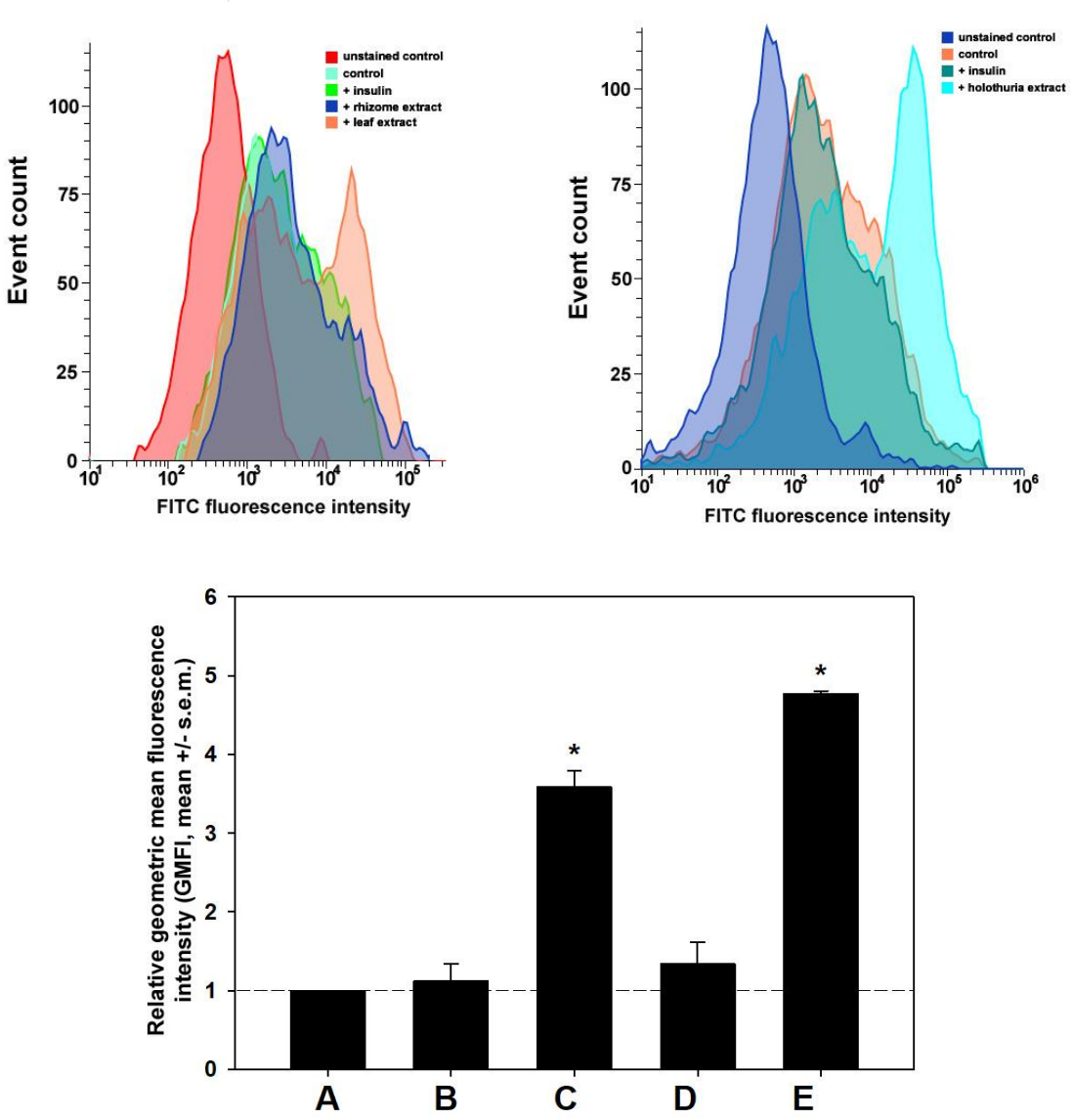

Figure 18. (Upper) Representative flow cytometric profiles of 2-NBDG uptake by HepG2 cells cultured for 1 h in control conditions or treated with 10^{-7} M insulin, (left) 60 µg/mL RE or 2.2 µg/mL GLE and (right) 2 µg/mL CFE. Fully-processed preparations without 2-NBDG were assayed in parallel to control for background derived from autofluorescence (unstained control). (Lower) Bar graph showing the relative geometric mean fluorescence intensity (GMFI) of control (A), insulin (B), GLE (C) RE (D) or CFE-treated (E) HepG2 cells. All the results from flow cytometry assays were analyzed for the GMFI of each condition and the GMFI of either treated cell population was divided by the GMFI of the controls to normalize the data. The error bars indicate the standard error of the mean (s.e.m.) of three independent measurements. *normality test *vs.* control passed.

3.3.3 *Expression levels of glucose transporters and upstream regulators in CFE- and GLE-treated HepG2 cells*

The effect of HepG2 cells' exposure to GLE and CFE on the respectively insuline-unresponsive and insuline-stimulated GLUT-2 and GLUT-4 transporters and other regulators such as the hepatocyte nuclear factor- 1α (HNF1α), a GLUT-2 transcription factor (Kim et al., 2017; Párrizas et al., 2001), as well as insulin receptor substrate-1(IRS-1) and protein kinase B(AKT) with its activated form pAKT, belonging to a signalling pathway responsible of GLUT-4 traslocation on the cell surface(Zhang et al., 2019;Świderska et al., 2020), was investigated at the gene expression and protein accumulation levels. The amplicon panel reported in Figure 19A and 20A, representative of triplicate experiment of conventional PCR and the densitometric analysis performed with ImageJ software, showed that in non stimulated-HepG2 cells, as expected (Chadt & Al-Hasani, 2020), *GLUT-2* was apparently up-regulated than *GLUT-4*. After exposure to CFE, about +6.1- and +2.4-fold increases in *AKT* and *IRS1* expression levels, respectively, were identified by analysis of the amplicon intensity with the ImageJ software and normalization set to *ACTB* level. Being undetectable by conventional PCR, the differential expression of *GLUT-2*, *GLUT-4*, and *HNF1α* was further studied through qRT-PCR. The bar graph in Figure 19B and 20B shows that the exposure to the CFE promoted the upregulation of *GLUT-4* (about +0.66-fold *vs.* control) and *HNF1α* (about +2.4-fold *vs.* control), whereas no significant change was found for the expression level of *GLUT-2*. Concerning GLE-treated cells, only *GLUT-4* and the two GLUT-4 externalization-related genes, i.e., *IRS1* and *AKT2,* were upregulated by 3.1 ± 0.01, 2.15 ± 0.07 and 2.84 ± 0.03 folds, respectively. Conversely, *HNF1α* was downregulated by 0.8 ± 0.02 folds, and no significant modification of band density was found for *GLUT2*. The Western blot data on both glucose transporters, HNF1α and AKT, with its phosphorylated forms are reported in Figure 19D and 20D. The obtained results demonstrate that in line with the mRNA expression data GLUT-4 was less abundant than GLUT-2 in control cells, and that the CFE and GLE induced an up-regulation of GLUT-4 (about +2.7-fold and 4.4 fold respectively). CFE increased HNF1α levels (about +1.3-fold) and, unexpectedly, also GLUT-2 (about +1.8-fold), unlike GLE that did not induce any change in HNF1α and the downregulation of GLUT-2 (about -0.6-fold). The sole GLE determined the increase of both activated pAKT (+1.3-fold) and pAKT/AKT ratio (+4.2-fold).

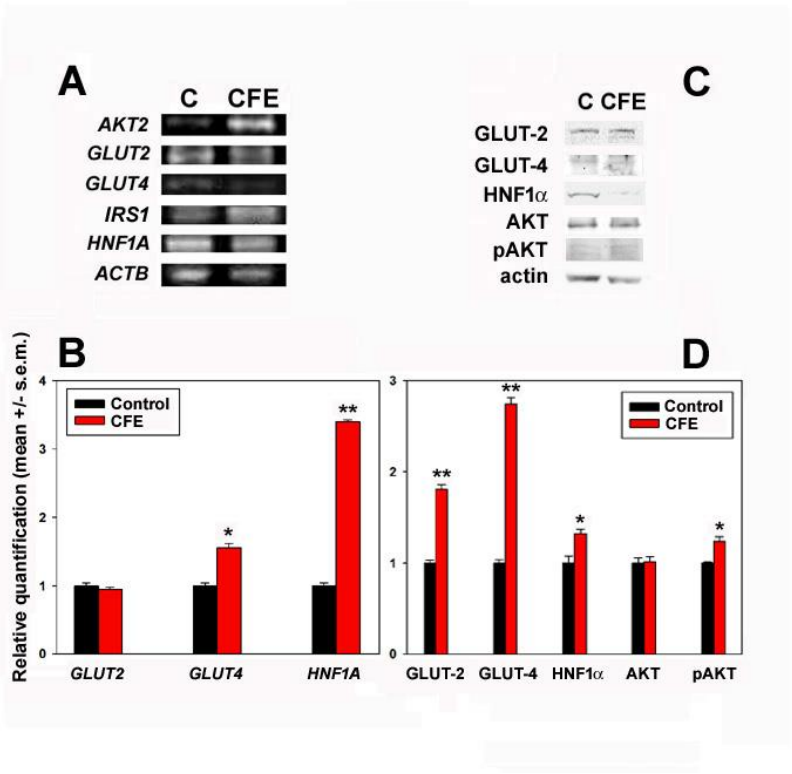

Figure 19 (A) Representative results of PCR analysis for the expression of genes coding for glucose transporters (*GLUT-2*, *GLUT-4*) and their regulators (*IRS1*, *AKT*, *HNF1α*) in HepG2 cells grown for 24 h under control conditions or in the presence of 2 µg/mL CFE. The bar graph in B) shows the relative quantification (treated/control) obtained by band densitometry, normalized to *ACTB* expression, of three independent experiments. (C) Representative results of Western blot analysis for accumulation of glucose transporters and regulators in HepG2 cells grown for 24 h under control conditions or in the presence of 2 µg/mL CFE. The bar graph in D) represents the relative quantification (treated/control) obtained by band densitometry, normalized to actin, of three independent experiments. The error bars indicate the standard error of the mean (s.e.m.). *p ≤ 0.05; ** p ≤ 0.01.

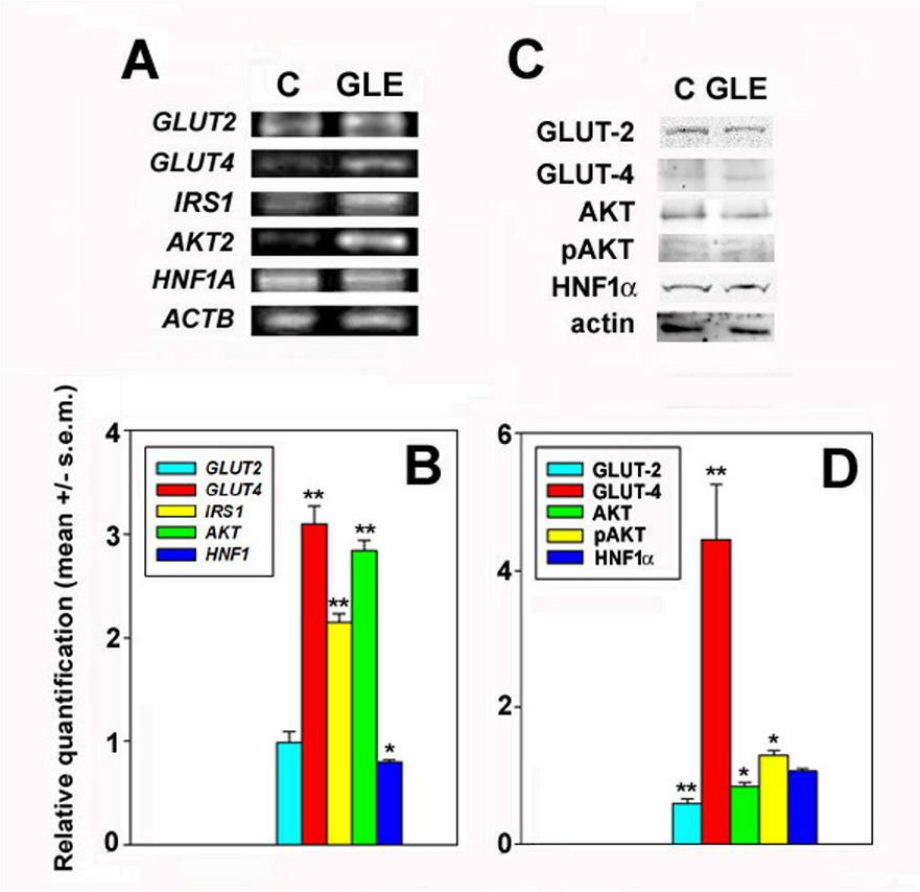

Figure 20 (A) Representative results of PCR analysis for the expression of genes coding for glucose transporters (*GLUT-2*, *GLUT-4*) and their regulators (*IRS1*, *AKT*, *HNF1α*) in HepG2 cells grown for 24 h under control conditions or in the presence of 2.2 µg/mL GLE. The bar graph in B) shows the relative quantification (treated/control) obtained by band densitometry, normalized to *ACTB* expression, of three independent experiments. (C) Representative results of Western blot analysis for accumulation of glucose transporters and regulators in HepG2 cells grown for 24 h under control conditions or in the presence of 2.2 µg/mL GLE (GLE). The bar graph in D) represents the relative quantification (treated/control) obtained by band densitometry, normalized to actin, of three independent experiments. The error bars indicate the standard error of the mean (s.e.m.). * $p \leq 0.05$; ** $p \leq 0.01$.

3.3.4 *Exposure of GLUT-2 and -4 on the plasma membrane in CFE and GLE -treated HepG2 cells*

Subsequently, to investigate more in detail the effect of CFE and GLE on the glucose transport system, especially their involvement in the traslocation and exposure of GLUT-2 and GLUT-4 on the plasma membrane, HepG2 cells were immunostained and analyzed by flow cytometry. Figure 21 and 22 show that unstimulated HepG2 cells displayed analogous values of the mean fluorescence intensities (GMFI) of the flow cytometric data for the two transporters. After treatment with 2 µg/mL CFE for 24 h, the cells showed a significant increase in the amount of GLUT-2 (about 38 %) and GLUT-4 proteins (about +72%) exposed

on the cell membrane. Concerning the treatment with 2.2 µg/mL GLE for 24 h, only an increase in surface-exposed GLUT-4 (about 52%) was identified.

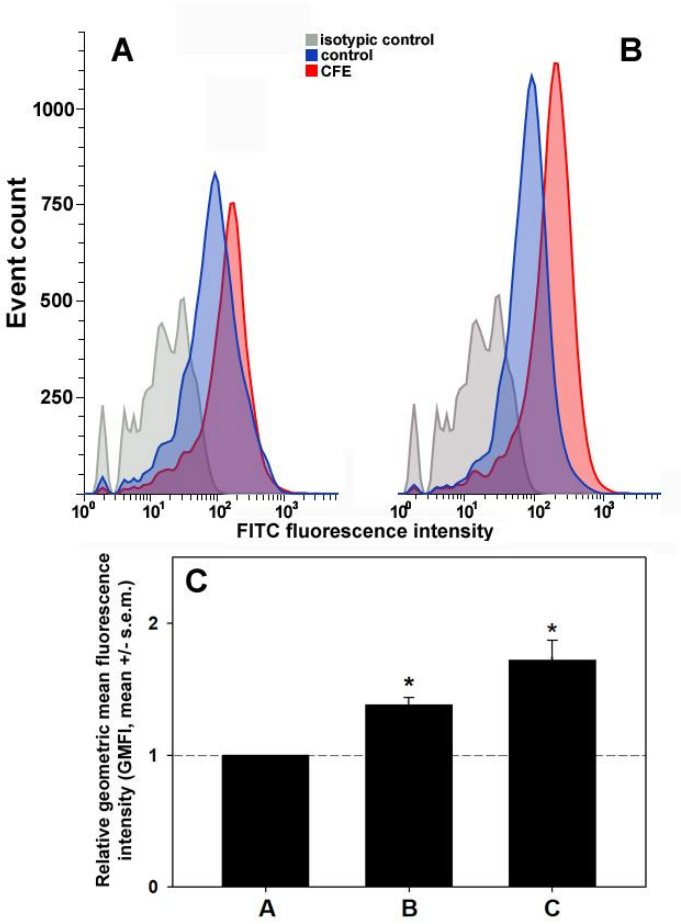

Figure 21. Representative flow cytometric profiles of immunostained GLUT-2 (A) and GLUT-4 (B) exposed on the plasma membrane of HepG2 cells cultured for 24 h in control conditions or treated with 2 µg/mL CFE. An isotype control was included in the analysis. (C) Bar graph showing the relative geometric mean fluorescence intensity (GMFI) of GLUT- 2 and GLUT-4 in HepG2 cells exposed to CFE and normalized to control. In each experimental condition the cumulative data obtained by flow cytometry were analyzed for the GMFI and the latter of either treated cell population was divided by the GMFI of the control for normalization. Three independent measurements were performed. Normality test *vs.* control passed.

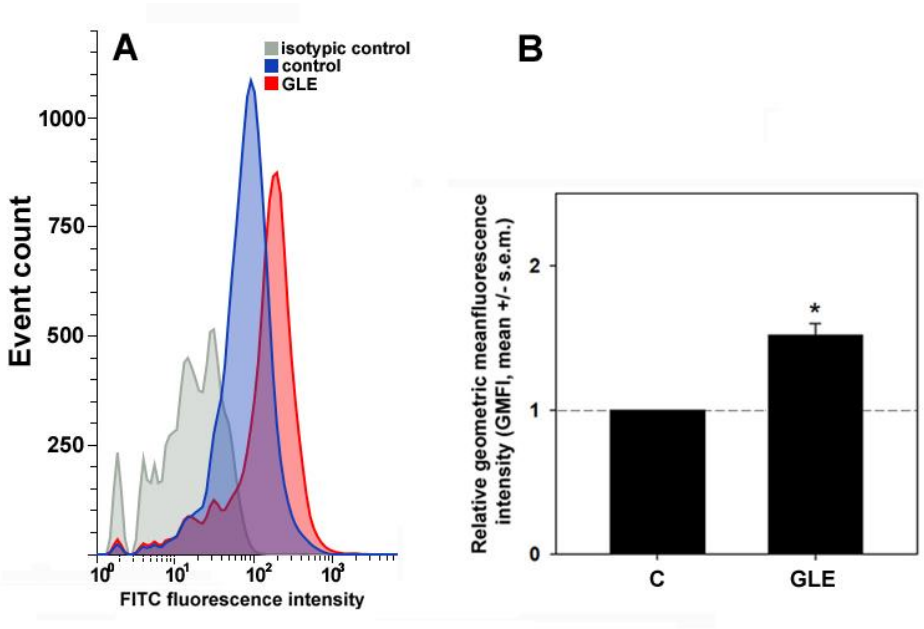

Figure 22. Representative flow cytometric profiles of immunostained GLUT-4 (A) exposed on the plasma membrane of HepG2 cells cultured for 24 h in control conditions or treated with 2.2 µg GLE/mL. An isotype control was included in the analysis. (B) Bar graph showing the relative geometric mean fluorescence intensity (GMFI) of GLUT-4 in HepG2 cells exposed to GLE and normalized to control. In each experimental condition the cumulative data obtained by flow cytometry were analyzed for the GMFI and the latter of either treated cell population was divided by the GMFI of the control for normalization. Three independent measurements were performed. Normality test *vs.* control passed.

4. ANTI-INFLAMMATORY AND PROTECTIVE EFFECT OF *P. OCEANICA* EXTRACTS (GLE AND RE) ON RAW 264.7 AND HUMAN *IN VITRO* BLOOD-BRAIN BARRIER MODEL

4.1 MATERIALS AND METHODS

4.1.1 Cell culture and viability assay

RAW 264.7 cells, taken from laboratory stocks, were cultured in D-MEM (Sigma), supplemented with 10% fetal calf serum (Sigma) and 100 U/mL penicillin-streptomicin (Gibco) at 37°C and 5% CO_2. For the viability test, the cells were seeded at a density of 10.000 cells/well in 96-well plates, allowed to adhere overnight and grown in control conditions or exposed to different concentrations of GLE or RE (1-20 µg/mL and 0.1-1 µg/mL respectively). After 24 h of incubation the standard MTT [3-(4,5- dimethylthiazol-2-yl) -2,5- diphenyltetrazolium bromide] assay was performed. The absorbance of samples was measured in an automated microplate reader at λ=600 nm. Cell viability% in each experimental condition was determined as the ratio between treated cells' and control cells' optical density (OD) *100.

4.1.2 Evaluation of nitrite production

The ability of the GLE and RE in scavenging the NO radical in the LPS-inflammed RAW 264.7 was evaluated using the Griess method. After 24 h of incubation with GLE, RE at different concentrations and 0.1 µg/mL LPS (Kim et al., 2024) the culture media from control and treated cells were collected and 150µL were transferred to a 96-well plate. Following manufacturer's recommendation after 30 minutes of incubation with the Griess reagent (Biotium, Fremont/CA, USA) at room temperature, the absorbance of the samples was measured in an automated microplate reader at λ = 548 nm. The NO release ratio in each experimental condition was determined as the ratio between the O.D. of the media from exposed cells and that of the controls.

4.1.3Human blood-brain barrier model (BBB)

For this study, a human in vitro blood-brain barrier (BBB) model was utilized. This model was created using *brain-like endothelial cells* (BLECs) following the protocol developed by (Cecchelli et al., 2014). CD34+ hematopoietic stem cells were isolated from human umbilical cord blood as described by (Pedroso et al., 2011) and subsequently differentiated into BLECs. The BLECs were then co-cultured with human brain pericytes to create a

functional BBB model. Briefly, 8×10^4 BLECs at passage 6 were seeded onto Matrigel-coated (Matrigel®, Growth Factors reduced, BD Biocoat 354230, Corning Inc., New York/NY, USA) inserts (pore size 0.4 μm, Costar Transwell inserts, Corning Inc., Corning, NY, USA). Then, the BLECs were co-cultured with human brain pericytes at passage 10 in a 12-well type I collagen-coated plates with Promocell medium (Promocell GmBH, Heidelberg, Germany). The co-cultures were incubated at 37°C under 5% CO2 in humidified air, and the medium was renewed every two days until the co-culture system was ready for use, that is, at the sixth day of incubation. Once the BLEC phenotype was established, the cells formed two distinct compartments: the apical compartment, representing the blood side, and the basolateral compartment, representing the brain side, allowing for treatment application.

4.1.4 Treatments

GLE and RE were prepared in basal endothelial cell growth medium with the addition of 0.1% BSA. In light of the previously obtained results about GLE and RE dose-response effect on HepG2 cells (Abruscato et al., 2023)10 μg/mL (for GLE) and 0.1 μg/mL (for RE) were selected as the maximum non-inhibitory concentrations and used for the present assays. The extracts were applied to the luminal compartment (blood side) and after 30 minutes of exposure, TNF-α (SRP3177; Sigma Aldrich, Lyon, France) was applied at a concentration of 5 ng/mL to the same compartment, either with or without GLE and RE, to establish an inflammatory condition for further 24 h.

4.1.5 Evaluation of nitric oxide release in culture media

The ability of the GLE and RE in scavenging the NO radical in the TNFα-treated BBB was evaluated using the Griess method as in paragraph 4.1.2

4.1.6 Evaluation of BBB permeability

The effects of GLE and RE on the integrity of the BBB monolayer following exposure to TNFα were assessed by calculating the endothelial permeability coefficient (Pe) of sodium fluorescein (NaFlu, GS291A Interchim Montluçon, France; working dilution 1:1000) translocating from the luminal to the basolateral compartment, as previously described in (Dehouck et al., 1992). NaFlu is a hydrophobic small molecule that displays a low rate of passage through the BBB under physiological conditions and whose Pe is therefore indicative of monolayer integrity. After 24 h of exposure to the extracts and TNFα, the BLECs-containing inserts were transferred to a 12-well plate containing HEPES-buffered

Ringer's solution (RH: 8.8 g NaCl, 0.387 g KCl, 0.244 g CaCl2, 0.0406 g MgCl2, 0.504 g NaHCO3, 1.19 g HEPES, 0.504 g Glucose) and then 10 µM sodium fluoresceine (NaFlu) in RH were injected into the luminal compartment. Every 20 minutes and for a total of one hour, the inserts were transferred to a new well containing 500 µL of heated RH. At the end of the incubation, the inserts were removed, and aliquots from the donor solution were taken at the beginning and end of the experiment. Fluorescence was measured using a microplate reader (Synergy H1®, BioTek) at 490/525 nm. The cleared volume was calculated by dividing the amount of NaFlu in the receiver compartment at the end by its initial concentration in the donor compartment, then dividing by the duration of the experiment (60 minutes) to obtain the permeability surface area product (PS, µL/min). Both the permeability of filters without cells (PSf) and with cells (PSt) were considered in the calculation.

$$1/PSe = 1/Pst - 1/Psf$$

The permeability surface area product of the endothelial cell monolayer (PSe, in µL/min) was calculated and then the PeNaFlu values referred to BLECs (Pe, in cm/min), were obtained dividing the PSe value by the surface area of the filter (1.12 cm^2) and therefore using this formula "PeNaF= PSe/ S".

4.1.7 Immunostaining

After 24 h of treatment with TNFα or co-treatment with TNFα and either GLE or RE, BLECs were rinsed with PBS for 5 min, then fixed and permeabilized as described in (Versele et al., 2022a). After blocking–with Sea Block Blocking Buffer (37527;Thermofisher, Rockford/IL, USA) for 30 minutes, BLECs were incubated for 1 h with one of the following rabbit primary antibodies in 5% Sea Blocking Buffer in PBS-CMF at room temperature: anti-claudin-5 (34-1600, Thermofisher; working dilution 1:200), anti VE-cadherin (ab33168, Abcam, Cambridge, UK; working dilution: 1:400) anti-ZO-1 (61-7300, Thermofisher; working dilution 1:200). Following additional washes, the cells were incubated with the flurochrome-conjugated secondary polyclonal antibodies (Goat anti-Rabbit Alexa Fluor 488, A11034, Molecular Probes, Eugene/OR, USA) diluted 1:500 in 5% sea blocking buffer in PBS-CMF for 30 minutes in the dark and at room temperature. After a final series of washes the filters were placed on glass slides and mounted under coverslips with ProLong Gold Antifade Mountant® containing DAPI (Thermo-Fisher). Images were taken and analyzed in a Axio Imager A2® fluorescence microscope (Leica Microsys-tems, Wetzlar, Germany) and processed using ImageJ software.

4.1.8 mRNA expression analysis

The analysis of mRNA expression was performed through qRT-PCR, as reported by Abruscato et al. (2023) and Versele et al. (2022). Essentially, total RNA from control and treated BLECs of the BBB was extracted using NucleoSpin® RNA/Protein minikit (Macherey-Nagel, Dueren, Germany) according to manufacturer's instructions. RNA purity was monitored by measuring the absorbance at 260, 280 and 320 nm using a Take 3 plate and Agilent's Synergy H1 spectrophotometer. The amount of extracted mRNA was assayed by spectrophotometry (Synergy H1, Biotek, Colmar, France). Reverse transcription was performed using iScript™ reverse transcription supermix (Bio-Rad, Hercules/CA, USA). The SYBR Green-based qPCR was performed in 96-well plates on triplicate samples. The differential gene expressions in BLECs were assayed using the SsoFast™ Evagreen SuperMix (Bio-Rad) in a CFX96 Real-Time System thermal cycler (Bio-Rad). The primer pairs used are reported in Table 5. Gene expression levels were assessed using the ΔΔCt method and normalized to *GAPDH* as reference gene.

Gene (Primer)	Sequence (5′ → 3 ′)	Reference
ICAM-1 (Forward)	GCAGACAGTGACCATCTACAGC	(M. Kim et al., 2014)
ICAM-1 (Reverse)	CCTCACACTTCACTGTCACCTC	
VCAM-1 (Forward)	AGTGGTGGCCTCCTGAATGG	(T. Chen et al., 2020)
VCAM-1 (Reverse)	CTGTGTCTCCTGTCTCCGCT	
CLAUDIN-5 (Forward)	GAGGCGTGCTCTACCTGTTTT	(Versele et al., 2022b)
CLAUDIN-5 (Reverse)	CACAGACGGGTCGTAAAACTC	
VE-CADH (Forward)	GATCTCCGCAATAGACAAGGAC	(Versele et al., 2022b)
VE-CADH (Reverse)	TCCGTGAGGGTAAAGTTGTTCT	
GAPDH (Forward)	GATGACATCAAGAAGGTGGTGA	(Dib et al., 2023)
GAPDH(Reverse)	GCTGTTGAAGTCAGAGGAGACC	

Table 5. Primers used for PCR amplification

4.1.9 Western blotting

Following treatments, cells were harvested in RIPA buffer (Millipore) supplemented with protease and phosphatase inhibitor cocktails (Sigma Aldrich). The cell lysates were then centrifuged at 10,000 rpm for 10 minutes at 4°C. Protein concentrations were measured using a Bradford assay (Bio-Rad) according to the manufacturer's instructions. Equal amounts of protein lysates (20 μg) were combined with Laemmli reagent (Bio-Rad), heated at 95°C for 5 minutes, and subjected to SDS-PAGE on 4-15 % acrylamide gels (Bio-Rad) at 200 V for 45 minutes. The separated proteins were transferred to nitrocellulose membranes (GE Healthcare) at 100 V for 1 hour. Membranes were then blocked with TBS-T containing 1% Tween 20 and 5% skim milk for 1 hour, followed by incubation with primary antibodies at 4°C overnight, except for β-actin. The rabbit and mouse primary antibodies used to probe the blots were: anti-claudin-5 (GTX49370, Genetex, Irvine/CA,USA; working dilution 1:500), anti-ZO-1 (Ab216880; working dilution 1:1000), anti-VE-cadherin (Ab33168; working dilution 1:1000), anti-ICAM-1 (Ab53013; working dilution 1:2000) all from Abcam, anti-VCAM (PA5-80213, Invitrogen; working dilution 1:1000) and, as an internal control, either anti-GAPDH (GTX627408, Genetex; working dilution 1:20000) or anti-actin (A5441, Sigma; working dilution 1:20000). After reaction with the peroxidase-conjugated secondary antibodies, (P0447, Dako/Agilent Technologies, Inc., Santa Clara, CA, USA; working dilution 1:5000) (P0448, Dako/Agilent Technologies, Inc., Santa Clara, CA, USA; working dilution 1:8000) at room temperature for 1 h and after membranes incubation with enhanced chemiluminescence reagent (ECL, Cytiva TM Amersham, UK) the bands were revealed by the Western immunoblotting Imaging system Azure c600 (Azure Biosystems, Dublin, Ireland). Protein band intensities were quantified using ImageJ software, and the data were normalized to the band intensity of the internal control.

4.2 STATISTICS

Data are presented as mean ± SEM. The one-way variance analysis ANOVA and t- test were performed. Statistical analyses were performed using the GraphPad 9 Prism software (GraphPad Software, San Diego, CA).

4.3 RESULTS

4.3.1 Preliminary viability test and evaluation of NO levels in LPS-inflamed RAW 264.7 cells

With the aim of beginning the analysis of the potential anti-inflammatory effect at a peripheral level and to exclude the cytotoxic effect by GLE and RE on RAW 264.7 cells, preliminary MTT assays were performed. As shown in Figure 23A and B, cells exposure for 24 h to GLE and RE did not affect cell viability.

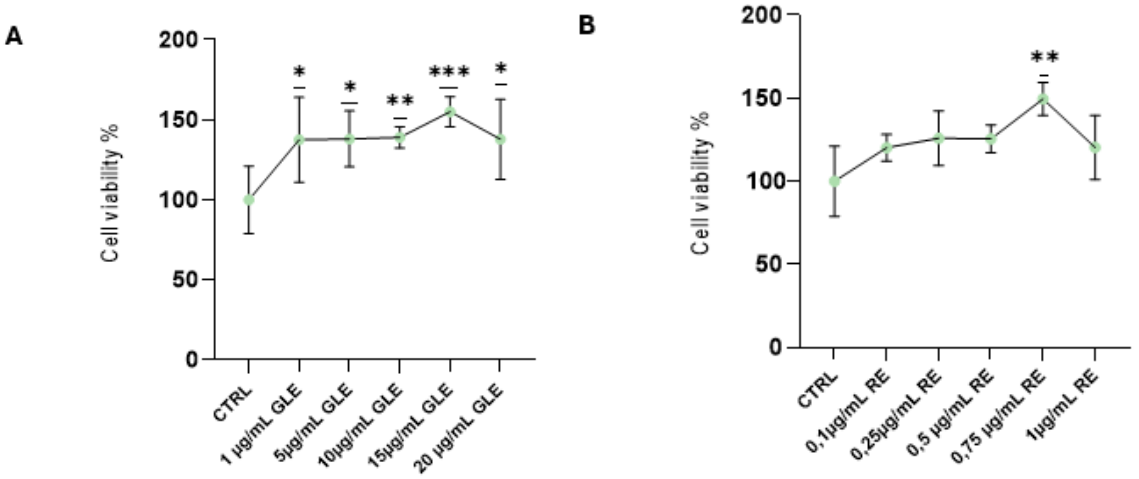

Figure 23. Representative graphs of cell viability rates following exposure of RAW 264.7 cells to different concentrations of GLE and RE (mean ± s.e.m of three independent experiments). Unpaired *t-test* was performed.

In light of the results obtained and as reported in literature, RAW cells were inflamed using 0.1µg/mL LPS and then treated for 24 h with GLE and RE at different concentrations to evaluate the nitric oxide release in the culture media. As shown in Figure 24A and B GLE and RE differently modulate NO release. In order to proceed with the evaluation of GLE and RE potential anti-inflammatory effects at the BBB level, we determined the concentrations to be used by selecting the highest tested concentrations at which the lowest release of NO was detected.

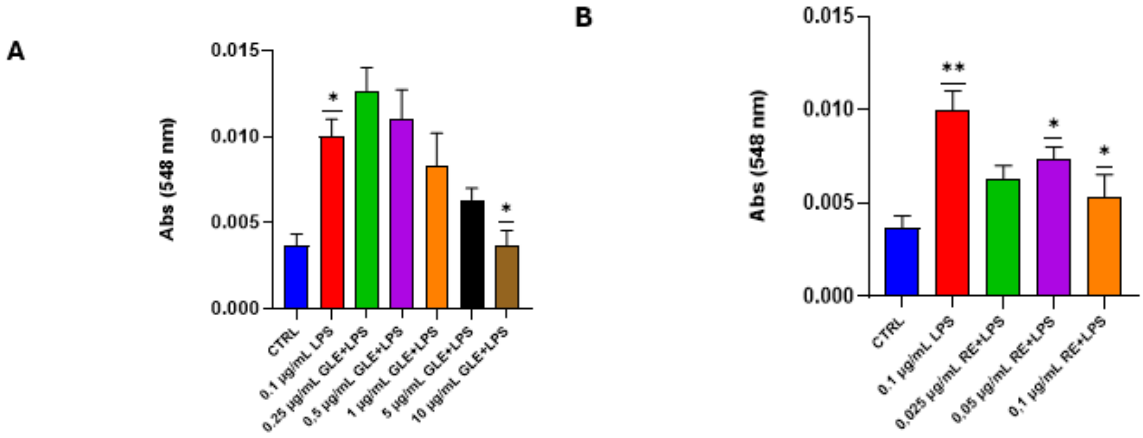

Figure 24. Effects of GLE and RE on nitric oxide release in RAW 264.7 culture media following 0.1 µg/ mL LPS exposure. Nitric oxide levels were quantified using the Griess reagent. The histogram shows a significant increase in nitric oxide levels after 24 hours of 0.1 µg/mL exposure (*p*-value in fig. A = 0.01, in fig. B= 0.0015) However, treatment with GLE and RE, in combination with LPS, resulted in OD values comparable to or lower than the LPS alone, indicating a variable modulation of the potential anti-inflammatory effect at the concentrations tested. For all the above graphs, each bar is representative of at least three independent experiments performed in triplicate. The one-way ANOVA test was used. The threshold for statistical significance compared to the LPS-treatment condition was set to * $p < 0.05$; ** $p < 0.01$; *** $p < 0.001$.

4.3.2 Evaluation of NO release in BLECs culture media

Turning then to the *in vitro* model of BBB, in order to mimic CNS inflammation, TNFα was added at a concentration of 5 ng/mL for 24 h to the luminal compartment of the BBB model, corresponding to the blood side. Next, we assessed the nitric oxide levels - a critical biomarker in inflammation processes in BLECs culture media after exposure to TNFα, as well as after treatment and co-treatment with GLE and RE, performing the Griess reaction. Consistent with an inflammatory state and as shown in Figure 25 the NO level was higher after 24h TNFα exposure (*p*-value= 0.0001) and returned to levels comparable to the control when treated with GLE or RE alone or in the presence of TNFα.

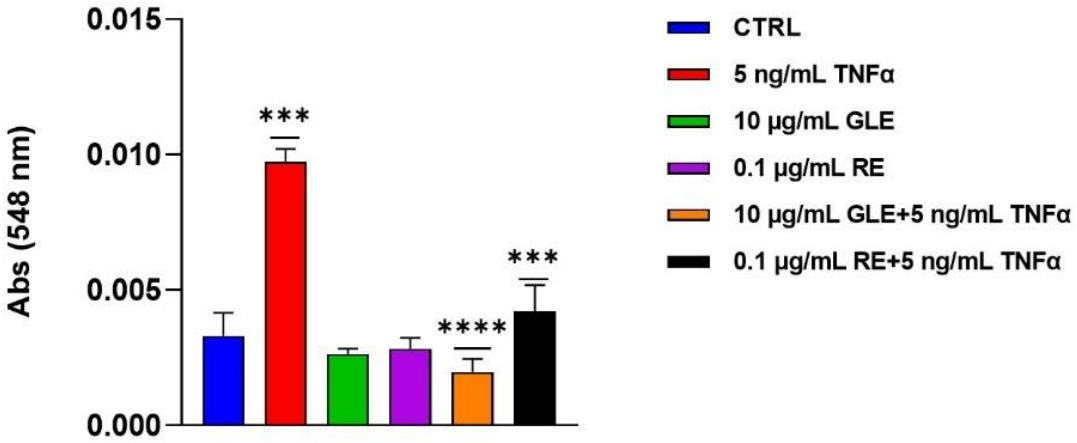

Figure 25. Effects of GLE and RE on nitric oxide release in BLECs culture media following TNFα exposure. NO levels were quantified using the Griess reagent. The histogram shows a significant increase in NO levels after 24 hours of TNFα exposure (*p*-value= 0.0001) However, treatment with GLE and RE, either alone or in combination with TNFα, resulted in OD values comparable to or lower than the control, indicating a potential anti-inflammatory effect at the concentration tested. In the graph each bar is representative of at least three independent experiments performed in triplicate. The one-way ANOVA test was used. The threshold for statistical significance compared to the control condition (for the TNFα, GLE and RE alone) and to the TNFα treatment- condition (for both co-treatments) was set to * $p < 0.05$; ** $p < 0.01$; *** $p < 0.001$; **** $p < 0.0001$.

4.3.3 Effects of GLE and RE on BBB permeability after TNFα exposure

To investigate the potential protective effects of GLE and RE on BBB permeability following TNFα-induced inflammation, we monitored the physical integrity of the BLECs by measuring the rate of sodium fluoresceine (NaFlu) passage, a small hydrophobic molecule, from the luminal to the abluminal compartment to calculate the endothelial permeability coefficient (Pe). As shown in Figure 26, treatment with GLE or RE alone resulted in Pe values similar to the control (0,54 x 10^{-3} cm·min^{-1} and 0,59 x 10^{-3} cm·min^{-1} respectively), confirming that these extracts do not alter the baseline permeability of the BBB. Instead, BLECs treated with TNFα for 24 h showed a significant increase in Pe values from 0,55 to 2,7 x 10^{-3} cm·min^{-1} compared to untreated controls. This increase in endothelial permeability coefficient (Pe), as expected, indicates a disruption of the BBB's integrity under inflammatory conditions.

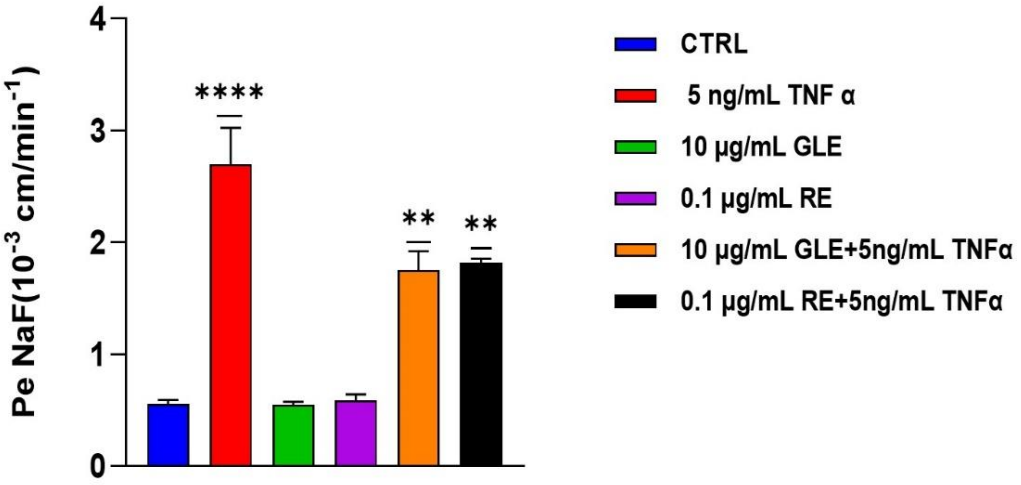

Figure 26. Effects of GLE and RE treatments alone and after TNFα exposure on BLECs permeability determined by measuring the endothelial permeability coefficient (Pe) of Sodium Fluoresceine. After TNFα exposure the Pe value is 2,7 x 10^{-3} cm·min^{-1} and increased compared to the control (0.55 x 10^{-3} cm·min^{-1}). Co-treatment with GLE and RE in the presence of TNF α reduced Pe values to 1,75 and 1,81 x 10^{-3} cm·min^{-1} respectively. When administered alone, both GLE and RE maintained Pe values comparable to those of the control (0,54 and 0,59 x 10^{-3} cm·min^{-1} respectively) indicating their potential role in preserving BBB integrity. In the graph each bar is representative of at least three independent experiments performed in triplicate. The one-way ANOVA test was used. The threshold for statistical significance compared to the control condition (for the TNFα, GLE and RE alone) and to the TNFα treatment- condition (for both co-treatments) was set to * $p < 0.05$; ** $p < 0.01$; *** $p < 0.001$; **** $p < 0.0001$.

However, when co-exposed to TNFα, Pe values were significantly reduced compared to TNFα treatment alone, indicating that both GLE and RE effectively attenuate TNFα-induced increase in BBB permeability (1,75 and 1,81 x 10^{-3} cm·min^{-1} respectively).

4.3.4 Effects of GLE and RE on Tight and Adherens Junctions at the BBB level

The integrity and functionality of the BBB are closely related to the various junctional complexes that regulate its permeability. Given that TNFα can induce modifications in BBB permeability that could be related to changes in the expression of proteins of tight and adherens junctions, the expression levels of Claudin-5 and VE-cadherin following treatment with GLE or RE, both in the presence or absence of TNFα were assessed by qRT-PCR, Western Blot, and immunostaining. This allowed us to determine whether GLE and RE can

counteract TNFα-induced changes in the expression of these key proteins. As shown in Figure 27A, the mRNA level of *CLAUDIN-5* significantly increased after TNFα exposure (by about 138.87%) compared to the control. The co-treatment with GLE or RE and TNFα result in an increase of *CLAUDIN-5* mRNA expression compared to TNFα treatment alone (respectively by 68% and 164.7%). In contrast, treatments with GLE or RE alone maintained *CLAUDIN-5* mRNA levels at values higher than the control (respectively 176.39% and 257.55%). Western blot analysis, presented in Figure 27B, further revealed that protein expression levels of CLAUDIN-5 were decreased across all experimental conditions compared to the control especially following TNFα treatment (about 0.4 fold). This suggest that while GLE and RE do not alter *CLAUDIN-5* mRNA levels in the presence of TNFα, they may influence protein expression in a manner that warrants further investigation.

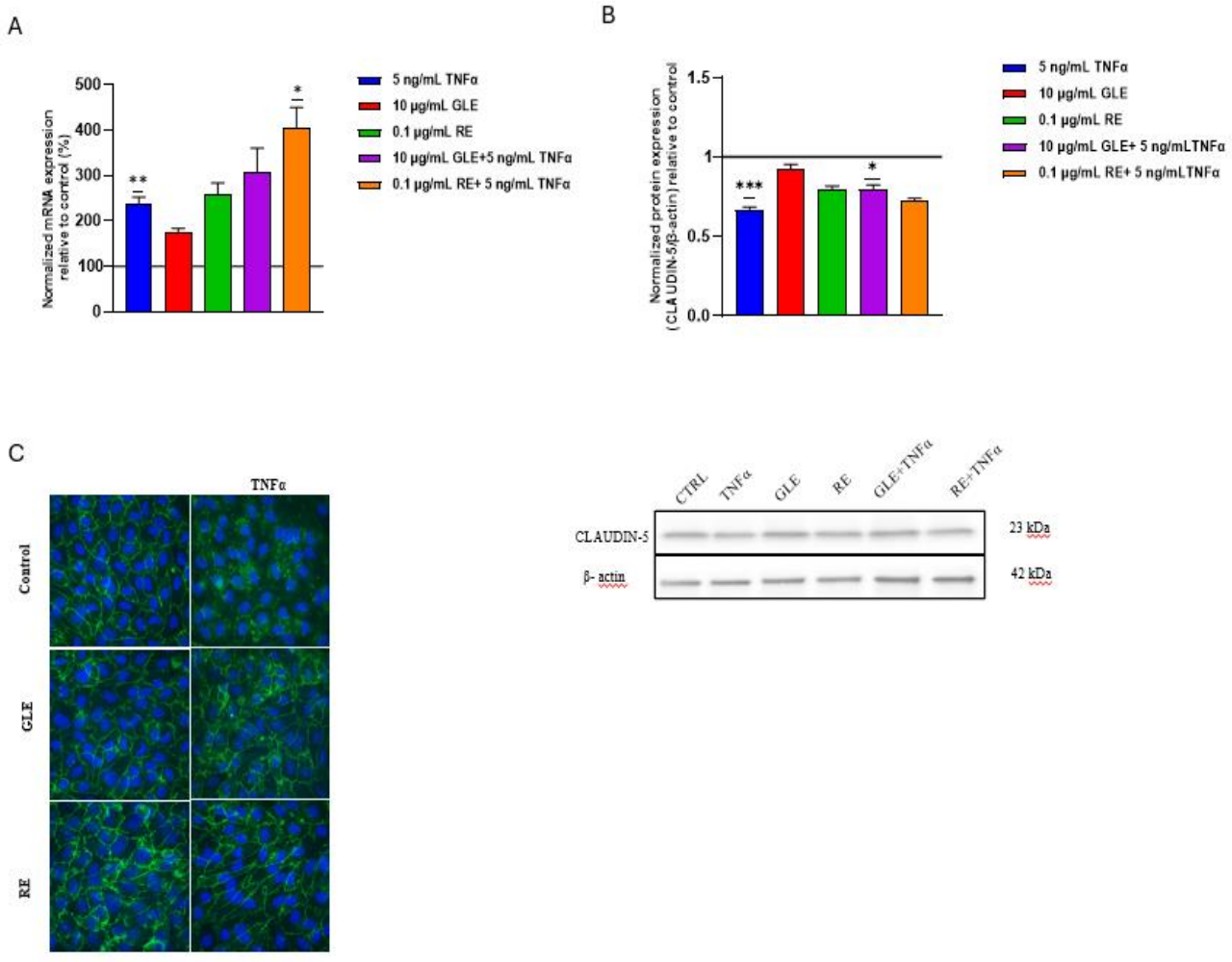

Figure 27. Effects of GLE and RE after TNFα exposure on the expression and the localization of the tight junction Claudin-5 determined by qRT-PCR (A), Western Blotting (B) and immunostaining (C). After 24 h treatment and co-treatment with TNFα, GLE or RE, mRNA (A) and protein (B) levels were quantified and

compared to the control condition. Staining of Claudin-5 (C), obtained using immunofluorescence, visualize the protein in green and the nuclei aee counterstained in blue. For all the above graphs, each bar is representative of at least three independent experiments performed in triplicate. Each bar represents the mean ± SEM relative to the control. The one-way ANOVA test was used. The threshold for statistical significance compared to the control condition (for the TNFα, GLE and RE alone) and to the TNFα treatment- condition (for both co-treatments) was set to * $p < 0.05$; ** $p < 0.01$; *** $p < 0.001$; **** $p < 0.0001$.

Changes in tight junctions protein expression induced by TNFα may be associated with changes in the localization of tight junction proteins.This latter event was investigated by immunofluorescence analysis. As shown in Figure 27C TNFα treatment alone led to the expected delocalization of tight junction proteins to cytosolic compartments. In contrast, co-treatment with TNFα and GLE or RE restored the proper localization of these proteins at the cell borders . Treatment with GLE or RE alone maintained protein localization comparable to control conditions. These findings indicate that GLE and RE can counteract TNFα-induced disruptions in protein localization, thereby potentially preserving BBB integrity. Referring to the *VE-cadherin*, its mRNA level (Figure 28A) was not significantly different following all experimental conditions except for the co-treatment with RE and TNFα, where an increase of 135.15 % compared to TNFα treatment alone was observed. At the same time, Western Blot analyses (Figure 28B) showed an increase in VE-cadherin protein across all experimental conditions, with a significant increase (0.47 fold) following TNFα exposure compared to the control. In this case, we also examined localization by immunofluorescence, that showed an increase in protein levels at the cell border, despite the observed change in morphology in the presence of TNFα. This increase confirms the protein's role in maintaining barrier architecture, especially under inflammatory conditions.

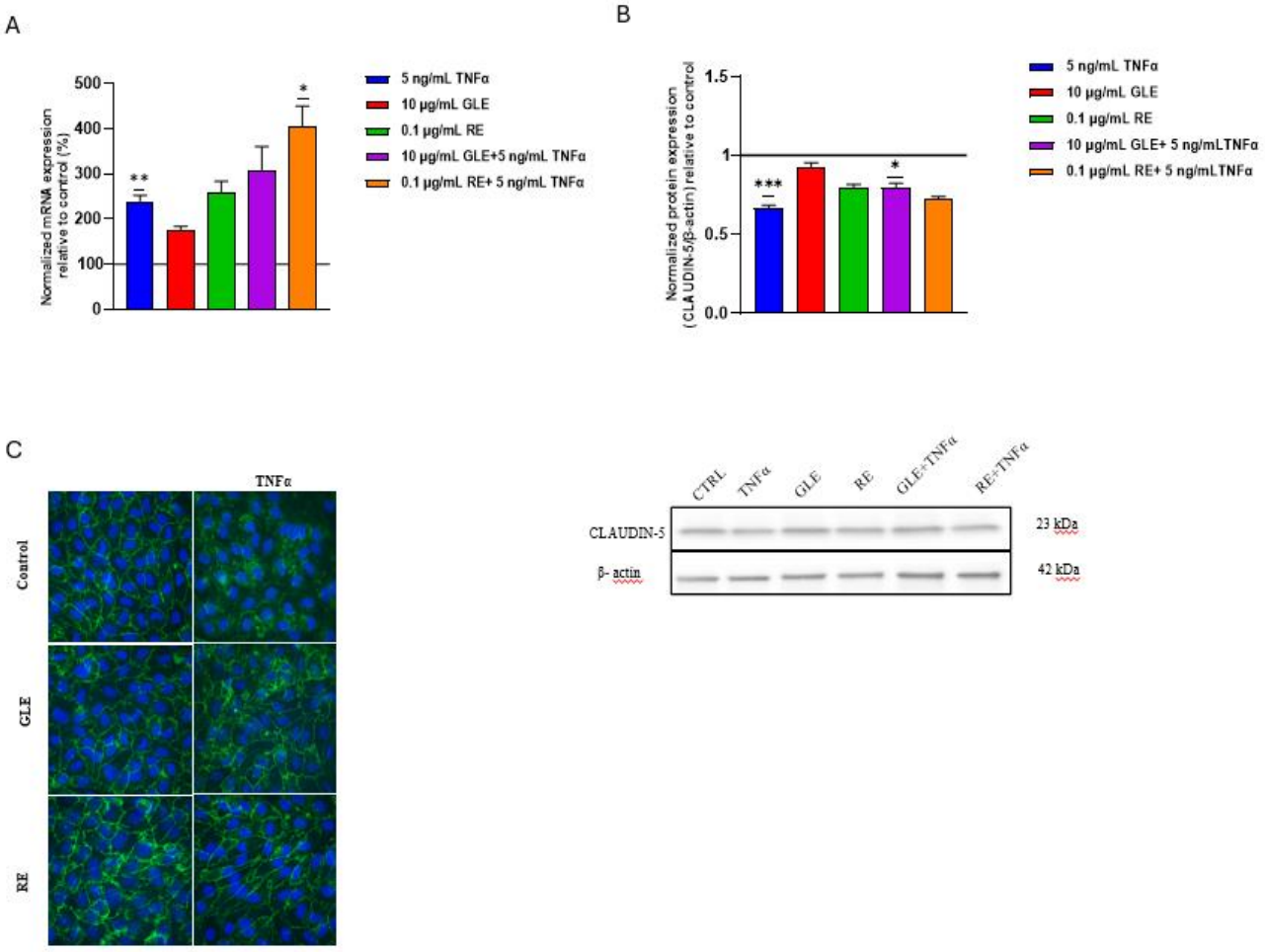

Figure 28. Effects of GLE and RE after TNFα exposure on the expression and the localization of the adherens junction VE-Cadherin determined by qRT-PCR (A), Western Blotting (B) and immunostaining (C). After 24 h treatment and co-treatment with TNFα, GLE or RE, mRNA (A) and protein (B) levels were quantified and compared to the control condition. Staining of VE-Cadherin (C), obtained using immunofluorescence, visualize the protein in green and the nuclei are counterstained in blue. For all the above graphs, each bar is representative of at least three independent experiments performed in triplicate. Each bar represents the mean ± SEM relative to the control. The one-way ANOVA test was used. The threshold for statistical significance compared to the control condition (for the TNFα, GLE and RE alone) and to the TNFα treatment- condition (for both co-treatments) was set to * $p < 0.05$; ** $p < 0.01$; *** $p < 0.001$; **** $p < 0.0001$.

4.3.5 Assessment of BBB inflammatory markers following treatment with GLE and RE

It is well known that ICAM-1 and VCAM-1 are important cell adhesion molecules typical of endothelial cells whose expression, absent or nearly absent under basal conditions, increases upon exposure to pro-inflammatory factors;therefore, they are widely recognized as markers of BBB inflammation. Given that GLE and RE have shown potential anti-

inflammatory properties, we assessed their effects on the expression levels of ICAM-1 and VCAM-1 by qRT-PCR and Western Blot analysis. As shown in Figure 28 and 29 mRNA and protein expression levels of both markers increase after TNFα exposure (by 401.74% and 1.29 fold for ICAM-1 - by 181.67 % and 19.13 fold for VCAM-1). Following treatment with the sole GLE or RE, ICAM-1 mRNA and protein levels were basal and absent, respectively, as in the control ; in contrast VCAM-1 mRNA and protein were maintained at basal levels. Following co-treatment with GLE or RE and TNFα, no reduction was observed for both markers at the transcriptional level compared with the treatment with the sole TNFα. ICAM-1 protein expression level was reduced after co-treatment with RE (by 0.4 fold) but not after co-treatment with GLE, in contrast VCAM-1 expression level was significantly reduced after both co-treatment (respectively by 8.53 and 12.46 fold).

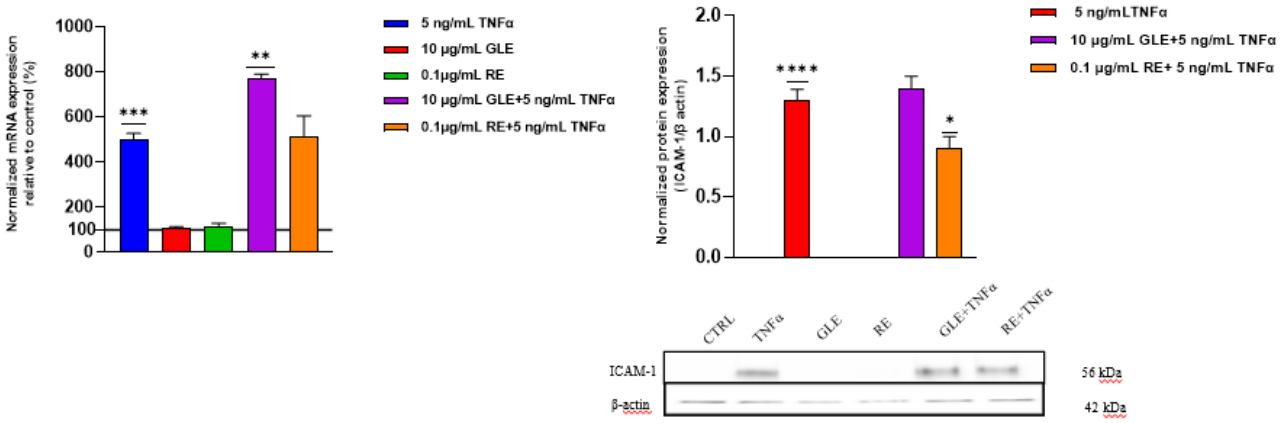

Figure 29. Effects of GLE and RE treatments after TNFα exposure on the mRNA and protein expression levels of the cell adhesion molecule ICAM-1. (Left) The black line correspond to the control (100%). After 24 h of TNFα exposure the mRNA level was increased (by 401.7 %) compared to the control. Co-treatments with GLE or RE and TNFα did not reduce mRNA levels but increased them or kept them to the level of the treatment with the sole TNFα. A condition comparable to the control was found after treatment with the sole GLE or RE (about 109.25% and 110.9% respectively). (Right) After 24 h of TNFα exposure the protein level was increased (by 1.29-fold). The increased levels were downregulated following co-treatment with RE (by about 0.4-fold) but not GLE. In control condition and after treatment with the sole GLE or RE alone, no protein expression was detected. For all the above graphs, each bar is representative of at least three independent experiments performed in triplicate. Each bar represents the mean ± SEM relative to the control. The one-way ANOVA test was used. The threshold for statistical significance compared to the control condition (for the TNFα, GLE and RE alone) and to the TNFα treatment- condition (for both co-treatments) was set to * $p < 0.05$; ** $p < 0.01$; *** $p < 0.001$; **** $p < 0.0001$.

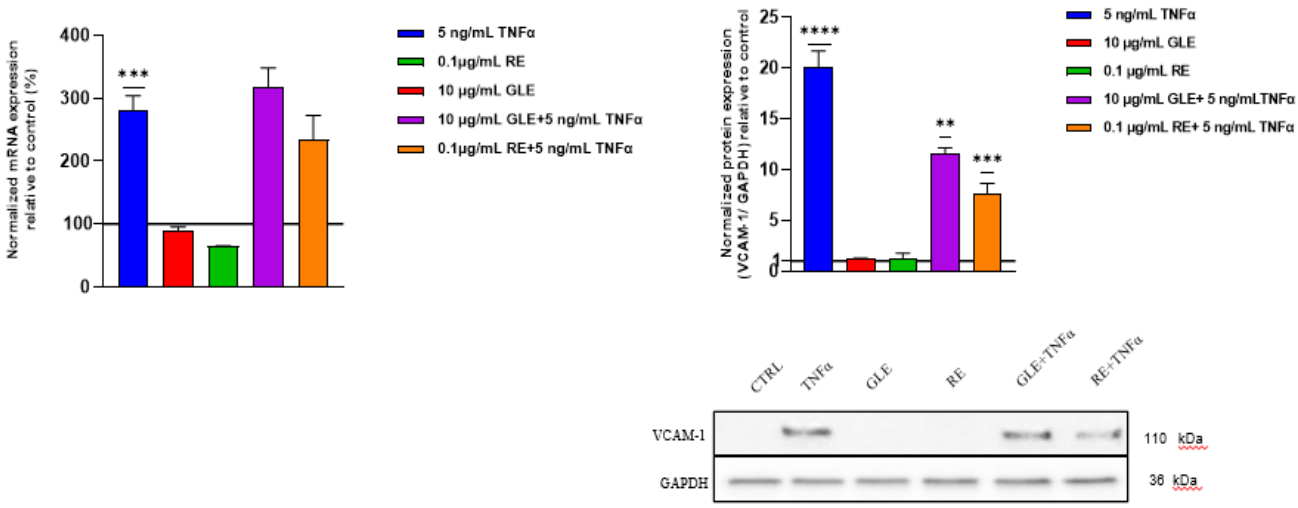

Figure 30. Effects of GLE and RE treatments after TNFα exposure on the mRNA and protein expression levels of the cell adhesion molecule VCAM-1. (Left) The black line correspond to the control (100%). After 24 h of TNFα exposure the mRNA level was increased (by 181.67%) compared to the control. Co-treatments with GLE and TNFα did not reduce the mRNA levels but slightly increased them; in contrast, co-treatment with RE slightly reduced the values. Conditions comparable to the control and slightly lower than the control were found after treatment with the sole GLE or RE (88.59% and 64.44% respectively) (Right) After 24 h of TNFα exposure the protein level was increased (by 19.13-fold). A significant reduction in protein expression levels was shown following co-treatment with GLE or RE (respectively by 8.53 and 12.46-fold). Treatment with the sole GLE or RE showed a condition comparable to control (1.21 and 1.31-fold) For all the above graphs, each bar is representative of at least three independent experiments performed in triplicate. Each bar represents the mean ± SEM relative to the control. The one-way ANOVA test was used. The threshold for statistical significance compared to the control condition (for the TNFα, GLE and RE alone) and to the TNFα treatment-condition (for both co-treatments) was set to * $p < 0.05$; ** $p < 0.01$; *** $p < 0.001$; **** $p < 0.0001$.

5. DISCUSSION

The aquatic ecosystem constitutes the largest habitat of Earth, hosting an enormous diversity of animal and plant organisms and representing an underexploited source rich in natural bioactive molecules, which only to a small extent have been investigated for their potential utilization as treatment agents for numerous disease states, e.g., (Lazzara et al., 2019; Luparello et al., 2020a; 2020b) ; Mauro et al., 2020; Punginelli et al., 2023).The present study was aimed to ascertain whether the water-soluble extracts from different anatomical parts of the seagrass *P. oceanica* grown in the northwestern Sicilian coast could exert any cytotoxic effect on HepG2 liver cancer cells (chosen as an *in vitro* model of a cancer histotype of the digestive system), anti-inflammatory effect at the central nervous system level using an *in vitro* human blood-brain barrier model and, along with the coelomic fluid of *H. tubulosa*, *in vitro* antidiabetic effect on HepG2 cancer cells, in this case chosen as a liver cell model for the study of glucose metabolism.

GLE and RE as modulators of autophagy and apoptosis on HepG2 liver cancer cells

The obtained results suggest the potential antitumoral effect of GLE and RE, whereas BLE failed to show any effect on cell numbers at all the concentrations tested. On the other hand, although we showed that 24 hour exposure to both RE and GLE reduced the number of cancer cells in a dose–response manner, with regard to the biological endpoints chosen, the two extracts did not appear appeared to produce completely overlapping effects. Referring to the number and nature of the polyphenolic compounds found in the two different biologically active Posidonia matrices, they were mostly in agreement with the data present in the literature (Messina et al., 2021; Ammar et al., 2021; Farid, 2018). The differences could be related to the extraction method followed and the volume/weight amounts extracted. Delphinidin-3-glucoside and quercetin 3-O-galactoside were the most abundant polyphenols in RE, while lower amounts of vanillic acid and some procyanidin dimers were above the threshold for quantification. Interestingly, Maciel et al., (2018)reported that a low amount (5.39 µg/mL) of the delphinidin-3-glucoside-rich aqueous extract from *Hibiscus sabdariffa* acted as LC_{50} (50% lethal concentration) in HepG2 cells, while Martínez-Alonso et al., (2022) showed that the delphinidin-rich red bean extract acted by reducing ROS production. In addition, quercetin 3-O-galactoside (also known as hyperoside) has been reported to arrest the cell cycle of HepG2 cell through down-regulation of the BMP-7/PI3K/AKT signaling (Wei et al., 2021). Akbar et al. (2021) demonstrated a substantial

inhibition of HepG2 cell viability by vanillic acid, which induced cell-cycle disruption through inhibition of cyclin-dependent kinase 2. In addition, procyanidin B2 and B3 showed antiproliferative activity against HepG2 cells, the former being a proven cell-cycle inhibitor and promoter (Huang et al., 2021 ; Ibrahim, 2019). Caffeic acid methyl ester is the most abundant polyphenol in GLE and its cytotoxic activity against HepG2 cells has been demonstrated by (Zhou et al., 2022). In addition, according to the data by Razali et al., (2015), it may be responsible for the prolonged reduction in ROS amount observed during GLE treatment. Furthermore, the reduced dissipation of MMP observed after exposure of HepG2 cells to GLE could be due to the recognized protective effect of the compound against mitochondrial dysfunctions in this cell line (Tsai et al., 2017). However, we cannot rule out the cooperation of other trace components of both GLE and RE in inducing the effects observed in our assays on HepG2 cells. In the search of other molecular components that might be involved in the cytotoxic activity described, we performed a proteomic analysis of GLE and RE, which allowed us to predict a number of protein signatures putatively responsible for the panel of biological implications observed. In addition, the protein component showed a certain degree of heterogeneity between the two preparations. Among the identified signatures, some may be associated with the down-regulation of autophagy. Indeed, it is known that hepatocytic autophagy is suppressed by adenosine kinase-mediated AMP formation and leucyl aminopeptidase overexpression(Samari & Seglen, 1998 ;Feng et al., 2022); acyl-CoA binding (ACB) protein has also been described as a suppressor of autophagy in breast cancer cells through its ability to bind to phosphatidylethanolamine of the phagophore membrane, resulting in the inhibition of LC3 lipidation (Udupa et al., 2023). Other protein signatures may be primarily associated with the onset of apoptosis, also in relation to the impairment of mitochondrial function and modulation of the autophagic flux. Zheng et al. (2022) demonstrated the cell-cycle inhibition and apoptosis activation effect of phosphoglucomutase over-expression on colorectal tumor cells via the PI3K/AKT pathway. Human CutA1 protein has been shown to sensitize HeLa cells to copper-induced inhibition of cell proliferation and promotion of apoptosis the mechanosensitive ion channel proteins have been reported to induce mitochondrial dysfunctions leading to reduced autophagy and intensified apoptosis (Shi et al., 2022). Adenosylhomocysteinase is known to promote adenosine-induced apoptosis in HepG2 and esophageal cancer cells, also blocking their motility, and to inhibit autophagy in osteosarcoma cells in an MTORC1-independent manner (Hermes et al., 2007 ; Huang et al., 2022 ; Li et al., 2014). In the mitochondria, the nucleoside-diphosphate kinase NME4 participates in supporting the externalization of cardiolipin following organelle dysfunction, thus signaling apoptosis (Schlattner et al.,

2018). Finally, a group of proteins exhibit antioxidant properties. High ROS scavenging capacity has been found for recombinant 2-Cys peroxiredoxin from *Citrus sinensis* in Vero cells, for heterologous ferredoxin-NADP reductase in Cos-7 cells, and for recombinant peptidylprolyl cis-trans isomerase from *Pyropia yezoensis* in HepG2 cells (Mediavilla et al., 2010) (Kim et al., 2017 ;Gupta et al., 2022).On the other hand, the protective effect of glutathione reductase, glutathione transferase, and superoxide dismutase against oxidative damages is well-known (Couto et al., 2016; Elhusseiny et al., 2021). Interestingly, Aniya & Imaizumi (2011) reported that glutathione transferase bound to the mitochondrial membrane can form a permeability transition pore, which leads to the loss of MMP. Given the selective presence of this protein in RE, it may be responsible for the increased population of cells showing mitochondrial depolarization following exposure to this extract. At present, we have no data confirming whether these proteins present in the aqueous samples can be effectively internalized by the cells and can exert their putative functions, apart from peptidyl-prolyl cis-trans isomerase that has been successfully administered as an antioxidant to HepG2 cells and superoxide dismutase that, together with its conjugates and mimetics, possesses a significant recognized therapeutic action/potential against several diseases in humans and animals (Aniya & Imaizumi, 2011; Kim et al., 2017; Younus, 2018; Elhusseiny et al., 2021). A study carried out on experimentally edematous mice assessed the anti-inflammatory role of a methanolic extract from *H. tubulosa* through the partial inhibition of cyclooxygenase-2 activity. On the other hand, it is worth-mentioning that we (Punginelli et al., 2023; Abruscato et al., 2023) have recently shown that an isolated peptide obtained from RE exhibits an apoptotic-promoting ability on HepG2 cells, thus providing a first direct indication of the contribution of the protein component of the extract to the cytotoxic effect. Exposure to both extracts was found to reduce ROS accumulation as early at 4h of exposure, while after 24 h, although RE-induced ROS generation on individual cells was comparable to that of the control, the fraction of ROS+ cells was drastically reduced in the entire population. The decrease in intracellular ROS levels has been documented in quercetin-treated HepG2 cells by Jeon et al. (2019) and linked to the anti-proliferative effect of the compound. The apoptotic-promoting role of ROS reduction in HepG2 cells was explained by Liu et al. (2014), in terms of lacking the necessary amount of an important class of redox-active signaling molecules required for cell survival and growth. Autophagy is an important pathway that plays a key role in normal physiological processes, under various stress conditions, i.e., in the presence of damaged organelles or misfolded aggregated proteins, and under conditions of nutrient deprivation. The modulation of autophagy plays dual roles in tumor suppression and promotion in many types of cancers. Much evidence supports

modulation of autophagy as a promising and potential therapeutic target (Mizushima, 2007; Morel et al., 2017;Yun & Lee, 2018). High levels of basal autophagy, such as those observed in HepG2 cells, enable cancer-cell survival, growth, and motility by meeting the high metabolic and energetic demands (Luparello, 2021). Therefore, the suppression of "protective" autophagy could be one of the cytotoxicity mechanism of the extracts under study leading to the inhibition of cell proliferation and the promotion of apoptosis. Interestingly, the reversion of autophagy inhibition by rapamycin was sufficient to restore cell viability in the presence of GLE, whose effect on the down-regulation of autophagy, as well as MMP dissipation and decrease in clonogenic potential was milder than in RE treatment, thus suggesting, in the latter case, a more extensive and multitarget cellular damage of death than simple autophagy inhibition. The more pronounced alteration of HepG2 cells' healthy state by RE also emerged from the stronger inhibition of cell motility, as observed in the wound-healing assays, thus suggesting that this preparation may be a potential potent suppressor of the metastatic attitude of liver cancer cells. At the molecular level, our data showed that autophagy in HepG2 cells has been modulated, especially from 14 to 24 h of exposure and with greater effect for RE- treated cells than for GLE-treated cells. However, in both cases there was a reduction in the early and late autophagic processes, monitored by Beclin-1 accumulation and LC3-II/LC3-I ratio, respectively. On the other hand, during the early stages of treatment (4 h), autophagy levels seemed to be more evident in the treated sample than in the control, but this was recorded only for the late autophagy process (LC3-II/LC3-I ratio) and not for the early autophagic process (quantitation of Beclin-1). This result could be justified, considering that LC3-II marker levels do not depend directly on its translation but on a post-translation modification, i.e., the rapid conversion of LC3-I to LC3-II through a lipidation event. Therefore, in the early times of exposure, the cells already seemed to perceive the effect of the treatments, transiently triggering a defense mechanism represented by the rapid conversion of LC3. At the same time, AVOs levels were reduced at this early stage. As it is well known, by promoting the digestion of the content of autophagosome, the LC3-II protein itself begins to be degraded in these acidic vesicles. In fact, since there was a reduction in AVOs after both treatments, and thus a reduction in the number of autophagosomes fusing with lysosomes, the autophagic organelles were left with their membrane marker intact (LC3-II). A decrease in the levels of LC3-II/LC3-I ratio was observed in treated cells after 14 and 24 h of exposure (again with greater effect for RE treatment than GLE), when AVOs levels were very low. Therefore, this decline in the autophagic process could be attributed to the direct action of the treatments on autophagic protein expression. These data were confirmed by the Beclin-1 protein levels in the Western

blot assays, being the signals consistently very low in the treated samples compared with the control samples and showing a more pronunced effect for RE- than GLE-treated cells. The monitoring of the changes of the amount of proteins destined for autophagic degradation was accomplished by the analysis of the p62/SQSTM1 marker. It could be observed that, after 14 h, the GLE-treated cells showed a peak of this marker, indicating the possible activation of a cytoprotective mechanism. This result was confirmed by the peak for hsp60 detected after this treatment, confirming that a probable cytoprotection against the accumulation of damaged proteins was active. After 4 h of treatment, hsp60 levels detected in both treatments were low compared with the control, indicating a possible early reduction of stress due to the clearance process promoted by autophagy (high levels of LC3-II/LC3-I ratio). However, in general, there was a reduction in the autophagic processes for longer treatment times and this was conceivably related to the simultaneous activation of apoptotic processes, which were marked after 24 h of exposure. Indeed, at this stage, p62/SQSTM1 protein levels were elevated in GLE- and especially RE-treated cells, indicating the accumulation of protein aggregates that the cells were unable to eliminate due to the suspension of the autophagic clearance process and the simultaneous triggering of apoptotic cell death. In this context, as expected, a parallel reduction in the cytoprotective mechanisms exerted by hsp60 has been shown, thus confirming a synergistic effect of the treatments that reduce defense strategies, i.e., autophagy and cytoprotective mechanisms against stress, and increase cell death processes. Taken together, these data suggest that cells exposed to the extracts initially promote defense strategies, while they appear to offer less resistance to the persistence of the exposure and reduce the cell survival processes (autophagy) and the cytoprotection, giving way to the degenerative processes. We explored the cellular response following exposure to the extracts by studying the activation levels of caspases—key mediators of apoptosis—in order to identify also a possible relationship with other mechanism of cell survival or death. It is known that there is a crosstalk between autophagy and apoptosis in cancer(Yogev et al., 2010) and that caspases may be involved in autophagy (Tsapras & Nezis, 2017). Among the initiator caspases, we did not detect the increase in signals related to caspase-8 and -9 (indicative of the activation of the extrinsic and intrinsic pathway, respectively), but the presence of cleaved caspase-1 and -2 was observed after 24 h for both extracts. Cleavage of caspase-1 was shown to correspond to the increased rate of apoptosis recorded in xanthoangelol-treated HepG2 cells (Pang et al., 2021) and, similar to what we observed for RE- and GLE-treated cells, the increase in its activation in hepatocytes was accompanied by a reduction in autophagy, as evidenced by the loss of LC3 and Beclin-1. Caspase-2 possesses characteristics of both initiator and effector caspases (Vigneswara &

Ahmed, 2020) and has been identified as the only activated caspase involved in the onset of apoptosis following exposure of HepG2 cells to TNFα (Tsagarakis, 2011). In general, its activity is related to ROS scavenging and negative regulation of autophagy (Shalini et al., 2012; Tiwari et al., 2014). Our data are in line with these findings, since, under the experimental conditions used, we observed a decrease in ROS accumulation and ROS+ cell population and the down-regulation of AVOs and the autophagic markers LC3-II and Beclin-1, the latter especially in samples of RE-treated cells. Among the executing caspases, we observed a marked increase in cleaved caspase-3 signals after 24 h of GLE treatment and a significative increase in those of activated caspase-6 for both treatments compared with the controls. Apoptosis of HepG2 cells after bile acid treatments was reported to be caspase-6 dependent, while the activation of caspase-3 was found to be responsible for the apoptotic death of HepG2 cells after exposure to sulforaphane and ursolic acid, in the latter case due to the inactivation of the PI3K/Akt/survivin pathway; in addition, caspase-3 was shown to inhibit ROS generation, similarly to what was prominently observed in our experimental system in the presence of GLE. These two caspases have been located upstream or downstream of each other in different experimental systems, suggesting the existence of a complex pattern of reciprocal interactions (Park et al., 2007; Rust et al., 2009; Tang et al., 2009). Moreover, in this case, we found a correlation with the autophagic state observed in our assays for exposed cells. Indeed, as reported in the literature, several pro-apoptotic caspases directly interact with essential ATG proteins and cleave them, resulting in the inhibition of autophagy; for example, caspase-3 cleaves Beclin-1 and inhibits autophagy (Klionsky D.J. et al., 2021b). On the other hand, caspase-6 has a role in p62 cleavage, and N-terminal p62 cleavage product of caspase-6 (p62-N) plays a dominant negative role in blocking p62-droplet and autophagosome formation (Valionyte et al., 2022), confirming a modulation of autophagy through the caspase-6—p62 axis in the presence of certain stress stimuli. Similarly, this was also observed in our experiments, where, considering the whole treatment, the lowest levels of p62 were detected after 24 h of exposure, particularly in the presence of GLE. The results obtained on caspase activities, taken together, allow us to hypothesize that, in the response to the treatments on HepG2 cells, a crosstalk between autophagy and apoptosis exists, suggesting that the observed response is modulated through the orchestration of these processes.

GLE and CFE differently modulate the glucose uptake and metabolism in HepG2 cells

The studies conducted have also allowed us to attribute a promising efficacy of the GLE as another potential anti-diabetic agent to be added to the existing lists, while the RE showed no effect. The dysfunction of glucose metabolism that occurs in diabetes mellitus sees the nodal involvement of the GLUT transporters. In the hepatocytes, in particular, the glucose flux is mainly mediated by GLUT-2, the insulin-independent transporter, which is responsible for glucose uptake but, in some cases, also for glucose output, thus controlling the balance between the intracellular and extracellular glucose concentration (Thorens, 2015). Interestingly, Yonamine et al. (2017)reported that the resveratrol-mediated restoration of the glycemic homeostasis in diabetic mice resulted in decreased GLUT-2 expression in the liver, possibly due to reduced hepatic glucose outflow. On the other hand, GLUT-4 is characterized by its responsiveness to insulin signaling that triggers the translocation of GLUT4-containing vesicles to the membrane via the insulin-stimulated IRS1/PI3K/AKT pathway (Kouznetsova et al., 2017). Thus, an alteration in the expression level of GLUTs and a reduction in both the recruitment of GLUT-4 from cytoplasmic vesicles and its positioning on the cell surface are molecular alterations that contribute to the disruption of the glycemic control in diabetes mellitus. The data obtained show that, as reported for other natural products, e.g. Kim et al., 2017; Mokashi et al., 2017 ; Zhang et al., 2019; Chen et al., 2017), GLE resulted in an increased gene expression level of IRS1, an increased activation of AKT and in the up-regulation of GLUT-4 transcription and translation levels, followed by an increased exposure of the transporter on cell membranes. This is consistent with the increased glucose consumption and internalization observed with GLE treatment.In the present study, however, we found no significant change in HNF1α protein, whereas we observed a limited down-regulation of GLUT-2 in GLE-treated cells; this could be related to a reduction in the glucose efflux by HepG2 liver cells, as reported in (Yonamine et al., 2017), although further experiments will be needed to confirm this correlation. The polyphenolic and protein composition of the GLE used in the present experiments was studied and reported in Abruscato et al. (2023). In light of literature data, some of these molecules in the extract could be associated with its effects in reducing extracellular glucose and regulating GLUT in HepG2 cells. Regarding the polyphenols present in the GLE, but not in RE, methyl ester of caffeic acid, which is the most abundant compound found in the preparation, and the trace constituents ellagic acid, kaempferol, p-coumaric acid and procyanidin B2 were all shown to stimulate glucose uptake in different cell lines, including HepG2, mainly through the increased expression and translocation of GLUT-4 mediated by

insulin- and/or 5' AMP-activated protein kinase (AMPK)-dependent mechanisms (Chen et al., 2010; Yoon, 2013; Eid et al., 2017; Poulose et al., 2011; Yamashita et al., 2016) Dealing with the previously-cited proteomic analysis of GLE and RE based on mass spectrometry (Abruscato et al., 2023) we have performed a bioinformatic similarity search and identified five protein signatures contained exclusively in the GLE or over-represented in this preparation compared to RE, which may be potentially associated with the anti-diabetic property of the extract.

Accession number/ Protein description	**GLE amount**	**RE amount**
A0A0K9PU80 Glutamine synthetase	8.75E+04	0
A0A0K9NY84 Cysteine synthase	1.43E+05	0
A0A0K9P881 Leucyl aminopeptidase	9.56E+04	4.23E+04
O47254 Ribulose bisphosphate carboxylase large chain (Fragment)	1.81E+07	0
A0A7I8IZJ3 UTP:glucose-1-phosphate uridylyltransferase	3.01E+05	1.61E+05

Table 6. Glucose metabolism-associated proteins of the extracts from *P. oceanica.*

Table 6 shows the identity of the proteins and their relative semi-quantitative abundance in GLE and/or RE samples. Glutamine synthetase, essential in the liver to remove ammonia waste, is involved in glutamine synthesis by condensing NH_4^+ and glutamate (Frieg et al., 2021; Kohno et al., 1986). Wang (2018) reported that the over-exposure to glutamine lead to the glucose uptake of L6 myoblasts via the activation of the PI3K/AKT/GLUT-4 signalization and glycogen synthesis pathway. Leucyl aminopeptidase, metalloenzyme cleaving N-terminal residues from proteins and peptides, has been isolated from different tissues including human liver (Kohno et al., 1986). Interestingly, a leucyl aminopeptidase of 3T3-L1 adipocytes has shown a profound effect on GLUT-4 traffic through the regulation of the sorting of the carrier from endosomes to GLUT-4 specialized vesicles thus acting as an

important controller of the insulin-dependent pathway (Jordens et al., 2010). UTP: glucose-1-phosphate uridylyltransferase promotes the synthesis of UDP glucose, a glucosyl donor that is a direct precursor for the biosynthesis of glycogen in HepG2 cells (Bertram et al., 2015). The other two enzymes are not present in human cells however their products, possibly contained in the water-soluble GLE, could act on glucose metabolism. Particularly, cysteine synthase is the enzyme that produces L-cysteine and acetate from O3 -acetyl-L-serine and hydrogen sulfide. Achari & Jain (2016) indicated L-cysteine supplementation as decisive in the increase of GLUT-4 protein expression and glucose utilization in both 3T3-L1 adipocytes and a rodent model. Ribulose bisphosphate carboxylase/oxygenase (Rubisco) is the enzyme responsible for carbon dioxide fixation and photorespiration in the green leaves of plants; rubiscolin-6 is a six aminoacids-peptide obtained from Rubisco cleavage and characterized by high affinity with opioid receptors. Kairupan et al. (2019) indicated that after binding to the these receptors in the skeletal muscle cells, rubiscolin-6 enhanced the glucose uptake, maybe through an activation of AMPK leading to the up-regulation of GLUT-4 translocation. As previously reported, in parallel with *P. oceanica*'s extracts, the anti-diabetic effects of the coelomatic fluid of *H. tubulosa* were tested. Isolated compounds from other holothurians, such as the polysaccharides from *H. leucospilota* and *C. frondosa,* the AHG glycosaminoglycan from *A. japonicus*, the saponin from *H. thomasi*, and the eicosapentaenoic acid-enriched phosphatidylcholine from *C. frondosa*, have been proven able to reduce blood glucose levels and improve the biochemical and histological markers of diabetes mellitus in experimental animal models through the nodal involvement of the GLUT transporters (El Barky et al., 2016; Chen et al., 2019; Zhao et al., 2020; Zhu et al., 2020; Hu et al., 2014). In addition, an ethanolic extract of the golden sea cucumber *S. hermanii* was found to restore the glucose uptake and utilization in the muscles of diabetic rodents by enhancing the level of GLUT-4 protein (Purwanto et al., 2019). Here we report the first evidence linking the treatment of liver cells with an extract derived from *H. tubulosa* with the modulation of glucose metabolism, revealing a promising efficacy of the preparation as an additional potential anti-diabetic agent. Our study shows that, in analogy with other natural substances, e.g., (Chen ; Kim et al., 2017; Mokashi et al., 2017) , the CFE induced the upregulation of IRS1 gene expression and increased transcription and translation levels of AKT and GLUT-4. In addition, the phosphorylation level of AKT was increased by the treatment. On the other hand, the transcription and translation of HNF1α were equally increased, whereas, although an increase in GLUT-2 was observed, we were unable to find any upregulation of GLUT-2 mRNA expression. As reported in other model systems (Fu et al., 2023; Zhang et al., 2012), this suggests the existence of a mechanism of GLUT-2 protein

regulation at the level of translation or by post-transcription stabilization, which has yet to be determined. In parallel with the increased synthesis of GLUT-2 and -4 transporters, their significantly higher membrane translocation following treatment was also found. This molecular reprogramming plausibly enhanced the glucose response by HepG2 cells, leading to a clear increase in the glucose consumption/uptake and glycogen accumulation to levels comparable to those of insulin treatment. Proteins are the main components of the cell-free coelomic fluid of echinoderms, and studies of its protein composition aimed at the identifying factors related to regeneration- and response to injury have appeared in the literature (Shabelnikov et al., 2019; Gomes et al., 2022b). Previously we performed (Luparello et al., 2022) a proteomic profiling of the CFE from *H. tubulosa*, obtaining a final result of 115 forward and 20 reverse proteins and 321 unique forward peptides which were subjected to bioinformatic similarity search with different databases. We re-evaluated this result looking for entries that could be associated with the extracellular glucose-lowering effect of the CFE on HepG2 cells and made the following considerations: (i) No insulin or insulin analogs were found among the protein components of the CFE; (ii) As previously reported in Luparello et al. (2022), the analysis of the mixture showed the presence of proteins typical of the exosomes that are plausibly kept intact by the CFE preparation method and thus may stimulate the observed effects upon fusion with HepG2 cells and intracellular transfer of their cargo; (iii) Among the other protein signatures identified in the comprehensive analysis, three could be related to the increased GLUT-4 recruitment and activation. Their peptide sequences and the results of the selected alignments on the basis of best E value sorting are reported in Table 7. Specifically they are as follows : (1) Huntingtin-interacting protein 1 (HIP1), implicated in clathrin-mediated endocytosis and intracellular protein trafficking (Hyun & Ross, 2004). It is known that HIP1 interacts with the CHC22 clathrin isoform, which is also expressed in HepG2 cells (Esk et al., 2010), thus maintaining its proper functioning that targets the proper formation of the intracellular storage compartment for the GLUT-4 transporter (Ybe, 2014). The dysfunction of this mechanism has been related to the onset of diabetes mellitus (Vassilopoulos et al., 2009). (2) Small ubiquitin-like modifier (SUMO)/sentrin-specific protease 1 (SENP1), a cysteine protease that catalyzes the deSUMOylation of protein substrates, thus controlling the intracellular localization and function of the targets (Vertegaal, 2022). Among these, the transcription factor HIF1α, regulator of the mobilization of GLUT-4-containing vesicles to the plasma membrane in skeletal muscle cells (Sakagami et al., 2014), is stabilized by deSUMOylation through SENP1 activity. Therefore, it could plausibly stimulate increased glucose uptake through surface accumulation of GLUT-4 (Cheng et al., 2007). (3) TBC1 domain family

member 17 (TBC1D17), which is a Rab5 GTPase-activating protein. In myoblasts and skeletal muscle cells, the AMPK-induced phosphorylation of TBC1D17 leads to the activation of Rab5, recognized as recruiter of multiple molecules involved in GLUT-4 translocation (Rao et al., 2021).

Peptide sequence	Sequence ID (range)	Expected	Identities (%)	Positives (%)	Protein description (organism)
GRSAPSQGPNNGR	PIK47307.1 (459-471)	0.008	100	100	putative huntingtin-interacting protein 1 isoform X3 (*Apostichopus japonicus*)
MSVSILDSMDTGKG	PIK42614.1 (182-195)	$1e^{-04}$	100	100	putative sentrin-specific protease 1-like (*Apostichopus japonicus*)
KQVLTQAEGLVRE	PIK61193.1 (430-442)	0.002	100	100	putative TBC1 domain family member 17 (*Apostichopus japonicus*)

Table 7. Glucose metabolism-associated proteins of the CFE from *H. tubulosa.*

GLE and RE exert a protective effect on BLECs belonging to an in vitro model of BBB

It is also well known that in recent years, there has been an increasing interest in bioactive compounds, such as omega-3 fatty acids and antioxidants, due to their potential neuroprotective effects and their ability to support blood-brain barrier (BBB) health by reducing inflammation and oxidative stress (Wen et al., 2024). Within this context, extracts from *P. oceanica* are particularly noteworthy, as they are rich in polyphenols, which are recognized for their antioxidant and anti-inflammatory properties (Abruscato et al., 2023) Despite this promising profile, there is a notable lack of published studies specifically addressing the effects of these extracts on the BBB. However, it is essential to conduct specific studies to elucidate the mechanisms underlying this interaction and to assess the potential effects of these extracts on the integrity and function of this barrier. An *in vitro* approach is necessary for this purpose, as while *in vivo* models are valuable, they do not specifically focus on the endothelial cells of the cerebral capillaries that provide the anatomical support for the BBB. The *in vitro* model of the human blood-brain barrier developed by the LBHE was therefore utilized. This model consists of a co-culture of endothelial cells (derived from CD34+ cells) and brain pericytes (Cecchelli et al., 2014). To investigate the potential protective effects of GLE and RE against BBB permeability

following TNFα-induced inflammation, we first examined NO release in the culture media and the effects of these extracts on the physical integrity of the endothelial cell monolayer. Our findings reveal a typical increase in NO levels in the media of cells treated with TNFα alone, which aligns with the expected inflammatory response. Interestingly, this increase was not observed in the control conditions, it did not persist in the experimental conditions involving GLE and RE treatment. Consisting with our findings Shin et al. (2004) and Wu et al. (2023) attested, even though using an *in vitro* model of LPS-inflamed RAW 264.7 cells the reduction of nitric oxide levels in the culture medium after treatment of the same cells respectively with caffeic acid and its derivatives, present in various medicinal plants, and with the glycosidic fraction of *Picrorhiza scrophulariiflora Pennell (GPS).* Additionally Y. Kim et al. (2022) demonstrated that quercetin, administered in vivo to female rats subjected to oxidative stress from polychlorinated biphenyls, provided a protective effect on the BBB. This protection was evidenced by an increase in the expression levels of Claudin-5, coupled with a reduction in alterations in permeability and inducible nitric oxide synthase (iNOS) expression levels. Similarly, we found that both GLE and RE preserved the physical integrity of the endothelial monolayer, indicating their potential role in mitigating the inflammatory impact on BBB integrity. Moreover, both GLE and RE were shown to potentially mitigate TNFα-induced increases in BBB permeability, suggesting they may reduce the permeability disruptions caused by inflammatory signaling from TNFα. Based on these observations, we sought to explore whether these extracts could also influence the reorganization and function of junctional complexes within the BBB. To assess this, we examined the potential effects of GLE and RE on two key proteins: Claudin-5, a representative tight junction (TJ) protein essential for barrier integrity, and VE-cadherin, a crucial adherens junction (AJ) protein involved in endothelial cell adhesion. Based on our results, both GLE and RE demonstrated a potential protective effect on BBB integrity Consistent with the work of Versele et al. (2022), who demonstrated that TNFα alone modulates BLECs morphology and Claudin-5 expression, our Western blot and immunofluorescence analyses confirmed elevated Claudin-5 expression levels. Immunofluorescence further revealed cytosolic delocalization of Claudin-5 following TNFα treatment, indicating increased cell permeability in this condition. However, co-treatment with GLE or RE restored Claudin-5 localization at the cell borders, despite some morphological changes, suggesting a protective role of the extracts in maintaining TJ integrity. Similarly, our immunofluorescence analysis of Ve-Cadherin, responsible for maintaining barrier architecture, showed increased expression levels following co-treatment with GLE or RE, further supporting their protective effect on BBB structure, referred to the ability to preserve the functional organization of tight junctions,

during inflammatory conditions. Finally ICAM-1 and VCAM-1 expression levels were evaluated to test the inflammatory response of endothelial cells. Their expression is in fact suppressed under physiological conditions and increased under stress conditions, e.g. inflammation, ensuring the recruitment of leukocyte populations (Moon et al., 2009) and also driving via calcium-mediated pathways to the cytoskeleton deregulation (Kim et al., 2022). Given that inflammation typically upregulates ICAM-1 and VCAM-1, contributing to increased BBB permeability, we aimed to determine if GLE and RE could counteract this effect and help normalize their expression levels. The inflammatory response of BLECs to TNFα was confirmed by qRT-PCR and Western Blot analyses, which showed that following treatment with GLE and RE alone, as well as under basal conditions, these proteins are not expressed or expressed at basal levelsHowever following co-treatment GLE and RE the TNFα-induced increasein these adhesion molecules was significantly s with the most notable effect observed in the case of VCAM-1 and particularly following co-treatment with RE. This aligns with the findings of Kim et al., (2022) who reported that resveratrol, a key component of RE, inhibited the expression of the same adhesion molecule. Moreover, similar studies by Liu et al. (2018) demonstrated that other polyphenols could effectively downregulate ICAM-1 and VCAM-1 expression under inflammatory conditions, further supporting the potential anti-inflammatory effects of these extracts In support of the analysis performed and results obtained the research by Zhao et al. (2022) and Sweeney et al.(2019) reinforced the idea that these antioxidant compounds can enhance endothelial cell integrity and function, highlighting their importance in neuroprotection. Collectively, these findings suggest that GLE and RE may play a significant role in modulating endothelial cell inflammation and preserving BBB integrity thus they could represent a promising therapeutic strategy to counteract the neuroinflammatory processes.

6. CONCLUSION AND FUTURE PERSPECTIVES

In conclusion, we have demonstrated the cytotoxic and protective effects of aqueous extracts from different anatomical parts of the seagrass *P. oceanica*, (green leaves and rhizomes) in a liver cancer cell model system and an *in vitro* model of human blood-brain barrier. Our results identified respectively death-promoting mechanisms that include the modulation of autophagy, apoptosis, cell redox status and the impairment of MMP, and also a reparative mechanism on BBB alteration, caused by inflammation, through predominantly restoring the proper localization of Tight and Adherens junctions and a reduction of ICAM-1 and VCAM-1 expression levels. The effects found are probably attributable to specific phenolic compounds and proteins identified. Furthermore, it is necessary to underline that the comparative study made with the GLE and RE indicates that the phytocomplexes extracted from the different parts of the seagrass and possessing different constituents do not share the same bioactive potential (Abruscato et al., 2023). In addition, we have demonstrated, through *in vitro* studies on an experimental model of cultured liver cells and a panel of cellular and molecular analyses, an evident increase in glucose consumption/uptake and glycogen storage after the exposure of HepG2 cells to the CFE and GLE. The molecular reprogramming underlying this effect includes the upregulation of (i) IRS1 gene expression, (ii) the transcription and translation levels of HNF1α, AKT, and GLUT-4, (iii) the phosphorylation level of AKT, (iv) the synthesis of GLUT-2 protein, and (v) the translocation of GLUT-2 and - 4 transporters onto the plasma membrane. Also in this case the component(s) of the CFE and GLE responsible for the observed effects was (were) not isolated. However the analysis of the proteomic profile suggested the presence of some proteins that can apparently enhance GLUT-4 activity. Obviously, we cannot exclude the contribution of other trace proteins undetected in the proteomic analysis and/or non-protein and non-polyphenolic water-soluble constituents, as well as the occurrence of synergic activities between the compounds present. Future works will be aimed at identifying the substance(s) responsible for the reported effects and to a more thorough evaluation of the underlying molecular mechanism(s) responsible for the positive effects found. In the specific case of the BBB, analyses regarding transporters (influx and efflux pumps) and mechanisms underlying the inflammatory process will allow us to assess whether anti-inflammatory effects can effectively be attributed to GLE and RE and in which manner the passage of these molecules at the level of CNS cells occurs. The ultimate goal would be the development of novel alternative agents for prevention and/or treatment of liver tumors, diabetes mellitus, neuroinflammatory diseases and beneficial supplements for the formulation of functional

food and food packaging materials endowed with antioxidant, anticancer and antidiabetic properties.

7. REFERENCES

Abdel Raoof, G. F., & Mohamed, K. Y. (2018). *Natural Products for the Management of Diabetes* (pp. 323–374). https://doi.org/10.1016/B978-0-444-64179-3.00010-4

Abruscato, G., Chiarelli, R., Lazzara, V., Punginelli, D., Sugár, S., Mauro, M., Librizzi, M., Di Stefano, V., Arizza, V., Vizzini, A., Vazzana, M., & Luparello, C. (2023). In Vitro Cytotoxic Effect of Aqueous Extracts from Leaves and Rhizomes of the Seagrass Posidonia oceanica (L.) Delile on HepG2 Liver Cancer Cells: Focus on Autophagy and Apoptosis. *Biology*, *12*(4), 616. https://doi.org/10.3390/biology12040616

Achari, A. E., & Jain, S. K. (2016). l-Cysteine supplementation increases adiponectin synthesis and secretion, and GLUT4 and glucose utilization by upregulating disulfide bond A-like protein expression mediated by MCP-1 inhibition in 3T3-L1 adipocytes exposed to high glucose. *Molecular and Cellular Biochemistry*, *414*(1–2), 105–113. https://doi.org/10.1007/s11010-016-2664-7

Akbar, S., Ishtiaq, S., Jahangir, M., Elhady, S. S., Bogari, H. A., Alahdal, A. M., Ashour, M. L., & Youssef, F. S. (2021). Evaluation of The Antioxidant, Antimicrobial, and Anticancer Activities of Dicliptera bupleuroides Isolated Compounds Using In Vitro and In Silico Studies. *Molecules*, *26*(23), 7196. https://doi.org/10.3390/molecules26237196

Alper, M., & Güneş, M. (2020). Evaluation of cytotoxic, apoptotic effects and phenolic compounds of sea cucumber Holothuria tubulosa (Gmelin, 1791) extracts. *Turkish Journal Of Veterinary And Animal Sciences*, *44*(3), 641–655. https://doi.org/10.3906/vet-1909-80

American Diabetes Association (2013) Diagnosis and classification of diabetes mellitus. *Diabetes Care.* Jan; 36 Suppl 1(Suppl 1):S67-74. doi: 10.2337/dc13-S067.

Ammar, N. M., Hassan, H. A., Mohammed, M. A., Serag, A., Abd El-Alim, S. H., Elmotasem, H., El Raey, M., El Gendy, A. N., Sobeh, M., & Abdel-Hamid, A.-H. Z. (2021). Metabolomic profiling to reveal the therapeutic potency of *Posidonia oceanica* nanoparticles in diabetic rats. *RSC Advances*, *11*(14), 8398–8410. https://doi.org/10.1039/D0RA09606G

Aniya, Y., & Imaizumi, N. (2011). Mitochondrial glutathione transferases involving a new function for membrane permeability transition pore regulation. *Drug Metabolism Reviews*, *43*(2), 292–299. https://doi.org/10.3109/03602532.2011.552913

Aranda, P. S., LaJoie, D. M., & Jorcyk, C. L. (2012). Bleach gel: A simple agarose gel for analyzing RNA quality. *Electrophoresis*, *33*(2), 366–369. https://doi.org/10.1002/elps.201100335

Asafo-Agyei KO, S. H. (2023, June). *Hepatocellular Carcinoma*. https://www.ncbi.nlm.nih.gov/books/NBK559177/

Auten, R. L., & Davis, J. M. (2009). Oxygen Toxicity and Reactive Oxygen Species: The Devil Is in the Details. *Pediatric Research*, *66*(2), 121–127. https://doi.org/10.1203/PDR.0b013e3181a9eafb

Barletta, E., Ramazzotti, M., Fratianni, F., Pessani, D., & Degl'Innocenti, D. (2015). Hydrophilic extract from *Posidonia oceanica* inhibits activity and expression of gelatinases and prevents HT1080 human fibrosarcoma cell line invasion. *Cell Adhesion & Migration*, *9*(6), 422–431. https://doi.org/10.1080/19336918.2015.1008330

Bay-Nouailhat A. (2006, September). *Description of Holothuria tubulosa*. ttps://www.european-marine-life.org/30/holothuria-(holothuria)-tubulosa.php

Bellissimo, G., Sirchia, B., & Ruvolo, V. (2020). *Monitoring of Posidonia oceanica meadows in the Sicilian coasts under the Water Framework Directive (WFD)* (pp. 510–518). https://doi.org/10.36253/978-88-5518-147-1.51

Belyaeva, E. A., Dymkowska, D., Więckowski, M. R., & Wojtczak, L. (2008). Mitochondria as an important target in heavy metal toxicity in rat hepatoma AS-30D cells. *Toxicology and Applied Pharmacology*, *231*(1), 34–42. https://doi.org/10.1016/j.taap.2008.03.017

Berfad, M. A. and T. M. S. Alnour. (2014). Phytochemical analysis and Antibacterial activity of the 5 different extract from the seagrasses Posidonia oceanica. *Journal of Medicinal Plants Studies 2* ., 15–18.

Bernard, P., & Pesando, D. (1989). Antibacterial and Antifungal Activity of Extracts from the Rhizomes of the Mediterranean Seagrass *Posidonia oceanica* (L.) Delile. *Botm*, *32*(2), 85–88. https://doi.org/10.1515/botm.1989.32.2.85

Bertram, K., Valcu, C.-M., Weitnauer, M., Linne, U., & Görlach, A. (2015). NOX1 Supports the Metabolic Remodeling of HepG2 Cells. *Plos One*, *10*(3), e0122002. https://doi.org/10.1371/journal.pone.0122002

Brar, T. S., Hilgenfeldt, E., & Soldevila-Pico, C. (2018). *Etiology and Pathogenesis of Hepatocellular Carcinoma* (pp. 1–15). https://doi.org/10.1007/978-3-319-68082-8_1

Bruzzone, S., Ameri, P., Briatore, L., Mannino, E., Basile, G., Andraghetti, G., Grozio, A., Magnone, M., Guida, L., Scarfì, S., Salis, A., Damonte, G., Sturla, L., Nencioni, A., Fenoglio, D., Fiory, F., Miele, C., Beguinot, F., Ruvolo, V., … Zocchi, E. (2012). The plant hormone abscisic acid increases in human plasma after hyperglycemia and stimulates glucose consumption by adipocytes and myoblasts. *The Faseb Journal*, *26*(3), 1251–1260. https://doi.org/10.1096/fj.11-190140

Cecchelli, R., Aday, S., Sevin, E., Almeida, C., Culot, M., Dehouck, L., Coisne, C., Engelhardt, B., Dehouck, M.-P., & Ferreira, L. (2014). A Stable and Reproducible Human Blood-Brain Barrier Model Derived from Hematopoietic Stem Cells. *Plos ONE*, *9*(6), e99733. https://doi.org/10.1371/journal.pone.0099733

Chadt, A., & Al-Hasani, H. (2020). Glucose transporters in adipose tissue, liver, and skeletal muscle in metabolic health and disease. *Pflügers Archiv - European Journal of Physiology*, *472*(9), 1273–1298. https://doi.org/10.1007/s00424-020-02417-x

Chao, X., Zhou, X., Zheng, G., Dong, C., Zhang, W., Song, X., & Jin, T. (2014). Osthole induces G2/M cell cycle arrest and apoptosis in human hepatocellular carcinoma HepG2 cells. *Pharmaceutical Biology*, *52*(5), 544–550. https://doi.org/10.3109/13880209.2013.850517

Chen, L., Zheng, S., Huang, M., Ma, X., Yang, J., Deng, S., Huang, Y., Wen, Y., & Yang, X. (2017). β-ecdysterone from Cyanotis arachnoidea exerts hypoglycemic effects through activating IRS-1/Akt/GLUT4 and IRS-1/Akt/GLUT2 signal pathways in KK-Ay mice. *Journal of Functional Foods*, *39*, 123–132. https://doi.org/10.1016/j.jff.2017.09.061

Chen, Q. C. ; Z. W. Y. ; J. W. ; L. I. S. ; M. B. S. ; J. H. J. ; N. M. ; L. S. ; B. K. (2010). Flavonoids and isoflavonoids from Sophorae Flos improve glucose uptake in vitro. *Planta Med.*, *76*, 79–81.

Chen, T., Zhang, X., Zhu, G., Liu, H., Chen, J., Wang, Y., & He, X. (2020). Quercetin inhibits TNF-α induced HUVECs apoptosis and inflammation via downregulating NF-kB and AP-1 signaling pathway in vitro. *Medicine*, *99*(38), e22241. https://doi.org/10.1097/MD.0000000000022241

Chen, Y., Wang, Y., Yang, S., Yu, M., Jiang, T., & Lv, Z. (2019). Glycosaminoglycan from Apostichopus japonicus Improves Glucose Metabolism in the Liver of Insulin Resistant Mice. *Marine Drugs*, *18*(1), 1. https://doi.org/10.3390/md18010001

Cheng, J., Kang, X., Zhang, S., & Yeh, E. T. H. (2007). SUMO-Specific Protease 1 Is Essential for Stabilization of HIF1α during Hypoxia. *Cell*, *131*(3), 584–595. https://doi.org/10.1016/j.cell.2007.08.045

Chiarelli, R., Martino, C., Roccheri, M. C., & Cancemi, P. (2021). Toxic effects induced by vanadium on sea urchin embryos. *Chemosphere*, *274*, 129843. https://doi.org/10.1016/j.chemosphere.2021.129843

Cornara, L., Pastorino, G., Borghesi, B., Salis, A., Clericuzio, M., Marchetti, C., Damonte, G., & Burlando, B. (2018). Posidonia oceanica (L.) Delile Ethanolic Extract Modulates Cell Activities with Skin Health Applications. *Marine Drugs*, *16*(1), 21. https://doi.org/10.3390/md16010021

Couto, N., Wood, J., & Barber, J. (2016). The role of glutathione reductase and related enzymes on cellular redox homoeostasis network. *Free Radical Biology and Medicine*, *95*, 27–42. https://doi.org/10.1016/j.freeradbiomed.2016.02.028

Csepregi, R., Temesfői, V., Sali, N., Poór, M., W. Needs, P., A. Kroon, P., & Kőszegi, T. (2018). A One-Step Extraction and Luminescence Assay for Quantifying Glucose and ATP Levels in Cultured HepG2 Cells. *International Journal of Molecular Sciences*, *19*(9), 2670. https://doi.org/10.3390/ijms19092670

Decuypere, J.-P., Parys, J. B., & Bultynck, G. (2012). Regulation of the Autophagic Bcl-2/Beclin 1 Interaction. *Cells*, *1*(3), 284–312. https://doi.org/10.3390/cells1030284

Dehouck, M., Jolliet-Riant, P., Brée, F., Fruchart, J., Cecchelli, R., & Tillement, J. (1992). Drug Transfer Across the Blood-Brain Barrier: Correlation Between In Vitro and In Vivo Models. *Journal of Neurochemistry*, *58*(5), 1790–1797. https://doi.org/10.1111/j.1471-4159.1992.tb10055.x

Desquiret, V., Loiseau, D., Jacques, C., Douay, O., Malthièry, Y., Ritz, P., & Roussel, D. (2006). Dinitrophenol-induced mitochondrial uncoupling in vivo triggers respiratory adaptation in HepG2 cells. *Biochimica et Biophysica Acta (BBA) - Bioenergetics*, *1757*(1), 21–30. https://doi.org/10.1016/j.bbabio.2005.11.005

Dib, S., Loiola, R. A., Sevin, E., Saint-Pol, J., Shimizu, F., Kanda, T., Pahnke, J., & Gosselet, F. (2023). TNFα Activates the Liver X Receptor Signaling Pathway and Promotes Cholesterol Efflux from Human Brain Pericytes Independently of ABCA1. *International Journal of Molecular Sciences*, *24*(6), 5992. https://doi.org/10.3390/ijms24065992

Donato, M. T., Tolosa, L., & Gómez-Lechón, M. J. (2015). *Culture and Functional Characterization of Human Hepatoma HepG2 Cells* (pp. 77–93). https://doi.org/10.1007/978-1-4939-2074-7_5

Eid, H. M., Thong, F., Nachar, A., & Haddad, P. S. (2017). Caffeic acid methyl and ethyl esters exert potential antidiabetic effects on glucose and lipid metabolism in cultured murine insulin-sensitive cells through mechanisms implicating activation of AMPK. *Pharmaceutical Biology*, *55*(1), 2026–2034. https://doi.org/10.1080/13880209.2017.1345952

El Barky, A. R., Hussein, S. A., Alm-Eldeen, A. A., Hafez, Y. A., & Mohamed, T. M. (2016). Anti-diabetic activity of Holothuria thomasi saponin. *Biomedicine & Pharmacotherapy*, *84*, 1472–1487. https://doi.org/10.1016/j.biopha.2016.10.002

Elhusseiny, S. M., El-Mahdy, T. S., Awad, M. F., Elleboudy, N. S., Farag, M. M. S., Yassein, M. A., & Aboshanab, K. M. (2021). Proteome Analysis and In Vitro Antiviral, Anticancer and

Antioxidant Capacities of the Aqueous Extracts of Lentinula edodes and Pleurotus ostreatus Edible Mushrooms. *Molecules*, *26*(15), 4623. https://doi.org/10.3390/molecules26154623

Esk, C., Chen, C.-Y., Johannes, L., & Brodsky, F. M. (2010). The clathrin heavy chain isoform CHC22 functions in a novel endosomal sorting step. *Journal of Cell Biology*, *188*(1), 131–144. https://doi.org/10.1083/jcb.200908057

Farag, A. K., & Roh, E. J. (2019). Death-associated protein kinase (DAPK) family modulators: Current and future therapeutic outcomes. *Medicinal Research Reviews*, *39*(1), 349–385. https://doi.org/10.1002/med.21518

Farid, M., Marzouk, M., Hussein S. R., Elkhateeb A., & Abdel-Hameed,E.S. (2018) Comparative study of Posidonia oceanica L.: LC/ESI/MS analysis, cytotoxic activity and chemosystematic significance. *J.Mater.Environ.Sci*, *9*(6), 1676–1682.

Farzaneh, Z., Vosough, M., Agarwal, T., & Farzaneh, M. (2021). Critical signaling pathways governing hepatocellular carcinoma behavior; small molecule-based approaches. *Cancer Cell International*, *21*(1), 208. https://doi.org/10.1186/s12935-021-01924-w

Feng, L., Chen, Y., Xu, K., Li, Y., Riaz, F., Lu, K., Chen, Q., Du, X., Wu, L., Cao, D., Li, C., Lu, S., & Li, D. (2022). Cholesterol-induced leucine aminopeptidase 3 (LAP3) upregulation inhibits cell autophagy in pathogenesis of NAFLD. *Aging*, *14*(7), 3259–3275. https://doi.org/10.18632/aging.204011

Franken, N. A. P., Rodermond, H. M., Stap, J., Haveman, J., & van Bree, C. (2006). Clonogenic assay of cells in vitro. *Nature Protocols*, *1*(5), 2315–2319. https://doi.org/10.1038/nprot.2006.339

Frieg, B., Görg, B., Gohlke, H., & Häussinger, D. (2021). Glutamine synthetase as a central element in hepatic glutamine and ammonia metabolism: novel aspects. *Biological Chemistry*, *402*(9), 1063–1072. https://doi.org/10.1515/hsz-2021-0166

Fu, H., Vuononvirta, J., Fanti, S., Bonacina, F., D'Amati, A., Wang, G., Poobalasingam, T., Fankhaenel, M., Lucchesi, D., Coleby, R., Tarussio, D., Thorens, B., Hearnden, R. J., Longhi, M. P., Grevitt, P., Sheikh, M. H., Solito, E., Godinho, S. A., Bombardieri, M., … Marelli-Berg, F. M. (2023b). The glucose transporter 2 regulates CD8+ T cell function via environment sensing. *Nature Metabolism*, *5*(11), 1969–1985. https://doi.org/10.1038/s42255-023-00913-9

Furtado, L. M., Somwar, R., Sweeney, G., Niu, W., & Klip, A. (2002). Activation of the glucose transporter GLUT4 by insulin. *Biochemistry and Cell Biology*, *80*(5), 569–578. https://doi.org/10.1139/o02-156

Furth, E. E., Sprecher, H., Fisher, E. A., Fleishman, H. D., & Laposata, M. (1992). An in vitro model for essential fatty acid deficiency: HepG2 cells permanently maintained in lipid-free medium. *Journal of Lipid Research*, *33*(11), 1719–1726.

Gao, F., Zhou, L., Li, M., Liu, W., Yang, S., & Li, W. (2020). Inhibition of ERKs/Akt-Mediated c-Fos Expression Is Required for Piperlongumine-Induced Cyclin D1 Downregulation and Tumor Suppression in Colorectal Cancer Cells . *OncoTargets and Therapy*, *Volume 13*, 5591–5603. https://doi.org/10.2147/OTT.S251295

Gokce, G., & Haznedaroglu, M. Z. (2008). Evaluation of antidiabetic, antioxidant and vasoprotective effects of Posidonia oceanica extract. *Journal of Ethnopharmacology*, *115*(1), 122–130. https://doi.org/10.1016/j.jep.2007.09.016

Golestani Eimani, B., Sanati, M. H., Houshmand, M., Ataei, M., Akbarian, F., & Shakhssalim, N. (2014). Expression and prognostic significance of bcl-2 and bax in the progression and clinical outcome of transitional bladder cell carcinoma. *Cell Journal*, *15*(4), 356–363.

Gomes, L. P., Gouveia e Silva, C., Gaillard, J.-C., Armengaud, J., & Coelho, A. V. (2022a). *Characterization of Soluble Cell-Free Coelomic Fluid Proteome from the Starfish Marthasterias glacialis* (pp. 583–597). https://doi.org/10.1007/978-1-0716-2172-1_31

Gupta, D. N., Rani, R., Kokane, A. D., Ghosh, D. K., Tomar, S., & Sharma, A. K. (2022). Characterization of a cytoplasmic 2-Cys peroxiredoxin from Citrus sinensis and its potential role in protection from oxidative damage and wound healing. *International Journal of Biological Macromolecules*, *209*, 1088–1099. https://doi.org/10.1016/j.ijbiomac.2022.04.086

Hermes, M., Osswald, H., & Kloor, D. (2007). Role of S-adenosylhomocysteine hydrolase in adenosine-induced apoptosis in HepG2 cells. *Experimental Cell Research*, *313*(2), 264–283. https://doi.org/10.1016/j.yexcr.2006.10.003

Hossain, A., Dave, D., & Shahidi, F. (2022). Antioxidant Potential of Sea Cucumbers and Their Beneficial Effects on Human Health. *Marine Drugs*, *20*(8), 521. https://doi.org/10.3390/md20080521

Hu, S., Xu, L., Shi, D., Wang, J., Wang, Y., Lou, Q., & Xue, C. (2014). Eicosapentaenoic acid-enriched phosphatidylcholine isolated from Cucumaria frondosa exhibits anti-hyperglycemic effects via activating phosphoinositide 3-kinase/protein kinase B signal pathway. *Journal of Bioscience and Bioengineering*, *117*(4), 457–463. https://doi.org/10.1016/j.jbiosc.2013.09.005

Huang, H.-M., Ho, C.-Y., Chang, G.-R., Shia, W.-Y., Lai, C.-H., Chao, C.-H., & Wang, C.-M. (2021). HPLC/ESI-MS and NMR Analysis of Chemical Constitutes in Bioactive Extract from the Root Nodule of Vaccinium emarginatum. *Pharmaceuticals*, *14*(11), 1098. https://doi.org/10.3390/ph14111098

Huang, W., Li, N., Zhang, Y., Wang, X., Yin, M., & Lei, Q.-Y. (2022). AHCYL1 senses SAH to inhibit autophagy through interaction with PIK3C3 in an MTORC1-independent manner. *Autophagy*, *18*(2), 309–319. https://doi.org/10.1080/15548627.2021.1924038

Hyun, T. S., & Ross, T. S. (2004). HIP1: trafficking roles and regulation of tumorigenesis. *Trends in Molecular Medicine*, *10*(4), 194–199. https://doi.org/10.1016/j.molmed.2004.02.003

Ibrahim, T. A. et al. (2019). Chemical composition and antimicrobial and cytotoxic activities of Antidesm abunius L. *Pakistan Journal of Pharmaceutical Sciences*, 153–163.

Jeon, J.-S., Kwon, S., Ban, K., Kwon Hong, Y.-, Ahn, C., Sung, J.-S., & Choi, I. (2019). Regulation of the Intracellular ROS Level Is Critical for the Antiproliferative Effect of Quercetin in the Hepatocellular Carcinoma Cell Line HepG2. *Nutrition and Cancer*, *71*(5), 861–869. https://doi.org/10.1080/01635581.2018.1559929

Jiang, J., Briedé, J. J., Jennen, D. G. J., Van Summeren, A., Saritas-Brauers, K., Schaart, G., Kleinjans, J. C. S., & de Kok, T. M. C. M. (2015). Increased mitochondrial ROS formation by acetaminophen in human hepatic cells is associated with gene expression changes suggesting disruption of the mitochondrial electron transport chain. *Toxicology Letters*, *234*(2), 139–150. https://doi.org/10.1016/j.toxlet.2015.02.012

Jordens, I., Molle, D., Xiong, W., Keller, S. R., & McGraw, T. E. (2010). Insulin-regulated Aminopeptidase Is a Key Regulator of GLUT4 Trafficking by Controlling the Sorting of GLUT4 from Endosomes to Specialized Insulin-regulated Vesicles. *Molecular Biology of the Cell*, *21*(12), 2034–2044. https://doi.org/10.1091/mbc.e10-02-0158

Kairupan, T. S., Cheng, K.-C., Asakawa, A., Amitani, H., Yagi, T., Ataka, K., Rokot, N. T., Kapantow, N. H., Kato, I., & Inui, A. (2019). Rubiscolin-6 activates opioid receptors to enhance glucose uptake in skeletal muscle. *Journal of Food and Drug Analysis*, *27*(1), 266–274. https://doi.org/10.1016/j.jfda.2018.06.012

Kale, J., Osterlund, E. J., & Andrews, D. W. (2018). BCL-2 family proteins: changing partners in the dance towards death. *Cell Death & Differentiation*, *25*(1), 65–80. https://doi.org/10.1038/cdd.2017.186

Kang, Y. H., Kim, D. J., Kim, K. K., Lee, S. M., & Choe, M. (2014). Study of the mechanisms underlying increased glucose absorption in *Smilax china* L. leaf extract-treated HepG2 cells. *Journal of Nutrition and Health*, *47*(3), 167. https://doi.org/10.4163/jnh.2014.47.3.167

Karim, S. (2012). Hepatic expression and cellular distribution of the glucose transporter family. *World Journal of Gastroenterology*, *18*(46), 6771. https://doi.org/10.3748/wjg.v18.i46.6771

Kenny, T. C., Craig, A. J., Villanueva, A., & Germain, D. (2019). Mitohormesis Primes Tumor Invasion and Metastasis. *Cell Reports*, *27*(8), 2292-2303.e6. https://doi.org/10.1016/j.celrep.2019.04.095

Kim, D. J., Kang, Y. H., Kim, K. K., Kim, T. W., Park, J. B., & Choe, M. (2017). Increased glucose metabolism and alpha-glucosidase inhibition in *Cordyceps militaris* water extract-treated HepG2 cells. *Nutrition Research and Practice*, *11*(3), 180. https://doi.org/10.4162/nrp.2017.11.3.180

Kim, E.-Y., Choi, Y. H., Choi, C. G., & Nam, T.-J. (2017). Effects of the cyclophilin-type peptidylprolyl cis-trans isomerase from Pyropia yezoensis against hydrogen peroxide-induced oxidative stress in HepG2 cells. *Molecular Medicine Reports*, *15*(6), 4132–4138. https://doi.org/10.3892/mmr.2017.6517

Kim, M., An, J., Shin, S.-A., Moon, S. Y., Kim, M., Choi, S., Kim, H., Phi, K.-H., Lee, J. H., Youn, U. J., Park, H. H., & Lee, C. S. (2024). Anti-inflammatory effects of TP1 in LPS-induced Raw264.7 macrophages. *Applied Biological Chemistry*, *67*(1), 16. https://doi.org/10.1186/s13765-024-00873-y

Kim, M., Ham, A., Kim, K. Y.-M., Brown, K. M., & Lee, H. T. (2014). The Volatile Anesthetic Isoflurane Increases Endothelial Adenosine Generation via Microparticle Ecto-5′-Nucleotidase (CD73) Release. *PLoS ONE*, *9*(6), e99950. https://doi.org/10.1371/journal.pone.0099950

Kim, Y., Cho, A. Y., Kim, H. C., Ryu, D., Jo, S. A., & Jung, Y.-S. (2022a). Effects of Natural Polyphenols on Oxidative Stress-Mediated Blood-Brain Barrier Dysfunction. *Antioxidants*, *11*(2), 197. https://doi.org/10.3390/antiox11020197

Klionsky D.J. et al. (2021a). Guidelines for the use and interpretation of assays for monitoring autophagy (4th edition). *Autophagy*, 1–382.

Kohno, H., Kanda, S., & Kanno, T. (1986). Immunoaffinity purification and characterization of leucine aminopeptidase from human liver. *The Journal of Biological Chemistry*, *261*(23), 10744–10748.

Koshy, S., Alizadeh, P., Timchenko, L. T., & Beeton, C. (2010). Quantitative Measurement of GLUT4 Translocation to the Plasma Membrane by Flow Cytometry. *Journal of Visualized Experiments*, *45*. https://doi.org/10.3791/2429

L. Kouznetsova, V., Hauptschein, M., & Tsigelny, I. F. (2017). Glucose and Lipid Transporters Roles in Type 2 Diabetes. *Integrative Obesity and Diabetes*, *3*(5). https://doi.org/10.15761/IOD.1000192

Lazzara, V., Arizza, V., Luparello, C., Mauro, M., & Vazzana, M. (2019). Bright Spots in the Darkness of Cancer: A Review of Starfishes-Derived Compounds and Their Anti-Tumor Action. *Marine Drugs*, *17*(11), 617. https://doi.org/10.3390/md17110617

Leri, M., Ramazzotti, M., Vasarri, M., Peri, S., Barletta, E., Pretti, C., & Degl'Innocenti, D. (2018). Bioactive Compounds from Posidonia oceanica (L.) Delile Impair Malignant Cell Migration through Autophagy Modulation. *Marine Drugs*, *16*(4), 137. https://doi.org/10.3390/md16040137

Li, Q., He, Z., Liu, J., Wu, J., Tan, G., Jiang, J., Su, Z., & Cao, M. (2019). *Paris polyphylla 26* triggers G2/M phase arrest and induces apoptosis in HepG2 cells via inhibition of the Akt signaling pathway. *Journal of International Medical Research*, *47*(4), 1685–1695. https://doi.org/10.1177/0300060519826823

Li, Q., Mao, L., Wang, R., Zhu, L., & Xue, L. (2014). Overexpression of S-adenosylhomocysteine hydrolase (SAHH) in esophageal squamous cell carcinoma (ESCC) cell lines: effects on apoptosis, migration and adhesion of cells. *Molecular Biology Reports*, *41*(4), 2409–2417. https://doi.org/10.1007/s11033-014-3095-8

Librizzi, M., Longo, A., Chiarelli, R., Amin, J., Spencer, J., & Luparello, C. (2012). Cytotoxic Effects of Jay Amin Hydroxamic Acid (JAHA), a Ferrocene-Based Class I Histone Deacetylase Inhibitor, on Triple-Negative MDA-MB231 Breast Cancer Cells. *Chemical Research in Toxicology*, *25*(11), 2608–2616. https://doi.org/10.1021/tx300376h

Liu, B., Tan, X., Liang, J., Wu, S., Liu, J., Zhang, Q., & Zhu, R. (2014). A reduction in reactive oxygen species contributes to dihydromyricetin-induced apoptosis in human hepatocellular carcinoma cells. *Scientific Reports*, *4*(1), 7041. https://doi.org/10.1038/srep07041

Liu, C.-Y., Bai, K., Liu, X.-H., Zhang, L.-M., & Yu, G.-R. (2018). Hyperoside protects the blood-brain barrier from neurotoxicity of amyloid beta 1–42. *Neural Regeneration Research*, *13*(11), 1974. https://doi.org/10.4103/1673-5374.239445

Luparello, C. (2021). Marine Animal-Derived Compounds and Autophagy Modulation in Breast Cancer Cells. *Foundations*, *1*(1), 3–20. https://doi.org/10.3390/foundations1010002

Luparello, C., Asaro, D. M. L., Cruciata, I., Hassell-Hart, S., Sansook, S., Spencer, J., & Caradonna, F. (2019). Cytotoxic Activity of the Histone Deacetylase 3-Selective Inhibitor Pojamide on MDA-MB-231 Triple-Negative Breast Cancer Cells. *International Journal of Molecular Sciences*, *20*(4), 804. https://doi.org/10.3390/ijms20040804

Luparello, C., Branni, R., Abruscato, G., Lazzara, V., Drahos, L., Arizza, V., Mauro, M., Di Stefano, V., & Vazzana, M. (2022) a. Cytotoxic capability and the associated proteomic profile of cell-free coelomic fluid extracts from the edible sea cucumber Holothuria tubulosa

on HepG2 liver cancer cells. *EXCLI Journal*, *21*, 722–743. https://doi.org/10.17179/excli2022-4825

Luparello, C., Branni, R., Abruscato, G., Lazzara, V., Sugár, S., Arizza, V., Mauro, M., Di Stefano, V., & Vazzana, M. (2022) b. Biological and Proteomic Characterization of the Anti-Cancer Potency of Aqueous Extracts from Cell-Free Coelomic Fluid of Arbacia lixula Sea Urchin in an In Vitro Model of Human Hepatocellular Carcinoma. *Journal of Marine Science and Engineering*, *10*(9), 1292. https://doi.org/10.3390/jmse10091292

Luparello, C., Longo, A., & Vetrano, M. (2012). Exposure to cadmium chloride influences astrocyte-elevated gene-1 (AEG-1) expression in MDA-MB231 human breast cancer cells. *Biochimie*, *94*(1), 207–213. https://doi.org/10.1016/j.biochi.2011.10.009

Luparello, C., Mauro, M., Arizza, V., & Vazzana, M. (2020). Histone Deacetylase Inhibitors from Marine Invertebrates. *Biology*, *9*(12), 429. https://doi.org/10.3390/biology9120429

Luparello, C., Mauro, M., Lazzara, V., & Vazzana, M. (2020). Collective Locomotion of Human Cells, Wound Healing and Their Control by Extracts and Isolated Compounds from Marine Invertebrates. *Molecules*, *25*(11), 2471. https://doi.org/10.3390/molecules25112471

Luparello, C., Ragona, D., Asaro, D. M. L., Lazzara, V., Affranchi, F., Celi, M., Arizza, V., & Vazzana, M. (2019). Cytotoxic Potential of the Coelomic Fluid Extracted from the Sea Cucumber Holothuria tubulosa against Triple-Negative MDA-MB231 Breast Cancer Cells. *Biology*, *8*(4), 76. https://doi.org/10.3390/biology8040076

Luparello, C., Sirchia, R., & Lo Sasso, B. (2008). Midregion PTHrP regulates Rip1 and caspase expression in MDA-MB231 breast cancer cells. *Breast Cancer Research and Treatment*, *111*(3), 461–474. https://doi.org/10.1007/s10549-007-9816-0

Maciel, L. G., do Carmo, M. A. V., Azevedo, L., Daguer, H., Molognoni, L., de Almeida, M. M., Granato, D., & Rosso, N. D. (2018). Hibiscus sabdariffa anthocyanins-rich extract: Chemical stability, in vitro antioxidant and antiproliferative activities. *Food and Chemical Toxicology*, *113*, 187–197. https://doi.org/10.1016/j.fct.2018.01.053

Martínez-Alonso, C., Taroncher, M., Castaldo, L., Izzo, L., Rodríguez-Carrasco, Y., Ritieni, A., & Ruiz, M.-J. (2022). Effect of Phenolic Extract from Red Beans (Phaseolus vulgaris L.) on T-2 Toxin-Induced Cytotoxicity in HepG2 Cells. *Foods*, *11*(7), 1033. https://doi.org/10.3390/foods11071033

Mauro, M., Lazzara, V., Punginelli, D., Arizza, V., & Vazzana, M. (2020). Antitumoral compounds from vertebrate sister group: A review of Mediterranean ascidians. *Developmental & Comparative Immunology*, *108*, 103669. https://doi.org/10.1016/j.dci.2020.103669

Mecheta, A., Hanachi, A., Jeandel, C., Arab-Tehrany, E., Bianchi, A., Velot, E., Mezali, K., & Linder, M. (2020). Physicochemical Properties and Liposomal Formulations of Hydrolysate Fractions of Four Sea Cucumbers (Holothuroidea: Echinodermata) from the Northwestern Algerian Coast. *Molecules*, *25*(13), 2972. https://doi.org/10.3390/molecules25132972

Mediavilla, M. G., Di Venanzio, G. A., Guibert, E. E., & Tiribelli, C. (2010). Heterologous Ferredoxin Reductase and Flavodoxin Protect Cos-7 Cells from Oxidative Stress. *PLoS ONE*, *5*(10), e13501. https://doi.org/10.1371/journal.pone.0013501

Messina, C. M., Arena, R., Manuguerra, S., Pericot, Y., Curcuraci, E., Kerninon, F., Renda, G., Hellio, C., & Santulli, A. (2021). Antioxidant Bioactivity of Extracts from Beach Cast Leaves of Posidonia oceanica (L.) Delile. *Marine Drugs*, *19*(10), 560. https://doi.org/10.3390/md19100560

Mizushima, N. (2007). Autophagy: process and function. *Genes & Development*, *21*(22), 2861–2873. https://doi.org/10.1101/gad.1599207

Mokashi, P., Khanna, A., & Pandita, N. (2017). Flavonoids from Enicostema littorale blume enhances glucose uptake of cells in insulin resistant human liver cancer (HepG2) cell line via IRS-1/PI3K/Akt pathway. *Biomedicine & Pharmacotherapy*, *90*, 268–277. https://doi.org/10.1016/j.biopha.2017.03.047

Moon, M. K., Lee, Y. J., Kim, J. S., Kang, D. G., & Lee, H. S. (2009). Effect of Caffeic Acid on Tumor Necrosis Factor-Alpha-Induced Vascular Inflammation in Human Umbilical Vein Endothelial Cells. *Biological & Pharmaceutical Bulletin*, *32*(8), 1371–1377. https://doi.org/10.1248/bpb.32.1371

Morel, E., Mehrpour, M., Botti, J., Dupont, N., Hamaï, A., Nascimbeni, A. C., & Codogno, P. (2017). Autophagy: A Druggable Process. *Annual Review of Pharmacology and Toxicology*, *57*(1), 375–398. https://doi.org/10.1146/annurev-pharmtox-010716-104936

Mueckler, M., & Thorens, B. (2013). The SLC2 (GLUT) family of membrane transporters. *Molecular Aspects of Medicine*, *34*(2–3), 121–138. https://doi.org/10.1016/j.mam.2012.07.001

Ong, K. L., Stafford, L. K., McLaughlin, S. A., Boyko, E. J., Vollset, S. E., Smith, A. E., Dalton, B. E., Duprey, J., Cruz, J. A., Hagins, H., Lindstedt, P. A., Aali, A., Abate, Y. H., Abate, M. D., Abbasian, M., Abbasi-Kangevari, Z., Abbasi-Kangevari, M., Abd ElHafeez, S., Abd-Rabu, R., Vos, T. (2023). Global, regional, and national burden of diabetes from 1990 to 2021, with projections of prevalence to 2050: a systematic analysis for the Global Burden of Disease Study 2021. *The Lancet*, *402*(10397), 203–234. https://doi.org/10.1016/S0140-6736(23)01301-6

Pace, A., Barone, G., Lauria, A., Martorana, A., Palumbo Piccionello, A., Pierro, P., Terenzi, A., Maria Almerico, A., Buscemi, S., Campanella, C., Angileri, F., Carini, F., Zummo, G., Conway de Macario, E., Cappello, F., & J.L. Macario, A. (2013). Hsp60, a Novel Target for Antitumor Therapy: Structure-Function Features and Prospective Drugs Design. *Current Pharmaceutical Design*, *19*(15), 2757–2764. https://doi.org/10.2174/1381612811319150011

Pang, X., Gao, X., Liu, F., Jiang, Y., Wang, M., Li, Q., & Li, Z. (2021). Xanthoangelol modulates Caspase-1-dependent pyroptotic death among hepatocellular carcinoma cells with high expression of GSDMD. *Journal of Functional Foods*, *84*, 104577. https://doi.org/10.1016/j.jff.2021.104577

Park, S., Kim, G., Bae, S.-J., Yoo, Y., & Choi, Y. (2007). Induction of apoptosis by isothiocyanate sulforaphane in human cervical carcinoma HeLa and hepatocarcinoma HepG2 cells through activation of caspase-3. *Oncology Reports*. https://doi.org/10.3892/or.18.1.181

Párrizas, M., Maestro, M. A., Boj, S. F., Paniagua, A., Casamitjana, R., Gomis, R., Rivera, F., & Ferrer, J. (2001). Hepatic Nuclear Factor 1-α Directs Nucleosomal Hyperacetylation to Its Tissue-Specific Transcriptional Targets. *Molecular and Cellular Biology*, *21*(9), 3234–3243. https://doi.org/10.1128/MCB.21.9.3234-3243.2001

Pedroso, D. C. S., Tellechea, A., Moura, L., Fidalgo-Carvalho, I., Duarte, J., Carvalho, E., & Ferreira, L. (2011). Improved survival, vascular differentiation and wound healing potential of stem cells co-cultured with endothelial cells. *PloS One*, *6*(1), e16114. https://doi.org/10.1371/journal.pone.0016114

Philips, C. A., Rajesh, S., Nair, D. C., Ahamed, R., Abduljaleel, J. K., & Augustine, P. (2021). Hepatocellular Carcinoma in 2021: An Exhaustive Update. *Cureus*. https://doi.org/10.7759/cureus.19274

Podar, K., Raab, M. S., Tonon, G., Sattler, M., Barilà, D., Zhang, J., Tai, Y.-T., Yasui, H., Raje, N., DePinho, R. A., Hideshima, T., Chauhan, D., & Anderson, K. C. (2007). Up-Regulation of c-Jun Inhibits Proliferation and Induces Apoptosis via Caspase-Triggered c-Abl Cleavage in Human Multiple Myeloma. *Cancer Research*, *67*(4), 1680–1688. https://doi.org/10.1158/0008-5472.CAN-06-1863

Poulose, N., Prasad, V., Nidhina Haridas, P. A., & Gopalakrishnapillai, A. (2011). Ellagic acid stimulates glucose transport in 3T3-L1 adipocytes and C2C12 myotubes by AMP activated protein kinase mediated pathway. *The FASEB Journal*, *25*(S1). https://doi.org/10.1096/fasebj.25.1_supplement.lb85

Punginelli, D., Catania, V., Abruscato, G., Luparello, C., Vazzana, M., Mauro, M., Cunsolo, V., Saletti, R., Di Francesco, A., Arizza, V., & Schillaci, D. (2023). New Bioactive Peptides from the Mediterranean Seagrass Posidonia oceanica (L.) Delile and Their Impact on Antimicrobial

Activity and Apoptosis of Human Cancer Cells. *International Journal of Molecular Sciences*, *24*(6), 5650. https://doi.org/10.3390/ijms24065650

Purwanto, B., Wiyasihati, S. I., Masyitha, P. A., Wigati, K. W., & Irwadi, I. (2019). Golden sea cucumber extract revives glucose transporter-4 and interleukin-6 protein level in diabetic mouse muscle. *Veterinary World*, *12*(5), 684–688. https://doi.org/10.14202/vetworld.2019.684-688

Ramachandran, V., & Saravanan, R. (2015). Glucose uptake through translocation and activation of GLUT4 in PI3K/Akt signaling pathway by asiatic acid in diabetic rats. *Human & Experimental Toxicology*, *34*(9), 884–893. https://doi.org/10.1177/0960327114561663

Rao, X. S., Cong, X. X., Gao, X. K., Shi, Y. P., Shi, L. J., Wang, J. F., Ni, C.-Y., He, M. J., Xu, Y., Yi, C., Meng, Z.-X., Liu, J., Lin, P., Zheng, L. L., & Zhou, Y. T. (2021). AMPK-mediated phosphorylation enhances the auto-inhibition of TBC1D17 to promote Rab5-dependent glucose uptake. *Cell Death & Differentiation*, *28*(12), 3214–3234. https://doi.org/10.1038/s41418-021-00809-9

Razali, N., Mat Junit, S., Ariffin, A., Ramli, N. S. F., & Abdul Aziz, A. (2015). Polyphenols from the extract and fraction of T. indica seeds protected HepG2 cells against oxidative stress. *BMC Complementary and Alternative Medicine*, *15*(1), 438. https://doi.org/10.1186/s12906-015-0963-2

Ronchetti, S. A., Miler, E. A., Duvilanski, B. H., & Cabilla, J. P. (2013). Cadmium Mimics Estrogen-Driven Cell Proliferation and Prolactin Secretion from Anterior Pituitary Cells. *PLoS ONE*, *8*(11), e81101. https://doi.org/10.1371/journal.pone.0081101

Rust, C., Wild, N., Bernt, C., Vennegeerts, T., Wimmer, R., & Beuers, U. (2009). Bile Acid-induced Apoptosis in Hepatocytes Is Caspase-6-dependent. *Journal of Biological Chemistry*, *284*(5), 2908–2916. https://doi.org/10.1074/jbc.M804585200

Sakagami, H., Makino, Y., Mizumoto, K., Isoe, T., Takeda, Y., Watanabe, J., Fujita, Y., Takiyama, Y., Abiko, A., & Haneda, M. (2014). Loss of HIF-1α impairs GLUT4 translocation and glucose uptake by the skeletal muscle cells. *American Journal of Physiology-Endocrinology and Metabolism*, *306*(9), E1065–E1076. https://doi.org/10.1152/ajpendo.00597.2012

Saltiel, A. R., & Kahn, C. R. (2001). Insulin signalling and the regulation of glucose and lipid metabolism. *Nature*, *414*(6865), 799–806. https://doi.org/10.1038/414799a

Samari, H. R., & Seglen, P. O. (1998). Inhibition of Hepatocytic Autophagy by Adenosine, Aminoimidazole-4-carboxamide Riboside, and N 6-Mercaptopurine Riboside. *Journal of Biological Chemistry*, *273*(37), 23758–23763. https://doi.org/10.1074/jbc.273.37.23758

Schillaci, D., Cusimano, M., Cunsolo, V., Saletti, R., Russo, D., Vazzana, M., Vitale, M., & Arizza, V. (2013). Immune mediators of sea-cucumber Holothuria tubulosa (Echinodermata) as source of novel antimicrobial and anti-staphylococcal biofilm agents. *AMB Express*, *3*(1), 35. https://doi.org/10.1186/2191-0855-3-35

Schlattner, U., Tokarska-Schlattner, M., Epand, R. M., Boissan, M., Lacombe, M.-L., & Kagan, V. E. (2018). NME4/nucleoside diphosphate kinase D in cardiolipin signaling and mitophagy. *Laboratory Investigation*, *98*(2), 228–232. https://doi.org/10.1038/labinvest.2017.113

Schlossberg, H., Zhang, Y., Dudus, L., & Engelhardt, J. F. (1996). Expression of c-fos and c-jun during hepatocellular remodeling following ischemia/reperfusion in mouse liver. *Hepatology*, *23*(6), 1546–1555. https://doi.org/10.1002/hep.510230635

Shalini, S., Dorstyn, L., Wilson, C., Puccini, J., Ho, L., & Kumar, S. (2012). Impaired antioxidant defence and accumulation of oxidative stress in caspase-2-deficient mice. *Cell Death & Differentiation*, *19*(8), 1370–1380. https://doi.org/10.1038/cdd.2012.13

Shi, S., Kang, X.-J., Zhou, Z., He, Z.-M., Zheng, S., & He, S.-S. (2022). Excessive mechanical stress-induced intervertebral disc degeneration is related to Piezo1 overexpression triggering the imbalance of autophagy/apoptosis in human nucleus pulpous. *Arthritis Research & Therapy*, *24*(1), 119. https://doi.org/10.1186/s13075-022-02804-y

Shin, K.-M., Kim, I.-T., Park, Y.-M., Ha, J., Choi, J.-W., Park, H.-J., Lee, Y. S., & Lee, K.-T. (2004). Anti-inflammatory effect of caffeic acid methyl ester and its mode of action through the inhibition of prostaglandin E2, nitric oxide and tumor necrosis factor-α production. *Biochemical Pharmacology*, *68*(12), 2327–2336. https://doi.org/10.1016/j.bcp.2004.08.002

Shou, Y., Feng, C., Lu, Q., Mao, X., Huang, H., Su, Z., Guo, H., & Huang, Z. (2023). Research progress on the chemical components and biological activities of sea cucumber polypeptides. *Frontiers in Pharmacology*, *14*. https://doi.org/10.3389/fphar.2023.1290175

Singh, P., Ravanan, P., & Talwar, P. (2016). Death Associated Protein Kinase 1 (DAPK1): A Regulator of Apoptosis and Autophagy. *Frontiers in Molecular Neuroscience*, *9*. https://doi.org/10.3389/fnmol.2016.00046

Singh, R., & Czaja, M. J. (2007). Regulation of hepatocyte apoptosis by oxidative stress. *Journal of Gastroenterology and Hepatology*, *22*(s1). https://doi.org/10.1111/j.1440-1746.2006.04646.x

Strober, W. (2015). Trypan Blue Exclusion Test of Cell Viability. *Current Protocols in Immunology*, *111*(1). https://doi.org/10.1002/0471142735.ima03bs111

Sweeney, M. D., Zhao, Z., Montagne, A., Nelson, A. R., & Zlokovic, B. V. (2019). Blood-Brain Barrier: From Physiology to Disease and Back. *Physiological Reviews*, *99*(1), 21–78. https://doi.org/10.1152/physrev.00050.2017

Świderska, E., Strycharz, J., Wróblewski, A., Szemraj, J., Drzewoski, J., & Śliwińska, A. (2020). Role of PI3K/AKT Pathway in Insulin-Mediated Glucose Uptake. In *Blood Glucose Levels*. IntechOpen. https://doi.org/10.5772/intechopen.80402

Tang, C., Lu, Y.-H., Xie, J.-H., Wang, F., Zou, J.-N., Yang, J.-S., Xing, Y.-Y., & Xi, T. (2009). Downregulation of survivin and activation of caspase-3 through the PI3K/Akt pathway in ursolic acid-induced HepG2 cell apoptosis. *Anti-Cancer Drugs*, *20*(4), 249–258. https://doi.org/10.1097/CAD.0b013e328327d476

Taniguchi, C. M., Emanuelli, B., & Kahn, C. R. (2006). Critical nodes in signalling pathways: insights into insulin action. *Nature Reviews Molecular Cell Biology*, *7*(2), 85–96. https://doi.org/10.1038/nrm1837

Thorens, B. (2015). GLUT2, glucose sensing and glucose homeostasis. *Diabetologia*, *58*(2), 221–232. https://doi.org/10.1007/s00125-014-3451-1

Tiwari, M., Sharma, L. K., Vanegas, D., Callaway, D. A., Bai, Y., Lechleiter, J. D., & Herman, B. (2014). A nonapoptotic role for CASP2/caspase 2. *Autophagy*, *10*(6), 1054–1070. https://doi.org/10.4161/auto.28528

Tsagarakis, N. J. (2011). Octreotide induces caspase activation and apoptosis in human hepatoma HepG2 cells. *World Journal of Gastroenterology*, *17*(3), 313. https://doi.org/10.3748/wjg.v17.i3.313

Tsai, T.-H., Yu, C.-H., Chang, Y.-P., Lin, Y.-T., Huang, C.-J., Kuo, Y.-H., & Tsai, P.-J. (2017). Protective Effect of Caffeic Acid Derivatives on tert-Butyl Hydroperoxide-Induced Oxidative Hepato-Toxicity and Mitochondrial Dysfunction in HepG2 Cells. *Molecules*, *22*(5), 702. https://doi.org/10.3390/molecules22050702

Tsapras, P., & Nezis, I. P. (2017). Caspase involvement in autophagy. *Cell Death & Differentiation*, *24*(8), 1369–1379. https://doi.org/10.1038/cdd.2017.43

Udupa, P., Kumar, A., Parit, R., & Ghosh, D. K. (2023). Acyl-CoA binding protein regulates nutrient-dependent autophagy. *Metabolism*, *145*, 155338. https://doi.org/10.1016/j.metabol.2022.155338

Valionyte, E., Yang, Y., Griffiths, S. A., Bone, A. T., Barrow, E. R., Sharma, V., Lu, B., & Luo, S. (2022). The caspase-6–p62 axis modulates p62 droplets based autophagy in a dominant-negative manner. *Cell Death & Differentiation*, *29*(6), 1211–1227. https://doi.org/10.1038/s41418-021-00912-x

Vasarri, M., Barletta, E., Ramazzotti, M., & Degl'Innocenti, D. (2020). In vitro anti-glycation activity of the marine plant Posidonia oceanica (L.) Delile. *Journal of Ethnopharmacology*, *259*, 112960. https://doi.org/10.1016/j.jep.2020.112960

Vasarri, M., Leri, M., Barletta, E., Pretti, C., & Degl'Innocenti, D. (2021). Posidonia oceanica (L.) Delile Dampens Cell Migration of Human Neuroblastoma Cells. *Marine Drugs*, *19*(10), 579. https://doi.org/10.3390/md19100579

Vassilopoulos, S., Esk, C., Hoshino, S., Funke, B. H., Chen, C.-Y., Plocik, A. M., Wright, W. E., Kucherlapati, R., & Brodsky, F. M. (2009). A Role for the CHC22 Clathrin Heavy-Chain Isoform in Human Glucose Metabolism. *Science*, *324*(5931), 1192–1196. https://doi.org/10.1126/science.1171529

Versele, R., Sevin, E., Gosselet, F., Fenart, L., & Candela, P. (2022a). TNF-α and IL-1β Modulate Blood-Brain Barrier Permeability and Decrease Amyloid-β Peptide Efflux in a Human Blood-Brain Barrier Model. *International Journal of Molecular Sciences*, *23*(18), 10235. https://doi.org/10.3390/ijms231810235

Vertegaal, A. C. O. (2022). Signalling mechanisms and cellular functions of SUMO. *Nature Reviews Molecular Cell Biology*, *23*(11), 715–731. https://doi.org/10.1038/s41580-022-00500-y

Vigneswara, V., & Ahmed, Z. (2020). The Role of Caspase-2 in Regulating Cell Fate. *Cells*, *9*(5), 1259. https://doi.org/10.3390/cells9051259

Wang, C. ; D. Y. ; Y. Y. ; C. W. ; Z. Y. ; S. G. ; W. Z. (2018). Glutamine Enhances the Hypoglycemic Effect of Insulin in L6 590 Cells via Phosphatidylinositol-3-Kinase (PI3K)/Protein Kinase B (AKT)/Glucose Transporter 4 (GLUT4) Signaling Pathway. *Med. Sci. Monit.*, *24*, 1241–1250.

Wei, S., Sun, Y., Wang, L., Zhang, T., Hu, W., Bao, W., Mao, L., Chen, J., Li, H., Wen, Y., & Chen, Z. (2021). Hyperoside suppresses BMP-7-dependent PI3K/AKT pathway in human hepatocellular carcinoma cells. *Annals of Translational Medicine*, *9*(15), 1233–1233. https://doi.org/10.21037/atm-21-2980

Wen, J., Satyanarayanan, S. K., Li, A., Yan, L., Zhao, Z., Yuan, Q., Su, K.-P., & Su, H. (2024). Unraveling the impact of Omega-3 polyunsaturated fatty acids on blood-brain barrier (BBB) integrity and glymphatic function. *Brain, Behavior, and Immunity*, *115*, 335–355. https://doi.org/10.1016/j.bbi.2023.10.018

Wu, P., Chang, C., Zhu, G., Zhai, L., Zhang, X., Huan, Q., Gao, Z., Deng, H., Liang, Y., & Xiao, H. (2023). Network Pharmacology Study of Bioactive Components and Molecular Mechanisms of the Glycoside Fraction from Picrorhiza scrophulariiflora Against Experimental Colitis. *Drug Design, Development and Therapy*, *Volume 17*, 1531–1546. https://doi.org/10.2147/DDDT.S407339

Xie, X., Zhu, H., Zhang, J., Wang, M., Zhu, L., Guo, Z., Shen, W., & Wang, D. (2017). Solamargine inhibits the migration and invasion of HepG2 cells by blocking epithelial-to-

mesenchymal transition. *Oncology Letters*, *14*(1), 447–452. https://doi.org/10.3892/ol.2017.6147

Yamashita, Y., Wang, L., Nanba, F., Ito, C., Toda, T., & Ashida, H. (2016). Procyanidin Promotes Translocation of Glucose Transporter 4 in Muscle of Mice through Activation of Insulin and AMPK Signaling Pathways. *PLOS ONE*, *11*(9), e0161704. https://doi.org/10.1371/journal.pone.0161704

Yang, C.-W., Lee, Y.-Z., Hsu, H.-Y., Wu, C.-M., Chang, H.-Y., Chao, Y.-S., & Lee, S.-J. (2013). c-Jun-mediated anticancer mechanisms of tylophorine. *Carcinogenesis*, *34*(6), 1304–1314. https://doi.org/10.1093/carcin/bgt039

Ybe, J. A. (2014). Novel clathrin activity: developments in health and disease. *Biomolecular Concepts*, *5*(2), 175–182. https://doi.org/10.1515/bmc-2013-0040

Yogev, O., Goldberg, R., Anzi, S., Yogev, O., & Shaulian, E. (2010). Jun Proteins Are Starvation-Regulated Inhibitors of Autophagy. *Cancer Research*, *70*(6), 2318–2327. https://doi.org/10.1158/0008-5472.CAN-09-3408

Yonamine, C., Pinheiro-Machado, E., Michalani, M., Alves-Wagner, A., Esteves, J., Freitas, H., & Machado, U. (2017). Resveratrol Improves Glycemic Control in Type 2 Diabetic Obese Mice by Regulating Glucose Transporter Expression in Skeletal Muscle and Liver. *Molecules*, *22*(7), 1180. https://doi.org/10.3390/molecules22071180

Yoon, S. A. ; K. S. I. ; S. H. S. ; K. S. W. ; K. J. H. ; K. H. C. ; K. S. J. (2013). p-coumaric acid modulates glucose and lipid metabolism via AMP-activated protein kinase in L6 skeletal muscle cells. *Biochem. Biophys. Res. Commun*, *432*, 553–557.

Younus, H. (2018). Therapeutic potentials of superoxide dismutase. *International Journal of Health Sciences*, *12*(3), 88–93.

Yuan, Z., Gong, S., Luo, J., Zheng, Z., Song, B., Ma, S., Guo, J., Hu, C., Thiel, G., Vinson, C., Hu, C.-D., Wang, Y., & Li, M. (2009). Opposing Roles for ATF2 and c-Fos in c-Jun-Mediated Neuronal Apoptosis. *Molecular and Cellular Biology*, *29*(9), 2431–2442. https://doi.org/10.1128/MCB.01344-08

Yun, C. W., & Lee, S. H. (2018). The Roles of Autophagy in Cancer. *International Journal of Molecular Sciences*, *19*(11), 3466. https://doi.org/10.3390/ijms19113466

Zaidieh, T., Smith, J. R., Ball, K. E., & An, Q. (2019). ROS as a novel indicator to predict anticancer drug efficacy. *BMC Cancer*, *19*(1), 1224. https://doi.org/10.1186/s12885-019-6438-y

Zhang, C., Niu, W., Wang, Z., Wang, X., & Xia, G. (2012). The Effect of Gonadotropin on Glucose Transport and Apoptosis in Rat Ovary. *PLoS ONE*, *7*(8), e42406. https://doi.org/10.1371/journal.pone.0042406

Zhang, X., Xue, X.-C., Wang, Y., Cao, F.-F., You, J., Uzan, G., Peng, B., & Zhang, D.-H. (2019). Celastrol Reverses Palmitic Acid-Induced Insulin Resistance in HepG2 Cells via Restoring the miR-223 and GLUT4 Pathway. *Canadian Journal of Diabetes*, *43*(3), 165–172. https://doi.org/10.1016/j.jcjd.2018.07.002

Zhao, F., Liu, Q., Cao, J., Xu, Y., Pei, Z., Fan, H., Yuan, Y., Shen, X., & Li, C. (2020). A sea cucumber (Holothuria leucospilota) polysaccharide improves the gut microbiome to alleviate the symptoms of type 2 diabetes mellitus in Goto-Kakizaki rats. *Food and Chemical Toxicology*, *135*, 110886. https://doi.org/10.1016/j.fct.2019.110886

Zhao, Y., Gan, L., Ren, L., Lin, Y., Ma, C., & Lin, X. (2022). Factors influencing the blood-brain barrier permeability. *Brain Research*, *1788*, 147937. https://doi.org/10.1016/j.brainres.2022.147937

Zheng, J., Shao, Y., Jiang, Y., Chen, F., Liu, S., Yu, N., Zhang, D., Liu, X., & Zou, L. (2019). Tangeretin inhibits hepatocellular carcinoma proliferation and migration by promoting autophagy-related BECLIN1 . *Cancer Management and Research*, *Volume 11*, 5231–5242. https://doi.org/10.2147/CMAR.S200974

Zheng, Z., Zhang, X., Bai, J., Long, L., Liu, D., & Zhou, Y. (2022). PGM1 suppresses colorectal cancer cell migration and invasion by regulating the PI3K/AKT pathway. *Cancer Cell International*, *22*(1), 201. https://doi.org/10.1186/s12935-022-02545-7

Zhou, M.-N., Liu, P., Jing, S.-J., Sun, M., Li, X., Zhang, W., & Liu, B. (2022). [Chemical constituents of Scrophulariae Radix and their antitumor activities in vitro]. *Zhongguo Zhong Yao Za Zhi = Zhongguo Zhongyao Zazhi = China Journal of Chinese Materia Medica*, *47*(1), 111–121. https://doi.org/10.19540/j.cnki.cjcmm.20211126.201

Zhu, Q., Lin, L., & Zhao, M. (2020). Sulfated fucan/fucosylated chondroitin sulfate-dominated polysaccharide fraction from low-edible-value sea cucumber ameliorates type 2 diabetes in rats: New prospects for sea cucumber polysaccharide based-hypoglycemic functional food. *International Journal of Biological Macromolecules*, *159*, 34–45. https://doi.org/10.1016/j.ijbiomac.2020.05.043

Zmemlia, N., Bejaoui, S., Khemiri, I., Bouriga, N., Louiz, I., El-Bok, S., Ben-Attia, M., & Souli, A. (2020). Biochemical composition and antioxidant potential of the edible Mediterranean sea cucumber Holothuria tubulosa *Grasas y Aceites*, *71*(3), 364. https://doi.org/10.3989/gya.0452191

8. ACKNOWLEDGEMENTS